POLITECNICO DI TORINO

Department of Mechanical and Aerospace Engineering

**Master's degree in Biomedical Engineering**

# Exploring the Role of Photobiomodulation in Cellular Responses: Implications for Cancer and Alzheimer's Disease


Politecnico di Torino

UNIVERSITY OF ALBERTA


ALMA MATER STUDIORUM
UNIVERSITÀ DI BOLOGNA

**Supervisor**
Prof. Jacek Adam Tuszynski

**Candidate**
Sara Castria

Academic Year 2024-2025

# ABSTRACT

This project was intended to conduct experimental studies on the effects of two types of electromagnetic (EM) waves on living states with potential applications as novel therapeutic modalities. The first part of this study, conducted in collaboration with the University of Alberta, involved cancer research and specifically explored potential therapeutic applications of photobiomodulation (PBM). PBM involves the use of non-ionizing EM radiation in the range between infrared and ultraviolet to induce biological effects on cells, tissues and organisms. The devices used for the experiments were the Bioptron device, which emits a hyperpolarized light beam (HPL) at 40 mW/cm², and the Vielight NeuroPro device, which utilizes an infrared light beam at 60 mW/cm² with a 10 Hz frequency sweep. Three different cancer cell lines were used in the experiments, namely: PC3, HeLa, and MCF7. The study focused on analyzing cell viability, morphological changes, ATP production, and metabolic shifts. The first step of the experiment involved culturing the aforementioned cells under standard conditions to promote proliferation and obtain statistically significant data for analysis. Subsequently, part of the samples was exposed to HPL (via Bioptron), while the remaining samples were exposed to infrared light (via Vielight). After irradiation, cell viability was first assessed using the Alamar Blue assay, followed by the analysis of key cytoplasmic proteins: actin, tubulin, and mitochondrial morphological changes through immunofluorescence staining. Finally, ATP production and metabolic shifts were quantified using the Glycolysis/OXPHOS Assay Kit.

The study highlighted a biphasic cellular response to light irradiation: short exposure reduced cell viability, suggesting initial stress, whereas longer exposure produced variable effects, promoting proliferation in some cases and cell death in others. The Bioptron device induced more pronounced cellular changes than the Vielight NeuroPro device, with morphological alterations such as cytoplasmic shrinkage and potential mitochondrial damage. Metabolic assessments indicated a shift in energy production pathways following irradiation. Some experimental sets showed increased glycolytic activity with reduced mitochondrial ATP production, while others exhibited the opposite trend. This metabolic reprogramming appeared to be influenced by both the irradiation conditions and the specific cell line. An interesting finding was the role of the culture medium, which seemed to mediate the effects of electromagnetic waves, suggesting a complex interaction between light, the extracellular environment, and cellular response. The results suggest the therapeutic potential of PBM and HPL but emphasize the need for precise optimization of treatment protocols.

In the second part of the thesis, conducted in collaboration with the University of Bologna, experiments were performed to study the effects of PBM on the Tau protein, which is involved in Alzheimer's disease (AD). The experiments were conducted on rat brain slices obtained using a Vibratome and preserved in artificial cerebrospinal fluid (ACSF) at 4°C to maintain slice viability throughout the process. Before applying the discussed therapy, a subset of samples underwent Tau protein hyperphosphorylation mimicking a key aspect of the AD through a gradual temperature reduction. The samples were analyzed using WesternBlot to assess the behavior of the Tau protein and its potential phosphorylation under the experimental conditions.

# Indice

# 1 INTRODUCTION

This thesis explores the potential therapeutic applications of photobiomodulation (PBM) and hyperpolarized light (HPL) in two distinct areas of significant medical concern: cancer treatment and Alzheimer's disease (AD). By investigating the effects of these light-based therapies on various cellular processes and protein dynamics, this research aims to contribute to the growing body of knowledge in these fields and potentially uncover new avenues for treatment.
The motivation behind this study stems from the urgent need for innovative therapeutic approaches in both cancer and Alzheimer's disease. Cancer remains one of the leading causes of death worldwide, with conventional treatments often accompanied by severe side effects and limited efficacy in certain cases. Similarly, Alzheimer's disease represents a growing global health crisis as populations age, with current treatments offering limited benefits in slowing disease progression. Recent studies have highlighted the potential of light-based therapies in modulating cellular processes and neurological functions, sparking interest in their application to these challenging medical conditions.

In the realm of cancer research, photobiomodulation has shown promise in influencing cancer cell behavior, potentially offering a non-invasive approach to complement existing treatments. Research have demonstrated that PBM can induce apoptosis in certain cancer cell lines while potentially enhancing the efficacy of chemotherapeutic agents. However, the effects appear to be highly dependent on factors such as light parameters, cancer type, and experimental conditions. This variability underscores the need for comprehensive investigations to elucidate the complex interplay between PBM and the molecular landscapes of different cancer types.

For Alzheimer's disease, recent research has shown promising results in using light therapy to modulate neural activity and potentially mitigate disease progression. Recent studies have demonstrated that PBM can improve mitochondrial function, increase ATP production, and reduce oxidative stress in neural tissues, all of which are crucial factors in maintaining neuronal health. Furthermore, investigations into the effects of light therapy on key proteins involved in AD pathology, such as Tau and beta-amyloid, have opened new avenues for potential interventions.

The primary objective of this thesis is to systematically investigate the effects of PBM and HPL on cancer cells and AD-related proteins under various experimental conditions. For the cancer-focused portion of the study, we aim to elucidate the impact of different irradiation parameters on cell viability, morphology, and metabolic activity across three distinct cancer cell lines: PC3, HeLa, and MCF7. This comparative approach allows us to explore the cell-specific nature of responses to light therapy and potentially identify optimal treatment protocols for different cancer types.

In the Alzheimer's disease component, our goal is to examine how PBM and HPL influence key proteins involved in AD pathology, specifically Tau1, pGSK3β, and p-tau205. By conducting experiments under different temperature conditions and exposure durations, we seek to uncover the potential of these light-based therapies in modulating protein dynamics relevant to AD progression.

The methodology employed in this research involves a combination of in vitro cellular experiments and protein analysis techniques. For the cancer studies, we utilized two distinct light sources: the NeuroPro Device Module A, emitting near-infrared light, and the Bioptron Pro 1 device, producing hyperpolarized light. Cell viability was assessed using the Alamar Blue assay, while morphological changes were evaluated through immunofluorescence staining. Metabolic shifts were analyzed using a Glycolysis/OXPHOS Assay kit to provide insights into the impact of light therapy on cellular energetics.

For the Alzheimer's disease experiments, we employed a novel approach of using rat brain slices subjected to different temperature conditions to mimic aspects of AD pathology. Western blot analysis was used to quantify changes in protein levels and phosphorylation states following light therapy treatments.

The structure of this thesis is organized into several key chapters. Following this introduction, Chapter 2 provides a comprehensive review of the current state of the art in photobiomodulation and hyperpolarized light therapy, with specific focus on their applications in cancer and Alzheimer's disease. Chapter 3 details the materials and methods used in our experiments, ensuring reproducibility and transparency in our research approach. Chapters 4 and 5 present the results of our cancer and Alzheimer's disease studies, respectively, offering detailed analyses of our findings. Chapter 6 provides a comprehensive discussion of these results, contextualizing them within the broader scientific literature and exploring their implications for future research and potential clinical applications. Finally, Chapter 7 concludes the thesis by summarizing our key findings and outlining future directions for research in this promising field.

Our preliminary findings suggest complex and often cell-specific responses to light therapy in cancer cells, with variations in viability, morphology, and metabolic activity depending on irradiation parameters and cell type. In the Alzheimer's disease experiments, we observed intriguing changes in protein levels and phosphorylation states following light therapy, particularly under different temperature conditions. These results highlight the potential of PBM and HPL as therapeutic modalities while also underscoring the critical need for careful optimization of treatment protocols.

In conclusion, this thesis aims to provide a comprehensive exploration of the effects of photobiomodulation and hyperpolarized light on cancer cells and Alzheimer's disease-related proteins by elucidating the cellular and molecular responses to these innovative light-based therapies. The complexity of our findings emphasizes the need for continued rigorous investigation in this field, paving the way for potential breakthroughs in the treatment of cancer and Alzheimer's disease.

# 2 STATE OF THE ART

## 2.1 Background on Electromagnetic fields

Electromagnetic fields (EMFs) are a fundamental part of the physical world. This chapter looks at the complex traits of these fields, examining their features, sources, and possible impacts on living beings, particularly focusing on how they interact with human bodies (Markov, 2015a; Vecchia P. et al., 2009). EMFs consist of both electric and magnetic fields that work together in a balanced way. Understanding the details of this balance is important for explaining the basic rules that govern how they act.

Electric fields come from groups of stationary charges and affect charged particles around them (Popović & Popović, 1999). These fields can store and transfer energy and direct the paths of charged particles using forces. On the other hand, magnetic fields are created by moving charges or currents. These fields appear as invisible lines of force that surround and impact the movement of charged particles in their area (Rein, 2004).
In static conditions the electric and magnetic fields are clearly distinguishable, although their real nature is seen only in dynamic contexts where they are closely connected. When electric and magnetic fields are time-varying, they are indistinguishable, spreading in space as electromagnetic waves, which are controlled by the fundamental principles of electromagnetism.

These foundational principles simplify the immense understanding offered by the laws of electromagnetism and are a quantitative tool for analyzing and predicting electromagnetic behavior. They are the cornerstone of many applications across various fields including electrical engineering, optics and quantum physics, and thus enable us to harness the electromagnetic system to advance scientific and technological progress.

In this framework, electromagnetic fields are involved in human physiological processes (Markov, 2015a) from internal biological activities (endogenous EMFs) generated EMFs. In addition, there is an external factor that has a significant impact on these fields (exogenous EMFs).

These are not only secondary effects but are important in many physiological functions and cellular communication mechanisms (Funk, 2015a; Raines, 1981b; Zura et al., 2015a). On the cellular level, research has revealed that cells produce and react to electromagnetic fields during normal physiological functions (Markov, 2015b). The movement of ions across cell membranes - a process facilitated by ion channels and pumps that regulate their selective permeability - establishes electrical gradients and currents called membrane potentials.
These factors play a role in shaping the overall electromagnetic environment within the body (Levin, 2014; Thar & Kühl, 2004a). The potentials arise from the movement of charged particles, which create localized electromagnetic fields that are part of the body's natural EMF landscape. Metabolic processes that include oxidation-reduction reactions and electron transfer also generate localized electromagnetic fields. Therefore, energy production driven by metabolism encompasses all biosynthetic pathways (Funk, 2015b; Hammerschlag et al., 2015; Zura et al., 2015b).

As the “powerhouses of the cell”, mitochondria are also important in the generation of endogenous electromagnetic fields (EMFs). The process of ATP production involves creating electrochemical gradients through a series of redox reactions in the mitochondrial inner membrane known as the electron transport chain (Amaroli et al., 2021; Fantin et al., 2006; Thar & Kühl, 2004a). In addition to singularly acting reactive oxygen species, these signaling molecules aid in tuned modulation of electromagnetic fields and eventually cellular signaling pathways. Electron movement within proteins enables them to act as electromagnetic transceivers, enhancing the complex web of endogenous EMFs. (Thar & Kühl, 2004b).

Above the level of the individual cells, the human body displays large-scale electromagnetic phenomena. The nervous system uses action potentials, which are electrical signals generated by the movement of ions through neuronal membranes and create localized electromagnetic fields required for communication and brain activity. Such fields are responsible for diagnostic methods, including EEG and MEG. (DialoguesClinNeurosci – 16 – 93, Wiginton et al., 2022). The heart also produces powerful electromagnetic fields owing to the synchronized depolarization and repolarization of the cardiac cells that are necessary for the rhythmic contractions of the heart. These cardiac fields can be measured outside the body and are used for diagnosis with ECG and MCG. (Belenkov & Ryff, 1981). Both systems emphasize the astounding capacity of the human body to utilize endogenous electromagnetic fields for physiological processes and medical practices.

The existence of endogenous electromagnetic fields (EMFs) is well-documented, yet their precise functions and mechanisms in biological processes remain a topic of ongoing investigation. An intriguing theory suggests that these EMFs might facilitate long-range interactions between biomolecules, such as proteins, by enabling rapid and efficient binding beyond the constraints of Brownian diffusion. This proposed mechanism could enhance the coordination of complex biological processes.
Additionally, endogenous EMFs are hypothesized to play a role in facilitating intercellular communication and coordinating processes like circadian rhythms. This could provide a means for cells to synchronize their activities and respond to environmental cues, contributing to overall homeostasis and biological system regulation. Patterns of resting membrane potentials and endogenous EMFs have been suggested to guide developmental processes and tissue regeneration, potentially serving as a blueprint for cellular organization and differentiation.
In a more speculative context, endogenous EMFs have been proposed as a means for non-chemical communication between organisms, facilitating interactions such as plant-plant and animal-plant communication. This concept, often referred to as "biofield interactions," implies that living beings might exchange information and influence each other through the modulation of their electromagnetic fields, potentially revealing new insights into the interconnectedness of life.
Through this exploration of endogenous EMFs, we gain a deeper understanding of the intricate electromagnetic phenomena that permeate the human body. From cellular electrochemistry to larger-scale phenomena like neuronal conduction and cardiac rhythms, these fields are integral to our existence. As we continue to unravel the mysteries of life, studying endogenous EMFs promises to unveil new insights into the fundamental mechanisms governing biological processes, potentially leading to therapeutic applications and a deeper understanding of the natural world.

Exogenous electromagnetic fields (EMFs) originate from external sources and can interact with biological processes, influencing cellular functions. Research indicates that these external fields have various effects on bone cells, crucial for bone remodeling and homeostasis, depending on

factors like frequency, intensity, and exposure duration (Caliogna et al., 2021; Zhang et al., 2020). The effects on bone cells vary based on cell type, differentiation stage, and experimental conditions. Exogenous EMFs are categorized into low-frequency, radiofrequency, and pulsed electromagnetic fields (PEMFs), each with distinct effects on cell proliferation, differentiation, and signaling pathways.

Low-frequency EMFs influence bone cell proliferation and differentiation by modulating signaling pathways and calcium homeostasis (Costantini et al., 2022; Lei et al., 2017). Radiofrequency EMFs have been linked to increased osteoblast activity through specific signaling pathways (Atay et al., 2009; Gonul et al., 2016). PEMFs enhance bone repair by modulating calcium signaling and stimulating growth factors (Ceccarelli et al., 2013).
Additionally, natural EMFs like geomagnetic fields and cosmic rays contribute to the human EMF baseline, influencing physiological processes such as circadian rhythms (Füllekrug & Fraser-Smith, 2011; Vainio et al., 2009). However, more research is needed to fully understand these effects on human health.

## 2.2 Background on cancer

Cancer remains the second most common cause of death globally, claiming millions of lives each year. Its impact not only places a significant financial strain on healthcare systems but also profoundly affects individuals who must cope with the disease. Despite substantial progress in understanding cancer biology and developing new treatments, the disease's complexity and variability continue to present significant challenges.

Cancer is distinguished by unchecked cell proliferation and the capacity to invade and spread to other parts of the body. Hanahan and Weinberg's seminal work introduced a framework known as the "Hallmarks of Cancer," which outlines the fundamental characteristics of the disease. These hallmarks include sustained signalling for cell growth, evasion of growth inhibitors, resistance to cell death, acquisition of replicative immortality, induction of blood vessel formation, activation of invasion and metastasis, reprogramming of energy metabolism, evasion of immune responses, promotion of tumor-related inflammation, and genomic instability.

At the core of cancer lies a complex interaction of genetic and epigenetic changes that disrupt the delicate regulatory mechanisms governing cellular processes. These changes can result from inherited genetic predispositions, environmental exposures, and lifestyle factors, highlighting the multifaceted nature of cancer's development.

### 2.2.1 Cell-lines characteristics

This study sought to explore the potential impacts of photobiomodulation (PBM) and hyperpolarized light (HPL) on several cell lines by exposing them to two distinct electromagnetic field (EMF) spectrum ranges. Specifically, the investigation focused on three cancer cell lines, each with unique characteristics that are detailed below:

- The PC3 cell line is derived from a human prostatic adenocarcinoma and represents one of the most aggressive forms of prostate cancer. Originating from a bone metastasis of a grade IV prostate cancer, PC3 cells are characterized by their lack of functional androgen receptors (AR) and absence of prostate-specific antigen (PSA) expression. Additionally, they express neuroendocrine markers and the stem cell marker CD44, distinguishing them from other prostate cancer cell lines (Tai et al., 2011).

- The MCF7 cell line is derived from a human breast adenocarcinoma and serves as a model system for studying hormone receptor-positive breast cancers. Established from a pleural effusion of a 69-year-old woman with metastatic breast cancer, MCF7 cells exhibit a molecular profile similar to the luminal A subtype of breast cancer. Notably, they express estrogen receptor (ER) and progesterone receptor (PR) but are negative for human epidermal growth factor receptor 2 (HER2). Their well-defined molecular profile and responsiveness to hormonal stimuli make them a reliable platform for evaluating therapeutic agents (Baxter et al., 2017a; Welsh, 2013).

- The HeLa cell line is derived from a cervical adenocarcinoma and was established in 1951 from the tumor cells of Henrietta Lacks. HeLa cells have been instrumental in numerous scientific breakthroughs due to their unique ability to divide and proliferate indefinitely in culture. This property is attributed to the reactivation of the telomerase enzyme, which maintains telomere length. HeLa cells are also highly susceptible to viral infections, making them a valuable model for studying viral replication and pathogenesis (Masters, 2002).

### 2.2.2 Warburg effect

Cancer is characterized by uncontrolled cell proliferation and metastasis, accompanied by profound alterations in cellular metabolism (Ward & Thompson, 2012a). The Warburg effect, named after Otto Warburg, describes the unique metabolic phenotype observed in cancer cells, where they preferentially utilize aerobic glycolysis for energy production, even in the presence of sufficient oxygen (Otto, 2016a). This phenomenon was first observed by Warburg in the 1920s, who noted that cancer cells exhibit a significant increase in lactate production compared to normal cells, despite similar oxygen consumption rates (Liberti & Locasale, 2016a).

The Warburg effect is a hallmark of cancer metabolism, supporting rapid cell growth and survival by enhancing glucose uptake, increasing glycolytic flux, and reducing oxidative phosphorylation (Vander Heiden et al., 2009a). Cancer cells overexpress glucose transporters like GLUT1 to sustain high glycolytic rates, producing ATP rapidly, albeit less efficiently than oxidative phosphorylation (Hardie, 2022; Pascale et al., 2020). The reliance on glycolysis allows cancer cells to maintain redox balance through the pentose phosphate pathway, crucial for counteracting oxidative stress and supporting anabolic reactions (Vander Heiden et al., 2009a).
The elevated lactate production in cancer cells acts as a signalling molecule, influencing the tumor microenvironment by acidifying surrounding tissues, which promotes invasion and metastasis while suppressing immune responses (Liberti & Locasale, 2016a; Otto, 2016a). This metabolic shift contrasts with normal cells, which primarily rely on mitochondrial oxidative phosphorylation for ATP generation under aerobic conditions.

The Warburg effect is significant not only for its widespread presence across various cancer types but also for its potential as a diagnostic and therapeutic target. Its discovery has fundamentally altered our understanding of tumor biology, opening new avenues for cancer research and treatment strategies.

## 2.3 Background on Alzheimer's disease

Alzheimer's disease (AD) is a neurodegenerative disease first described in 1907 by Aloise Alzheimer, and, among other forms of dementia, it's considered the most common, accounting for up to 70% of cases, it is also classified as one of the leading causes of death for individuals over 65. As a matter of fact, age is the factor that contributes most to the development of AD, even though both genetic and environmental factors play a part. The typical symptoms of Alzheimer's disease are memory loss in the early stages, but as the disease develops, other symptoms such as anxiety, rage, petulance, sadness, sleeplessness, and delusions start to appear (Calabrò et al., 2020). Alzheimer's Disease is characterized by loss in cerebral function as neurons begin to die. Clinical signs are seen in the brain region affected by Alzheimer's disease because of damaged neuronal transmission. Gross atrophy of the affected areas is the outcome of this loss, including degeneration in the temporal and parietal lobes, as well as portions of the frontal cortex and cingulate gyrus.
Due to the progressive nature of this disease which leads to a severe cognitive decline, it is possible to identify four different stages of Alzheimer's disease based of the severity of the symptoms: preclinical, mild, moderate and severe (Calabrò et al., 2020).

The neuronal loss and nerve cell atrophy typical of AD are accompanied by the distribution of two other structures: the ω-Amyloid (Aω) plaques and the neurofibrillary tangles (NFT) (Delacourte, 1986; Karran, 2011). These are considered the major hallmarks of AD and are the subjects of the two main hypothesis, along with others, on how the disease pathologically evolves.
In this thesis, we will consider the second distinctive trait, which concerns the Tau protein, whose role focuses on promoting microtubule assembly (MTs).

### 2.3.1 Tau protein

Tau protein is a microtubule-associated protein first discovered in 1975 (Weingarten et al., 1975). It is encoded by the MAPT gene, which is located on human chromosome 17 (Himmler, 1989). Tau can be found in the central and peripheral nervous systems, in particular in the axons, where its main function consists of promoting microtubule assembly and stabilization. Tau is highly soluble but can aggregate into insoluble fibres and it is an intrinsically disordered protein (Mukrasch, 2009).

Tau protein is also subjected to several post-translational modifications, including phosphorylation, isomerisation, glycation, nitration, acetylation, oxidation and others, meaning that different tau-binding molecules share the same regulatory property of post-translational modifications, such as protein kinases and phosphatases (Yadikar, 2020). Among the possible modifications mentioned, the most common and impactful between these processes is phoshorylation, as tau protein contains approximately 85 phosphorylation sites.
Tau phosphorylation is regulated by a delicate balance between tau kinase and phosphatase activities, abnormal tau phosphorylation and subsequent aggregation in Alzheimer's disease might result from upregulated tau kinases or downregulated tau phosphatases, but these two possibilities are not mutually exclusive. Kinases are members of the enzyme class known as "transferases", since they transfer the phosphate group from high-energy donor molecules, like ATP or GTP, to specified substrates (Martin et al., 2013). GSK3β is a primary tau kinase that phosphorylates tau at multiple sites found in AD, it can phosphorylate tau at up to 42 different sites, making it one of the most effective kinases in promoting tau hyperphosphorylation. When GSK3β is phosphorylated (becoming pGSK3β), it is typically inactivated, which should lead to reduced tau phosphorylation. Under normal conditions, AKT (another kinase) phosphorylates GSK3β at Ser9, inhibiting its activity. However, in AD, this regulatory mechanism appears to be disrupted (Martin et al., 2013).

Under pathological conditions, conformational changes occur to the normal structure of tau, causing an increase of the protein in an hyperphosphorylated state, thus leading to the loss of tau's biological capacities. When it is hyperphosphorylated, Tau (PPTau) loses its primary function: Tau monomers detach from MTs, showing a tendency to aggregate in oligomers and then evolve toward the formation of NFT (Gerson et al., 2016; Wang and Mandelkow, 2016). This mechanism represents the main pathological marker of neurological diseases that are also termed as tauopathies (Kovacs, 2017), including Alzheimer's disease (AD) and other neurodegenerative disorders (Wang and Mandelkow, 2016; Kovacs, 2017).

For this reason, there are many studies in progress focusing on tau as a target for therapy. The principal strategies can be summarized as (Medeiros, 2011):
- Inhibition of abnormal tau hyperphosphorylation through modulation of specific protein kinases
- Induction of tau aggregates disassembly by using compounds like Methylene blue, Antharaquinones, etc.
- Stimulation of MTs stabilizing molecules with Taxol and Taxol-derived compounds
- Triggering of intracellular clearance pathways such as the ubiquitin-proteasome and/or autophagic system
- Tau immunotherapy
- Antiinflammatory therapy.

### 2.3.2 Deep Hypothermia and Synthetic Torpor

Tau hyperphosphorylation is not limited to neurodegenerative diseases but also occurs in response to hypothermic conditions in various physiological and experimental contexts (Squarcio et al., 2023; Luppi et al., 2019). This phenomenon has been observed in hibernation, deep anesthesia, and synthetic torpor (ST), a state induced in non-hibernating animals like rats through pharmacological inhibition of thermogenesis (Luppi et al., 2019). Unlike in pathological conditions, Tau hyperphosphorylation in these states is typically reversible and does not lead to neurodegeneration, with the exception of anesthesia-induced hypothermia in transgenic mouse models of tauopathy (Planel et al., 2009).

The accumulation of hyperphosphorylated Tau (PP-Tau) during ST is closely linked to the differential activity of key enzymes involved in Tau regulation, particularly glycogen synthase kinase-3β (GSK3β) and protein phosphatase 2A (PP2A) (Planel et al., 2004; Su et al., 2008).

At low temperatures, enzyme activity generally decreases in accordance with the Arrhenius equations (cf. Gutfreund, 1995; Marshall, 1997), however, PP2A activity decreases more rapidly than GSK3β, resulting in a temporary imbalance that favors Tau phosphorylation (Planel et al., 2004; Su et al., 2008).
While the Arrhenius equations explain the initial accumulation of PP-Tau during hypothermia, they do not account for the rapid dephosphorylation observed during recovery from ST. This suggests that active biochemical processes are involved in promoting Tau dephosphorylation during the recovery phase (Squarcio et al., 2023).

Indeed, the recovery from ST involves active biochemical processes that promote Tau dephosphorylation. These include the inhibition of GSK3β via phosphorylation at Ser9 and the activation of Akt, alongside an increase in melatonin levels, which may play a neuroprotective role by modulating these pathways (Squarcio et al., 2023; Luppi et al., 2019).

Such findings highlight ST as a model for studying adaptive neuronal mechanisms under hypothermia and suggest potential therapeutic avenues for tauopathies by mimicking these protective processes in normothermic conditions.

In this thesis work, brain samples were subjected to Tau protein hyperphosphorylation through a gradual reduction in temperature and then irradiated with the two devices, in order to analyze the levels of Tau-1 (non-phosphorylated form), pGSK3β (phosphorylated glycogen synthase kinase 3β), and p-205 Tau (Tau phosphorylated at threonine 205). The last one was analized because the levels of p[T205]-Tau form has been shown to have a neuroprotective role (Ittner et al., 2016).
This approach allowed for the examination of key markers involved in the phosphorylation state of Tau protein and its regulatory mechanisms during hypothermia-induced conditions, providing insights into the dynamics of Tau phosphorylation and its potential neuroprotective or pathological implications.

## 2.4 Background on Photobiomodulation

Photobiomodulation (PBM) is a new procedure involving EMFs, which consists of non-ionizing light stimulating cellular processes such as proliferation and tissue regeneration (Hamblin, 2016).

The discovery of PBM can be traced back to the work of Endre Mester in the 1960s. Mester, was attempting to replicate an experiment using a low-powered ruby laser on mice with tumors, expecting to observe tumor destruction. Instead, he noticed accelerated hair growth and enhanced wound healing in the shaved areas surrounding the tumors, despite the low power output of the laser (Anders et al., 2019). This unexpected finding was significant, as it highlighted the biological effects of low-intensity light.

Initially, this phenomenon was referred to as "Low Level Light Therapy" (LLLT), reflecting the low-power nature of the light sources used (Anders et al., 2019). However, subsequent research revealed that both lasers and light-emitting diodes (LEDs) could be effective in photobiomodulation applications, expanding the range of available light sources. As understanding of the underlying mechanisms improved and applications broadened, the scientific community adopted the more precise term "Photobiomodulation" in place of LLLT (Heiskanen & Hamblin, 2018).

Photobiomodulation (PBM) primarily targets cellular mitochondria, specifically interacting with Cytochrome C Oxidase (COX), which absorbs light within the red (600-700 nm) and near-infrared (700-1100 nm) spectrum (Hamblin, 2018a; Karu, 2014a; Ravera et al., 2019, 2021). Further research has identified several key mechanisms underlying the biological effects of PBM (de Freitas & Hamblin, 2016):

- Enhanced ATP Synthesis: PBM increases ATP production, thereby augmenting cellular metabolism and energy availability. This is crucial for facilitating cell repair and regeneration processes (Hamblin, 2016).
- Regulation of Reactive Oxygen Species (ROS) and Nitric Oxide (NO): The modulation of ROS and NO levels leads to improved cellular signaling pathways, reduced inflammation, and enhanced tissue repair mechanisms (Moriyama et al., 2009).
- Stimulation of Transcription Factors: PBM activates various transcription factors that regulate gene expression related to cell proliferation, migration, and anti-inflammatory responses, thereby influencing cellular behavior and tissue health (H. P. Kim, 2014; R Hamblin, 2017a).

The effectiveness of this novel light therapy is contingent upon several parameters that can substantially impact treatment outcomes (Hamblin et al., 2018). This therapeutic approach is guided by the Arndt-Schultz law, which outlines a biphasic dose-response curve in biological systems (Calabrese, 2001a, 2001b, 2002, 2004, 2013). According to this principle, low levels of light stimulate biological systems, while higher levels inhibit them. This concept highlights the importance of determining an optimal therapeutic range for photobiomodulation (PBM) treatments (Bensadoun et al., 2020a; Jo et al., 2023). Within this optimal range, the beneficial effects of the therapy can be maximized while minimizing potential adverse effects (Robijns et al., 2022a; Zein et al., 2018a). In particular:

- Wavelength: different wavelengths penetrate tissue to varying depths and interact with

specific cellular chromophores.

- Power density: the amount of energy delivered per unit area affects the depth of penetration and cellular response.
- Treatment duration: the length of exposure time influences the total energy delivered to the target tissue.
- Pulsing vs. continuous wave: some studies suggest that pulsed light may have different biological effects compared to continuous wave light.

Photobiomodulation (PBM) has demonstrated potential in several clinical applications:

- Skin Revitalization: Studies have shown that red and near-infrared light can significantly improve skin texture, appearance, and collagen density, leading to enhanced skin rejuvenation (Glass, 2023; Robijns et al., 2021a).

- Mood Disorders: Light therapy has proven effective in managing seasonal affective disorder (SAD) and non-seasonal depression. Meta-analyses indicate substantial reductions in depression symptoms with bright light treatment. For SAD, bright light therapy showed a considerable effect size, while dawn simulation also demonstrated significant benefits. In non-seasonal depression, bright light therapy yielded a notable effect size, highlighting its therapeutic potential (Gaggi et al., 2024; Montazeri et al., 2022).

Recently, photobiomodulation (PBM) has been explored as a potential adjunctive treatment for cancer, yielding mixed outcomes. Although PBM appears to hold promise in mitigating the adverse effects of conventional cancer therapies (R Hamblin, 2017b), emerging evidence suggests it may also serve as a viable complementary or alternative approach. In vivo studies have demonstrated that PBM can suppress the proliferation of cancer cells and impede tumor progression. For instance, research conducted by Hamblin et al. (Hamblin, 2018b) revealed that specific wavelengths of light can reduce the growth rate of certain cancer cell lines in animal models. These findings imply that PBM may exert a direct anti-cancer effect, potentially offering a non-invasive alternative to traditional treatments.

However, other research has reported conflicting outcomes. Some evidence suggests that PBM may not only be ineffective but could also worsen cancer progression. For instance, a study by Karu (Karu, 2014b; Karu et al., 2005) discovered that under certain conditions, PBM could lead to more aggressive tumor growth. These discrepancies emphasize the need for additional research to determine when PBM is beneficial versus harmful.
For this reason, it is essential to address the current research in terms of:

- Methodological heterogeneity: Many studies suffer from small sample sizes and varying treatment protocols.
- Placebo control: Designing appropriate placebo conditions for light therapy studies remains challenging.
- Long-term efficacy: More research is needed to assess the long-term effects of PBM therapy.

Future research should focus on standardizing treatment protocols, conducting larger randomized controlled trials, and exploring the potential synergistic effects of combining PBM with other therapeutic modalities.

Photobiomodulation (PBM) has also emerged as a promising therapeutic approach for Alzheimer's disease (AD), offering potential benefits in addressing the complex pathophysiology of this neurodegenerative disorder. As explained before, PBM utilizes non-thermal light from LEDs or lasers in the red to near-infrared spectrum to stimulate cellular processes, particularly in mitochondria, enhancing energy production and initiating a cascade of biological responses crucial for cellular health (Lim, 2024).
The mechanisms of PBM in AD treatment are multifaceted, targeting various aspects of the disease's pathology. PBM has been shown to reduce amyloid-beta (Aβ) plaques, a hallmark of AD, by enhancing microglial activation and promoting Aβ clearance (De Taboada et al., 2011). This reduction in Aβ burden is associated with improved cognitive function and decreased neuroinflammation (Saltmarche et al., 2017).
Furthermore, PBM has demonstrated the ability to mitigate tau pathology, another key feature of AD, by reducing hyperphosphorylated tau and neurofibrillary tangles in animal models (Purushothuman et al., 2015). The therapeutic effects of PBM extend beyond protein aggregation, addressing broader aspects of AD pathophysiology. PBM has been shown to enhance mitochondrial function, increase ATP production, and reduce oxidative stress, all of which are crucial for maintaining neuronal health and function (Hamblin, 2016). By improving cerebral blood flow and promoting angiogenesis, PBM supports vascular health and blood-brain barrier integrity, which are often compromised in AD (Yang et al., 2022).

PBM also modulates neuroinflammation by shifting microglial phenotypes from pro-inflammatory to anti-inflammatory states, potentially slowing disease progression (Zhang et al., 2021). Clinical studies have provided encouraging evidence for PBM's efficacy in AD treatment. Saltmarche et al. (2017) reported significant improvements in cognitive function and quality of life in patients with mild to moderately severe dementia following 12 weeks of PBM therapy. These improvements were associated with enhanced cerebral perfusion and increased connectivity within the default mode network, as observed in functional MRI studies (Chao, 2019). The application of PBM in AD treatment has also shown promise in modulating brain oscillations, particularly in the gamma frequency range. Studies have demonstrated that PBM can induce gamma oscillations, which are often disrupted in AD, potentially improving cognitive function and intra-brain communication (Zomorrodi et al., 2019).

Moreover, PBM has been found to stimulate neurogenesis and synaptogenesis, offering the potential for neural repair and regeneration in AD-affected brains (Hamblin, 2016). Despite these promising findings, it is important to note that the optimal parameters for PBM in AD treatment, including wavelength, power density, and treatment duration, are still under investigation. Large-scale clinical trials are needed to establish standardized protocols and confirm the long-term efficacy of PBM in AD management (Lim, 2024). In conclusion, the growing body of evidence supports PBM as a potential multifaceted approach to AD treatment, addressing various aspects of the disease's complex pathophysiology and offering hope for improved outcomes in patients with this devastating neurodegenerative disorder.

### 2.4.1 VieLight Devices

The device used in the experiments were the Vielight NeuroPro and Vielight NeuroPro alpha2. Both have a wearable brain photobiomodulation system developed by Vielight Inc. that delivers transcranial- intranasal photobiomodulation via a headset and intranasal applicator.
For the first part of the experiments, it was used just the Module A of the NeuroPro device without any other application device. For the second part of the experiments regarding Alzheimer's disease, it was used the intranasal device of the Vielight NeuroPro alpha2.

The Neuro Pro comes with the Neuro Pro app installed in a pre-synced smartphone provided with the Neuro Pro from Vielight Inc.
From the Neuro Pro app, it is possible to customize certain parameters such as power density and pulse rate as showed in the table.

| PARAMETER | SPECIFICATION |
|---|---|
| Light source | LED (810 nm) |
| Frequency pulse | 10 Hz |
| Power setting | 80% |
| Power density | 60 mW/cm$^2$ |
| Run time | Changeable |
| Duty cycle | 50% |

Table 1. VieLight NeuroPro setting for the Module A


Figure 1. VieLight NeuroPro modules and controller. The first on the right is the Module A which was used for this experimental study

The NeuroPro alpha2 device comes without the pre-synced smartphone, indeed the run time is not changeable, but it’s set at 20 minutes, and the power density is different.

| PARAMETER | SPECIFICATION |
|---|---|
| Light source | LED (810 nm) |
| Frequency pulse | 10 Hz |
| Power setting | 80% |
| Power density | 13.5 $mW/cm^2$ |
| Run time | 20 minutes |
| Duty cycle | 50% |

Table 2. VieLight NeuroPro Alpha2 setting for the intranasal module


Figure 2 Intranasal module of the Vielight Neuropro Alpha2 device

## 2.5 Hyperpolarized Light

Light, a fundamental concept of the physical sciences, is a form of electromagnetic radiation that crosses an extensive range of wavelengths within the electromagnetic spectrum. The visible part (400-700 nm) is just a small fraction of this spectrum but is crucial for human perception. Light exhibits both wave-like and particle-like properties, a duality that has been fundamental to the development of modern physics. In the 17$^{th}$ century, two competing theories emerged: Isaac Newton's corpuscular theory suggested that light consisted of particles, while Christiaan Huygens proposed a wave theory.

Thomas Young strongly support the latter theory doing a double-slit experiment, which demonstrated interference patterns characteristic of waves (Atkins & De Paula, 2006; Hecht, 2016). This experiment demonstrated the wave nature of light by showing an interference pattern on a screen when light passed through two closely spaced gaps. This pattern of alternating bright and dark fringes could only be explained by the constructive and destructive interference of light waves, providing strong evidence against the corpuscular theory of light (May 1801: Thomas Young and the Nature of Light, n.d.; Britannica, 2025). Young's findings also allowed him to measure the wavelengths of visible light and showed that different colors correspond to different wavelengths, revolutionizing our understanding of optics and laying the foundation for modern wave theory (Evident Scientific; Britannica, 2025).

However, the discovery of the photoelectric effect by Albert Einstein in 1905 restored the particle concept, showing that light consists of discrete packets of energy called Photons (Einstein, 1905). This dual nature was later combined in quantum mechanics under the concept of wave-particle duality (Born & Wolf, 2019; Britannica, 2025).

Following this concept, light is described as oscillating electric and magnetic fields that propagate perpendicularly to each other and to the direction of travel. These oscillations can occur in different planes, and when unpolarized light is emitted (e.g., from the Sun), its electric field vibrates randomly in all directions perpendicular to its propagation.
Polarization refers to the process by which the oscillations of the electric field are confined to a single plane or a specific pattern. This property is unique and has significant effects across scientific domains including optics, telecommunications, and medical therapies (Born & Wolf, 2019; Britannica, 2025).

There are three main types of polarization: linear, circular, and elliptical

- In linear polarization, the electric field oscillates along a single plane, this effect can be achieved using polarizing filters or by natural phenomena such as reflection and scattering.

- Circular polarization occurs when the electric field vector rotates in a circular motion as the wave propagates, with left- or right-handedness depending on the rotation direction.

- Elliptical polarization is a generalized form where the electric field traces an ellipse.

These forms can be manipulated using optical devices like wave plates (Goldstein, 2017; Vedantu, n.d.). Polarization has practical applications in areas such as glare reduction (e.g.,

polarized sunglasses), stress analysis in materials science, and even quantum communication systems (Vedantu, n.d.; AZoOptics, 2024).

A particularly advanced application of polarized light is the hyperpolarized light, also called Quantum Hyperlight (Willemse et al., n.d.). This complex form of light is generated through a nanophotonic process of fullerene C60 molecules. Fullerene C60 is a spherical molecule composed of 60 carbon atoms arranged in a structure resembling a soccer ball. In the light polarization process, these molecules are embedded within a polymeric matrix, these molecules create an icosahedral twisting structure that induces a Fibonacci-sequential effect on passing light. This effect rotates and twists the plane of photon polarization according to pentagonal patterns.
The process produces a two-dimensional energy membrane described by the following equation which “filters” photons based on Fibonacci law [Φ, φ] (Koruga, 2018; Willemse et al., n.d.).

$$[\Phi 2 + \varphi 2 = 3]$$

The result of this process is hyperpolarized light with both circular (left- and right-handed) and linear (vertical and horizontal) components. The unique polarization pattern generated is described as a "sunflower seeds photons pattern," reflecting its geometric arrangement, which lead to the final product of such process (Willemse et al., n.d.).

Hyperpolarized light has shown interesting promises in therapeutic applications. The “hyperlight therapy” penetrates tissues to stimulate cellular repair processes by stimulating photoacceptors within cells and enhancing mitochondrial function. This leads to increased nitric oxide production, improved blood flow, reduced inflammation, and enhanced immune responses. Additionally, it promotes collagen synthesis and fibroblast activity for tissue regeneration. Clinical studies have demonstrated its efficacy in managing chronic pain conditions such as neck pain by modulating inflammatory pathways and accelerating tissue repair mechanisms (BIOPTRON Hyperlight, n.d.; Tian et al., 2023; Raeissadat et al., 2014).

### 2.5.1 Bioptron Devices

The BIOPTRON devices are an advanced light therapy device that employs polarized light technology for medical and therapeutic applications. For the first part of the experiments the Bioptron Pro1 device was used to deliver the therapy, while for the second part of the experiments the Bioptron MedAll device was employed.

The Bioptron Pro1 incorporates user-friendly features such as a timer function, adjustable height and inclination, and an integrated distance rod to ensure optimal treatment positioning.
The filter diameter of BIOPTRON® Pro 1 (about 11 cm) allows for treatment of various medium-sized areas.
Certified to CE standards (CE0124), the BIOPTRON Pro 1 includes safety features like overheating protection and is operable within a temperature range of +10°C to +40°C, making it suitable for both clinical and home environments.

| PARAMETER | SPECIFICATION |
|---|---|
| Light source | Halogen Lamp |
| Wavelength range | 590-1550 nm |
| Polarization | 95% |
| Power setting | 100% |
| Power density | 40 mW/cm$^2$ |
| Run time | Changeable |
| Duty cycle | 50% |

Table 2. Setting used for Bioptron Pro1 experiments


Figure 3 Bioptron Pro1 device

The Bioptron MedAll device is also suitable for both clinical and home environments offering the same features as the other device. The primary differences lie in the size of the device and its filter. The 5 cm filter of this device allows to treat small but precise areas.


Figure 4 Bioptron MedAll device

# 3 MATERIALS AND METHODS

## 3.1 Cancer cells

### 3.1.1 Cell culture

The PC3 prostate cancer cell line was sourced from Dr. John Lewis's research facility at the Katz Group Center (Canada). The HeLa and MCF7 cell lines were procured from Dr. Godbout's laboratory at the Cross Cancer Institute (Canada). These cells were cultivated in Dulbecco's Modified Eagle Medium (DMEM) enhanced with 10% (V/V) Fetal Bovine Serum (FBS) and 1% antimicrobial compounds (100 U/ml penicillin and 100 µg/ml streptomycin). The cellular cultures were maintained in a regulated environment at 37°C with a 5% CO2 atmosphere.

### 3.1.2 Sample preparation and irradiation

Cells were cultured in T75 flasks until reaching approximately 80% confluence before subculturing into µ-Dish 35 mm high-wall glass-bottomed dishes (ibidi Inc, Gräfelfing, Germany). Upon attaining the desired confluence, the exhausted medium was removed, and the culture was washed with Phosphate-Buffered Saline (PBS). After removing the PBS, 2 mL of TrypLETM Express Enxyme 1X (Glibco, ThermoFisher Scientific, Burlington, Ontario, Canada) was added to detach cells. To boost such reaction, the flask was incubated at 37°C for a few minutes. Once trypsinization was complete, 8 mL of fresh culture medium (DMEM) was added. Subsequently, cells were counted using a hemocytometer, aiming for a cell density of $25 \times 10^4$ cells per dish. Finally, the cellular suspension of 10 µL was formulated in a 96-well plate with 40 µL of 0.4% Trypan Blue (Sigma Aldrich, St. Louis, Missouri, USA), resulting in a final dilution factor of 5.
Following cell seeding and overnight incubation, the medium was substituted with fresh DMEM supplemented solely with 1% antibiotics to synchronize the cells in the G0/G1 phase. This synchronization process required a 24-hour incubation period.

After synchronization, samples were irradiated using two different light exposure devices previously named. The module A of the Vielight NeuroPro device was employed to irradiate cells with a power density of 60 $mW/cm^2$ and a frequency of 10 Hz, while the Bioptron Pro1 device operates with a power density of 40 $mW/cm^2$.

Cells were irradiated with different time sets ambient temperature, in particular the PC3 cell line was divided into four group of exposure time (I) 10 minutes exposure (II) 15 minutes exposure, (III) 20 minutes exposure, (IV) 20 minutes exposure with a 10-minute intermission. The same exposure times were used to irradiate fresh growth medium in a 1.5 ml Eppendorf tube, which was subsequently transferred to the dishes containing the pre-seeded cells.

Regarding the irradiation of HeLa and MCF7 cells with the Bioptron device, the exposure times were the same as those used for the PC3 cell line. However, for the VieLight-treated

samples, the time set changed: (I) 15 minutes, (II) 33 minutes, (III) 60 minutes, (IV) 30 minutes with a 15-minute intermission.

Across all experimental groups and devices, the cell samples were positioned at a constant distance of 125 mm from the beam source during irradiation. This uniform distance ensured consistent exposure conditions and facilitated comparative analyses between the various treatment groups.

### 3.1.3 Cell viability

To evaluate the cellular viability the Alamar Blue assay was employed 24 hours post-irradiation. The test measures cell viability by utilizing the ability of metabolically active cells to reduce the non-fluorescent compound resazurin into the fluorescent and red-colored compound resorufin, which can be quantified using fluorescence or absorbance detection.

For this experiment, 100 µL of resazurin was introduced to 1 mL of pre-warmed medium and incubated for 2 hours. Cell viability was quantified using a fluorescence-based Fluostar Omega plate reader (BMG LABTECH, Ortenberg, Germany) with an excitation wavelength of 544 nm and an emission wavelength of 590 nm. Experiments were conducted in triplicate in a 96-well plate, utilizing fresh medium as a blank control.

### 3.1.4 Immunofluorescence

One gelatin-coated coverslip was inserted into each dish and allowed to dry. Cells were fixed with 3.7% of formaldehyde in Phosphate Buffer Solution (PBS) for 15 minutes at room temperature and washed twice with PBS. Then, cells were permeabilized with 0.1% Triton X-100 (Sigma Aldrich, St. Louis, Missouri, USA) in PBS for 15 minutes at room temperature, followed by a double washing with PBS.

For the actin staining, 1.4 µL of Alexa-Fluor 488 Phalloidin (Invitrogen, ThermoFisher Scientific, Burlington, Ontario, Canada) was diluted in 500 µL of 1% Working Buffer Solution (WBS) composed of MACS Bovine Serum Album (BSA) (Miltenyi Biotec, Bergisch Gladbach, Germany) in PBS. Then cells were incubated for 30 minutes at room temperature in the dark, washed again with PBS and mounted on microscope slides using the mounting media ProLong Gold Antifade Reagent with DAPI (Invitrogen, ThermoFisher Scientific, Burlington, Ontario, Canada).

For tubulin staining, 5 µL of Primary antibody ATN02 Anti-AlphaBeta Tubulin Sheep Polyclonal (Cytoskeleton Inc, Denver, Colorado, USA) in 1 mL of 1% WBS in PBS was applied to cells, incubated overnight, and rinsed with PBS the following day.
Subsequently, 2.5 µL of Donkey anti-Sheep IgG (H+L) Cross-Adsorbed Secondary Antibody Alexa Fluor 647 (Invitrogen, ThermoFisher Scientific, Burlington, Ontario, Canada) in 500 µL of WBS was introduced and incubated for 30 minutes at 4°C on a tilting plate in a dark environment. Samples were rinsed twice with PBS and then mounted following the procedure mentioned above for Phalloidin.

Immunofluorescence was used also to check mitochondrial activity: 250 nM of MitoTracker TM Orange CMTMRos (Invitrogen, ThermoFisher Scientific, Burlington, Ontario, Canada) in 1 mL of pre-warmed DMEM was added to the samples immediately after the irradiation and incubated at 37°C for 45 minutes. Then, the samples were washed three times with fresh new medium so that immunofluorescence could be performed.
Samples were analyzed using the Zeiss 710 confocal microscope (Carl Zeiss AG, Ober-kochen, Germany).
These tests were done for the PC3 and HeLa cell lines.

### 3.1.5 Glycolysis-Oxphosphorylation

Glycolysis/OXPHOS Assay kit (Dojindo Molecular Technologies, Minato City, Tokyo, Japan) was used to measure the total ATP, the glycolytic ATP, the mitochondrial ATP and the lactate production in cells following the manufactures specifications.

The ATP quantification kit provided a 5.5 mL ATP Buffer solution, to which 10 lyophilized luciferase enzyme was added to create the ATP working solution (ATP WS). The luciferase enzyme catalyzes the oxidation of luciferin, a process coupled to ATP consumption and light emission. A 96-well microplate was used for the assay setup. Each well received 100 µL of the prepared ATP WS, followed by 100 µL of cell supernatant from the respective samples. The microplate was then incubated at 25°C for 10 minutes in darkness.
The Fluostar Omega microplate reader (BMG LABTECH, Ortenberg, Germany) was used to measure the luminescence signal emitted from each well.

To assess the metabolic shift in cells due to mitochondrial activity, samples were treated with Oligomycin. Immediately after the radiation, 10 mmol/l Oligomycin stock solution was diluted 1:500 with culture medium to obtain a 2-fold solution. Each experiment included one dish treated with Oligomycin (Oligomycin +) and one with fresh medium only (Oligomycin -) for both control and treated samples.
Subsequently, cells were incubated for 3 hours at 37°C, then, ATP assay was performed following the protocol mentioned above, and luminescence was measured using the Fluostar Omega microplate reader.

For lactate production quantification, the assay compared absorbance values between the Lactate Standard, the sample, and the blank. The 10 mmol/l Lactate Standard provided in the kit was diluted to 1 mmol/l with double- deionized H2O (ddH2O). Cell culture supernatants were diluted 10-fold with ddH2O, and ddH2O served as the blank.
Subsequently, 20 µL of each solution was added in triplicate to a 96-well plate, followed by 80 µL of Lactate Working Solution. The plate was incubated at 37°C for 30 minutes.
Absorbance was measured at 450nm using the Fluostar Omega microplate reader.

## 3.2 Brain slices

### 3.2.1 Sample preparation

For the thesis experiments, two male Sprague–Dawley rats (300 g) were used. The experiments were conducted on two consecutive days, with one rat used on the first day and the other on the following day, replicating the same procedures for both animals.

The rats were deeply anesthetized with isoflurane before brain extraction. After the decapitation, the brain was carefully and meticulously extracted in ice-cold artificial cerebrospinal fluid (aCSF) solution, using precise dissection techniques to maintain the integrity of the neural tissue.
The brain area of interest, containing the hippocampus, was isolated. The front and back parts of the brain were cut away to get a roughly rectangular section with the hippocampus inside.

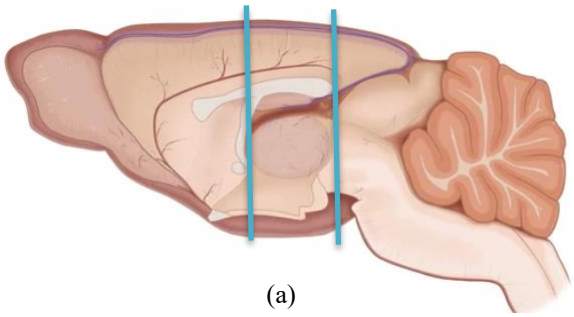

(a)

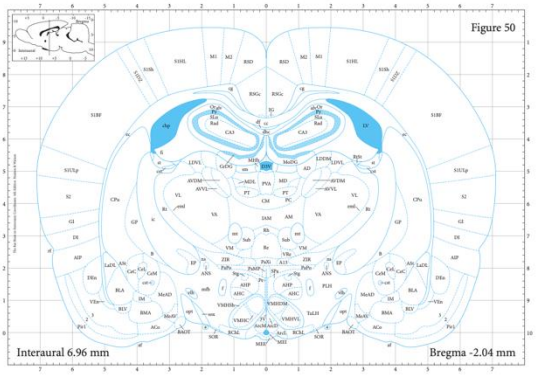


(b)

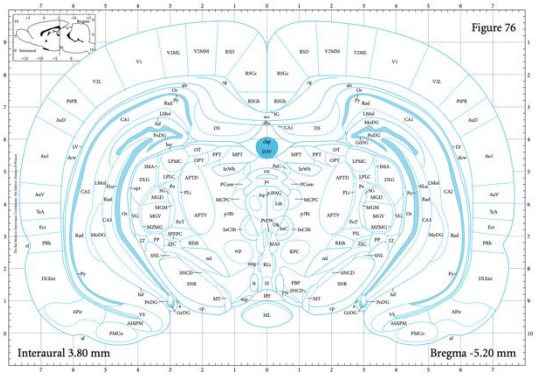


(c )

Figure 5 Rat brain (a) lateral section (b) Cranial slice (c) Caudal slice

Throughout the extraction and subsequent procedures, the brain tissue was kept at 3-4°C and bathed in ice-cold, oxygenated artificial cerebrospinal fluid (aCSF). The aCSF (295 mOsm/L, pH 7.4) was prepared in advance using the reagents listed in Table 3 and bubbled with 95% $O_2$ 5% $CO_2$.

| Reagent | nM | g |
|---|---|---|
| NaCl | 126 | 11.045 |
| KCl | 3 | 0.335 |
| $NaHCO_3$ | 26 | 3.276 |
| $CaCl_2$ | 2 | 0.441 |
| $MgSO_4$ | 1 | 0.370 |
| D-Glucose | 10 | 2.702 |
| $NaH_2PO_4$ | 1.25 | 0.225 |

Table 3. Reagent for 1 L of aCSF solution

To obtain brain slices, Vibroslice NVSLM1 (figure 6) vibrating microtome was used, which can cut fresh brain tissue into 50-700 µm thick slices. Vibrating blade slicers generally cause less tissue damage compared to other methods, helping preserve neurons in various brain regions.
The trimmed rectangular brain section was adhered to the specimen holder of the Vibroslice using superglue. The brain tissue was submerged in oxygenated aCSF at 3-4°C. After setting the vibration frequency and desired slice thickness to 300 µm, coronal slicing was performed. Each slice was carefully removed with a pipette and transferred to a petri dish containing oxygenated aCSF at 3-4°C for preservation.

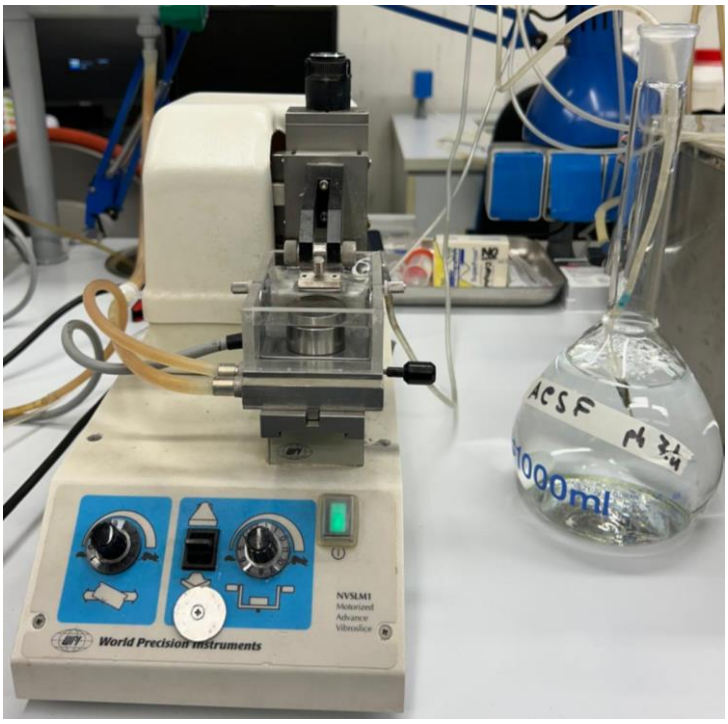


Figure 6 Vibroslice NVSLM1

This process was repeated until the entire brain section was sliced. The resulting tissue slices were immediately transferred to and maintained in aCSF oxygenated at 4°C to preserve their viability as shown in Figure 7.

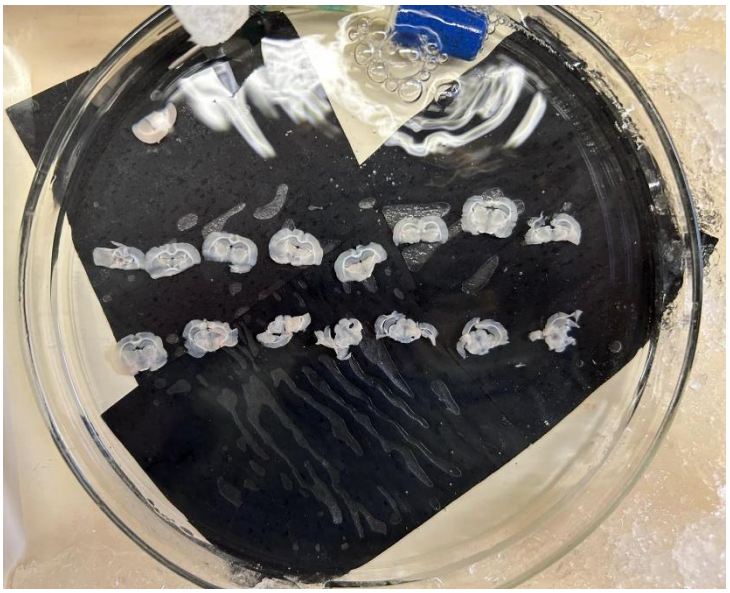

Figure 7 Brain slices in aCSF

The slices were then transferred into 8 becher, dividing the samples into two main groups: those that reached and remained at 37°C and those subjected to a temperature decrease.
The two groups were further divided in two sets: irradiated samples and control samples. The irradiated group was further subdivided based on the duration of exposure, either 10 minutes or 20 minutes, and the type of light source used. Specifically, for the 10-minute irradiation, two slices were exposed to Bioptron light and another two slices to Vielight. Similarly, for the 20-minute irradiation, two slices were exposed to Bioptron light and two slices to Vielight.
The control group, on the other hand, consisted of slices that were not subjected to any irradiation. This group included two slices for the 10-minute time point and two slices for the 20-minute time point, serving as a baseline for comparison with the irradiated samples. This protocol was replicated for the second group, subjected to a temperature decrease. This design allowed for the evaluation of the effects of different light sources and exposure durations on the samples.

### 3.2.2 Temperature

Prior to irradiation, the first group was brought to 37°C using a Liquid Bath Temperature Calibrator Ambient, which ensured stable and precise maintenance of the artificial cerebrospinal fluid (aCSF) temperature in which the brain slices were submerged.

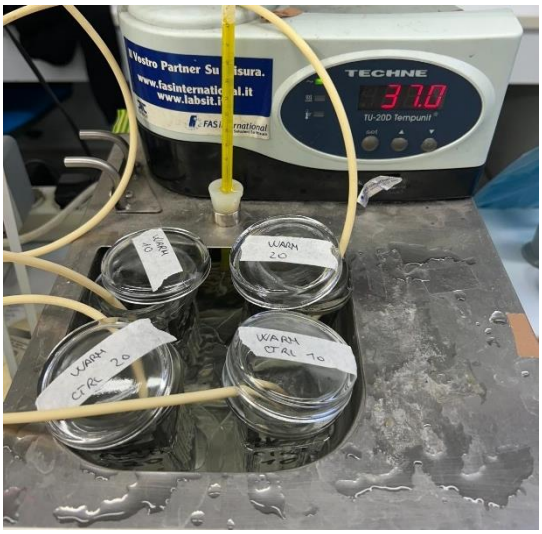


Figure 8 Liquid Bath Temperature

Similarly, the second group was initially brought to 37°C but subsequently underwent a controlled temperature gradient to reach 25°C. This protocol, involved lowering the temperature to 30°C over 30 minutes, followed by a gradual reduction to 25°C over the course of one hour. This process was achieved by immersing Coplin Staining Jars containing the samples into a temperature-regulated bath similar to that used for the first group.

After reaching 25°C, the samples were maintained at this temperature for an additional hour. This step was implemented based on findings from previous studies, which reported that AT8 staining, used to detect phosphorylated Tau at Ser202/Thr205, was not clearly detectable immediately upon reaching 25°C. Prolonging the exposure at 25°C allowed for enhanced AT8 signal detection, likely due to ongoing phosphorylation processes or stabilization of Tau epitopes during this period (Squarcio et al., 2023; Luppi et al., 2019).

### 3.2.3 Irradiation

The irradiation was performed using the two devices described in chapters 2.4.1 and 2.5.1, specifically the VieLight NeuroPro Alpha2 and Bioptron MedAll devices. Samples irradiated with HPL were placed at a distance of 12.5 cm, while those irradiated with NIR were positioned at a distance of 7.5 cm to maintain consistent power density across experiments. As detailed in chapter 3.2.1, the samples were irradiated for durations of 10 minutes and 20 minutes.

To irradiate the samples, the brain slices were removed from the becher and placed in dishes within a water bath maintained at the desired temperature. Specifically, the first group was kept at 37°C, while the second group was maintained at 25°C. The temperature was monitored using a thermal camera, as shown in the figure. It is crucial to ensure that the samples are not subjected to additional temperature gradients but rather remain at a constant temperature throughout the irradiation process.


Figure 9 Bioptron MedAll and VieLight NeuroPro Alpha2 devices

Finally, the hippocampus (the region used for analysis) was carefully dissected from the cortex and transferred to a 1.5 mL Eppendorf tube. The samples were then stored at -80°C until further analysis.

It is crucial to note that for the Bioptron irradiation, all four experimental conditions (Warm and Cold, 10 and 20 minutes) were conducted on both rats. However, for the Vielight exposure, only Rat 2 underwent this irradiation, and only two experimental conditions were analyzed (Warm and Cold for 20 minutes). This limitation was due to an insufficient number of brain slices obtained from Rat 1, which precluded Vielight irradiation for this subject. Furthermore, it is important to highlight that in Rat 2, the slices used for NIR irradiation were recovery slices, which may potentially yield less reliable results.

### 3.2.4 Western Blot

The brain slices were homogenized by ice-assisted sonication in RIPA lysis buffer [50 mM Tris buffer, 150 mM NaCl, 10% (v/v) NP-40, containing a cocktail of protease and phosphatase inhibitors (Sigma Aldrich), 1 mM dithiothreitol (DTT) and 1 mM PMSF]. The extract was then centrifuged and stored at -80°C.

Protein concentration was determined using the Bio-Rad DC protein assay kit (Bio-Rad Laboratories). The volume needed to obtain 20 µg of protein per lane was calculated using the following formula:

$$\textbf{Volume of sample } (\mu l) = \frac{\textbf{Protein amount } (\mu g)}{\textbf{protein concentration } (\frac{\mu g}{\mu l})}$$

Samples were diluted with H2O to a final volume of 15 µl, and 5 µl of loading buffer was added to each sample. The samples were then denatured by heating at 65°C for 10 minutes (450 rpm), briefly centrifuged, and kept on ice until loading.

Then, protein samples (XX µg) were loaded and separated electrophoretically using a 1.0 mm thick 4%–12% Bis-Tris gel with NuPAGE MOPS SDS Running Buffer (both by Invitrogen™ NuPAGE). Then the gel ran at 100-200 V until the dye front reaches the bottom of the gel (about 60-90 minutes).

The proteins were then electrotransferred onto nitrocellulose membranes (Hybond C Extra, Amersham Pharmacia) via wet transfer at 300 mA for a maximum of 3 hours at 4°C.
After the transfer, membranes were briefly rinsed to remove any excess buffer, incubated in Ponceau S solution for 1 minute to visualize the transferred proteins, then rinsed using distilled water until the background was clear, leaving only the protein bands visible. Membranes were then washed with PBS tween 0,1% (PBST).

Membranes were blocked using 5% (w/v) non-fat milk in PBST for at least 40 minutes at room temperature. Primary antibodies (shown in Table 4) were diluted in PBST and incubated with the membranes overnight at 4°C.
For secondary antibody incubation (table 5), membranes were washed 3 times for 10 minutes each in PBST, then incubated with HRP-conjugated secondary antibodies for 45 minutes at room temperature. Membranes were again washed 3 times for 10 minutes each in PBST.
In particular, the Anti-Rabbit HRP was used for P205, pGSK3β and Vinculin; while the Anti-Mouse HRP was employed for Tau-1.
For the detection, a substrate of ECL reagent was prepared and applied to the membranes. The signal was captured using an imaging system ChemiDoc™XRS+ (Image Lab™Software, Bio-Rad). A semi-quantitative measurement of the band intensity was performed using the same computer software. Results were expressed as a ratio of band intensity with respect to the loading control (vinculin), normalizing the different gels according to a randomly chosen sample used as an internal control.

| Antibody | Type | Species | Specificity | MW (kDa) | Source and dilution |
|---|---|---|---|---|---|
| Anti-Tau-1 | Mono | Mouse | Non-phosphorylated 189–207 residues | 52-68 | WB 1:1000 |
| Anti-p-Tau (P205) | Mono | Rabbit | p-Tau (T205) | 68-70 | WB 1:500 |
| Anti-p-GSK3β | Mono | Rabbit | p-GSK3β (S9) | 46 | WB 1:1000 |
| Vinculin | Mono | Rabbit | Vinculin | 116 | WB 1:8000 |

Table 4 Primary antibodies employed in this study

| Antibody | Type | Specificity | Source and dilution |
|---|---|---|---|
| Anti-Mouse HRP | Poly | Anti-Mouse IgG | WB 1: 10000 |
| Anti-Rabbit HRP | Poly | Anti-Rabbit IgG | WB 1: 10000 |

Table 5 Secondary antibodies employed in this study

# 4 RESULTS

## 4.1 Cancer disease

### 4.1.1 Bioptron Pro1 device

#### 4.1.1.1 Cellular Viability Assessment

The experimental results shown in Figure 10. demonstrate a significant decrease in cell viability across all experimental groups after just 10 minutes of exposure to the HPL. This initial drop suggests that the irradiation parameters used had an immediate harmful impact on the cell population. In particular, the fourth experimental group, which underwent 20 minutes of exposure with a 10-minute break in between, exhibited a marked increase in cell death, a phenomenon not seen in samples exposed continuously for 15 minutes. Interestingly, continuous exposure for 20 minutes did not yield a significant effect, as the number of viable cells remained nearly the same in both control and treated samples. This pattern in cell viability points to the possible activation of adaptive mechanisms or inherent cellular traits that influence the response to irradiation.

Additionally, as showed in the figure 12. experiments where only the culture medium was irradiated supported this trend, suggesting that the medium itself may play a key role in mediating the effects of electromagnetic waves on cellular populations.

The study also explored the effects of re-irradiating cells six days after the initial 10-minute exposure (figure 14.a; 14.b). A significant reduction in cell viability was observed, hinting at the potential for this approach as a treatment strategy. However, the experiment remains too limited to draw definitive conclusions or establish a general protocol. Nonetheless, it opens the door for further investigation to either confirm or challenge this observed trend.

When applying the same experimental conditions to the HeLa cell line (figure 15), the initial decrease in viability after 10 minutes of exposure mirrored the results observed in the PC3 cell line. However, while no significant reduction was detected after 15 minutes of exposure, an unexpected increase in viability was observed after 20 minutes, deviating from the anticipated trend. Similarly, no significant changes were noted in the fourth group (20 minutes of exposure with a 10-minute intermission).

In contrast, for the MCF7 cell line (figure 17), the only consistent finding was a significant decrease in viability following 10 minutes of exposure. Interestingly, while a non-significant reduction was observed after 15 minutes, both the third and fourth experimental groups showed a significant increase in cellular viability.

These results highlight the cell line-specific nature of responses to irradiation and suggest that different cell types may exhibit distinct adaptive or compensatory mechanisms.

### 4.1.1.2 Immunofluorescence – alteration in cellular structure

For what concern PC3 cell line, as shown in Figure 19.a, 19.b a noticeable contraction of the cytoplasm toward the nucleus was observed, a phenomenon commonly associated with the response of neoplastic cells to irradiation (10 minutes). This morphological change resulted in a more spherical cell shape and reduced spreading on the substrate, consistent with findings previously reported in the scientific literature. The same trend was confirmed following 20 minutes of exposure (figure 21.a, 21.b)

Regarding tubulin, no significant changes were observed between control and treated samples after 10 minutes of exposure (figure 19.c, 19.d). However, with 20 minutes of uninterrupted exposure, microtubule disassembly appeared to be promoted, as evidenced by cells adopting a rounder shape and exhibiting less spreading (figure 21.c, 21.d).

In contrast, mitochondria, as shown in figure 23.a, 23.b, displayed a marked reduction in fluorescence signal intensity in treated cells. This suggests potential toxicity affecting mitochondrial integrity. These findings point to mitochondrial damage induced by the specific irradiation parameters used (10 min, 40 mW/cm², 2.4 J/cm²), which may have harmful effects on cellular metabolism and energy production.

For the HeLa cells, figure 24.a, 24.b show the actin staining on cells irradiated with Bioptron for 10 minutes. The treated sample (figure 24.a), actin filaments appear more disorganized and fragmented, with fewer well-defined structures. The cytoskeletal network seems less structured compared to the control.
Considering the figure 25.a, 25.b, the microtubules appear more structured and organized, with a clear network radiating from the perinuclear region and the treated cells (figure 25.a) exhibit a more defined cellular shape.

### 4.1.1.3 Glycolysis-Oxphosphorylation – ATP production analysis

To gain a deeper understanding of the effects of irradiation on mitochondrial integrity, as suggested by the immunofluorescence analysis, a detailed evaluation of mitochondrial activity and cellular metabolic dynamics was carried out. The experiments were performed in triplicate and repeated three times to ensure reproducibility and statistical reliability. Cellular ATP production from both glycolytic and mitochondrial pathways was quantified using a biochemical assay provided by Dojindo (Dojindo Molecular Technologies, Minato City, Tokyo, Japan), as described in the Materials and Methods section. This approach offered valuable insights into the metabolic reprogramming triggered by the irradiation conditions.

The experimental results revealed distinct patterns in mitochondrial functionality and cellular energy metabolism across the three experimental sets. In the first set (Figure 26.b), a metabolic shift toward increased glycolytic activity was observed, accompanied by relatively low mitochondrial ATP production. In contrast, the second set (Figure 26.c) showed reduced

glycolytic activity compared to the control but significantly higher mitochondrial ATP production. Interestingly, the third set of experiments (Figure 26.d) displayed a slight increase in glycolytic ATP production compared to the control, along with a striking tenfold increase in mitochondrial ATP production relative to non-irradiated cells.

The findings from the first set of experiments were further supported by data shown in Figure 27.b, where a significant increase in lactate production was observed, confirming a marked drop-in glycolytic activity. These results collectively highlight the complex metabolic reprogramming induced by irradiation and its variable effects on cellular energy pathways.

### 4.1.2 VieLight NeuroPro device

#### 4.1.2.1 Cellular Viability Assessment

The trends in cellular viability observed in PC3 cells in figure 11, varied significantly depending on the duration of exposure with the VieLight device. Interestingly, the 15-minute irradiation protocol resulted in a statistically significant increase in viability compared to non-irradiated controls.
In contrast, a 10-minute exposure led to a non-significant decrease in viability, suggesting a relatively neutral effect on cellular processes at this duration. However, extending the exposure to 20 minutes caused a slight but statistically significant reduction in viable cells, indicating that prolonged light exposure may have detrimental effects on cell health or survival.

Following the experimental protocol established for the Biopropton device, cell culture media were irradiated across the four designated time groups (figure 13). Notably, a statistically significant increase in cellular viability was observed in samples exposed to 10 minutes of irradiation compared to non-irradiated controls. A similar trend of increased viability, though not statistically significant, was observed in the group subjected to 20 minutes of exposure with a 10-minute intermittent break. Conversely, the groups exposed to 15 minutes of continuous irradiation and 20 minutes of continuous irradiation exhibited a non-significant decrease in cell viability relative to controls.

These varying responses highlight the complex interplay between irradiation parameters such as dose, duration, and fractionation, and their impact on cellular outcomes.

Additionally, the effects of repeated irradiation on cell viability were explored (figure 14.c; 14.d). Notably, cells that were irradiated on day 1 and then re-irradiated on day 7 showed a decrease in viability compared to those exposed to a single 10-minute irradiation. This observation suggests that the growth state of the cells, potentially influenced by the number of subpassages during cell culture, may play a key role in their response to repeated irradiation. Specifically, cells re-irradiated six days after the initial exposure exhibited a significant reduction in viability, which was unexpected given that single-exposure samples did not show such pronounced effects.

This finding has led us to hypothesize that cellular growth dynamics and subpassage frequency may contribute to differences in response to repeated irradiation. Further research is required to uncover the mechanisms underlying this phenomenon and to better understand how repeated irradiation impacts cellular health and survival.

HeLa cells were exposed to irradiation for 15 minutes, 33 minutes, 60 minutes, and 30 minutes with a 15-minute intermittent break, all under a constant energy fluence of 2.4 J/cm² (figure 16). The first three exposure durations (15, 33, and 60 minutes) showed a non-statistically significant increase in cellular viability compared to control samples. This suggests that low to moderate doses of light exposure may have the potential to stimulate cellular proliferation or metabolic activity in HeLa cells, although the observed effects were not statistically conclusive.

However, the final exposure condition (30 minutes with a 15-minute break) did not result in any significant difference in viability between treated and untreated cells, possibly indicating a threshold beyond which the beneficial effects of light irradiation are diminished or negated by adverse processes.

For the MCF7 cell line, the viability trends across different exposure durations closely mirrored those observed in HeLa cells (figure 18). Interestingly, three out of the four exposure groups showed a significant decrease in viability following irradiation, except for the 15-minute exposure group, which exhibited a significant increase in viability. These findings suggest that optimizing the duration of exposure may be critical to achieving desired outcomes and avoiding detrimental effects.

#### 4.1.2.2 Immunofluorescence – alteration in cellular structure

Actin staining revealed noticeable structural changes in the cytoplasm of PC3 irradiated cells compared to non-irradiated controls after 15 minutes of exposure. Specifically, the cytoplasm appeared more condensed around the nucleus (figure 19.c; 19.d). In contrast, 20 minutes of exposure showed the opposite trend, seemingly promoting greater cell spreading (figure 21.c; 21.d).

For tubulin staining, no visible differences were observed in the treated cell population for both 15- and 20-minute exposures (figures 20.c; 20.d; 22.c; 22.d). However, in the 15-minute samples, the control group exhibited a slightly dimmer signal compared to cells exposed to NIR radiation.

Regarding mitochondria, as shown in Figure 23.c, 23.d, the fluorescence signal appeared relatively dim in both control and treated samples. However, a stronger signal was observed in the 15-minute irradiated cells, supporting the ATP analysis results that suggest increased mitochondrial activity under these conditions.

Regarding the HeLa cells, the figure 24.c, 24.d show the actin staining of cells irradiated with VieLight device for 15 minutes. The actin cytoskeleton of the treated sample (figure 24.c) appears more structured, with prominent stress fibres spanning the cytoplasm.

For the tubulin, the signal appears to be quite dimmer, but the red fluorescence is stronger and more uniform, suggesting enhanced tubulin polymerization or stabilization of microtubules (figure 25.c; 25.d).

#### 4.1.2.3 Glycolysis-Oxphosphorylation – ATP production analysis

Although not statistically significant, irradiated cells showed an increase in total ATP levels compared to controls (Figure 26.a). This trend was also observed for mitochondrial ATP, while glycolytic ATP levels were lower in irradiated samples relative to non-irradiated controls. This

reduction in glycolytic activity was further supported by the results of a lactate assay (Figure 27.a).

These findings suggest that light irradiation may induce a metabolic shift, promoting mitochondrial respiration over glycolytic pathways for energy production.

## 4.2 Alzheimer's disease

### 4.2.1 Bioptron MedAll device

#### 4.2.1.1 Tau 1

All the figures show four experimental conditions varying by sample temperature (warm or cold) and exposure duration (10 or 20 minutes) to the Bioptron MedAll device.

Figure 28 show the levels of Tau-1 protein measured in Rat 1, both cold samples (10- and 20-minutes exposure) show a decrease in Tau-1 levels, indicating a reduction in non-phosphorylated Tau. Similarly, in the warm sample exposed for 10 minutes, Tau-1 levels in the treated group are lower compared to the control group. However, the warm sample exposed for 20 minutes demonstrates an opposite trend: treated samples exhibit higher Tau-1 levels than those observed in the controls.

The graphs in figure 29 instead show the results of Tau 1 measured in Rat 2: for this experiment, two measurements were performed, yielding consistent results, except for the warm sample irradiated for 10 minutes. Cold samples exposed for 10- and 20- minutes, depicts an increase in Tau 1 levels. This trend contrasts with the warm samples exposed for 20 minutes that shows a decrease in Tau 1 levels.

The figure 30 compare the levels of Tau-1 protein between Rat 1 and Rat 2: for warm samples exposed for 10 minutes, Tau-1 levels in treated samples show a clear reduction in Rat 1 compared to controls, while Rat 2 exhibits minimal differences between treated and control groups. When the exposure duration is extended to 20 minutes for warm samples, both rats display increased Tau-1 levels in treated samples relative to controls, with Rat 2 showing a more pronounced increase than Rat 1.
In the case of cold samples exposed for 10 minutes, contrasting trends emerge: Rat 1 shows a marked reduction in Tau-1 levels in treated samples compared to controls, whereas Rat 2 displays an increase in Tau-1 levels under the same conditions. However, for cold samples exposed for 20 minutes, both rats exhibit elevated Tau-1 levels in treated samples relative to controls, with Rat 2 again demonstrating slightly higher levels than Rat 1.

Overall, these results reveal distinct patterns of Tau-1 modulation between the two rats across varying temperature and exposure conditions. While some trends are consistent (e.g., increased Tau-1 levels with longer exposure durations), others highlight individual variability, particularly under shorter exposure times or different temperature settings.

#### 4.2.1.2 PGSK3β

The following graphs display the levels of phosphorylated glycogen synthase kinase 3β (PGSK3β) measured in both rats under the same experimental conditions aforementioned.

The measurements concerning the rat 1 are showed in figure 31: two measurements were performed, yielding consistent results. However, the second measurement showed small differences between the treated and control samples, which were not statistically significant.
For warm samples exposed for 10 minutes, the treated group shows significantly lower PGSK3β levels compared to controls, indicating a marked reduction. Conversely, for warm samples exposed for 20 minutes, the trend reverses. This suggests that prolonged exposure under warm conditions may lead to an increase in PGSK3β levels.
In cold samples exposed for 10 minutes, treated samples display an increase in PGSK3β levels, contrasting with the reduction observed under warm conditions with the same exposure duration. For cold samples exposed for 20 minutes, treated samples again show elevated PGSK3β levels relative to controls, consistent with the trend seen in warm samples with extended exposure.

The figure 32 present the levels of PGSK3β in rat 2: with two measurements taken for all samples and an additional measurement for samples exposed for 20 minutes under both warm and cold conditions.
For warm samples exposed for 10 minutes, treated samples show a substantial increase in PGSK3β levels compared to controls, indicating heightened phosphorylation under these conditions. Conversely, the same time exposure in cold sample depicts a decrease in the kinases phosphorylation levels.
When the exposure duration is extended to 20 minutes, treated samples exhibit a further increase in PGSK3β levels, with the additional measurement confirming this trend. This suggests that prolonged exposure amplifies phosphorylation effects under warm conditions.
For the 20 minutes exposure in cold samples, the decreasing trend is confirmed by two measurements; yet the third measurement did not align with this trend.

Figure 33 compare the levels of PGSK3β between Rat 1 and Rat 2: for warm samples, short exposure (10 minutes) leads to decreased PGSK3β levels in Rat 1 but increased levels in Rat 2. With longer exposure (20 minutes), both rats show elevated PGSK3β levels, with Rat 2 exhibiting a more pronounced increase.
In cold samples, short exposure results in reduced PGSK3β levels for Rat 1 but higher levels for Rat 2. With longer exposure, both rats display increased PGSK3β levels, with Rat 2 showing slightly higher levels.

These comparisons highlight significant differences in the rats' responses to temperature and exposure duration variations. Rat 1 generally shows reductions in PGSK3β levels under shorter exposures, while Rat 2 tends to exhibit increases across most conditions, especially with prolonged exposure.

#### 4.2.1.3 P205

The graphs (figure 34) depict the levels of P205 measured in Rat 1: two measurements were taken for all samples to ensure reliability.
For warm samples exposed for 10- and 20- minutes, treated samples show higher P205 levels compared to controls, indicating an increase in phosphorylation under these conditions. Conversely, for cold samples exposed for 20 minutes the trend is inversed. The cold sample exposed for 10 minutes, show incoherent results between the two measurements.

Regarding the second rat (figure 35), two measurements were done only for the 20 minutes experiments, and they show a non-coherent result.
In the cold and warm samples exposed for 10 minutes, treated samples exhibit significantly higher P205 levels compared to controls. The 20 minutes exposure warm sample had the same trend, further confirmed by the first measure.

The comparison between the two rat is shown in figure 36: rat 2 consistently shows higher P205 levels in treated samples across all conditions compared to Rat 1. For warm samples exposed for 20 minutes, a notable distinction emerges: while treated samples display elevated P205 levels in both rats, no phosphorylation of Tau at the T205 residue is detected in the control group for Rat 2.
For cold samples, both rats exhibit increased P205 levels in treated samples relative to controls, with Rat 2 showing more pronounced elevations. These results emphasize individual variability, with Rat 2 generally demonstrating stronger phosphorylation responses across all experimental conditions.

### 4.2.2 VieLight NeuroPro Alpha2 device

#### 4.2.2.1 Tau 1

All the figures show two experimental conditions varying by sample temperature (warm or cold), with an exposure of 20 minutes to the VieLight NeuroPro Alpha2 device, only in rat 2.

The first graph (figure 37) shows two measurements of the levels of Tau1 for the warm sample and three measurements for the cold one. In particular, the measurements of warm sample were consistent, illustrating a decrease in levels of Tau 1 in the treated samples. In contrast, the measurement for the cold sample shows a non-coherent trend: the control seems to be higher than the treated samples in two out of three measures, suggesting an opposite effect of irradiation under cold conditions.

#### 4.2.2.2 PGSK3β

The levels of PGSK3β were analysed through two measurements, which yielded consistent trends (figure 38).
The warm slices represent higher levels of PGSK3β in controls compared to the treated samples, indicating a decrease in phosphorylation of the kinase, after the irradiation. Similarly, the cold slices show the same trend.

#### 4.2.2.3 P205

The data regarding the measurement of P205 levels, were quite difficult to analyse, indeed, for the warm sample, no data could be detected from either treated or control groups. This highlights a limitation in the current irradiation protocol and suggests that improvements are needed in future experiments, such as using fresh tissue slices instead of recovered ones. In contrast, for the cold sample, treated groups exhibit significantly higher P205 levels compared to controls, indicating increased phosphorylation under cold conditions (figure 39).

# 5 DATA FIGURES

## 5.1 Cancer

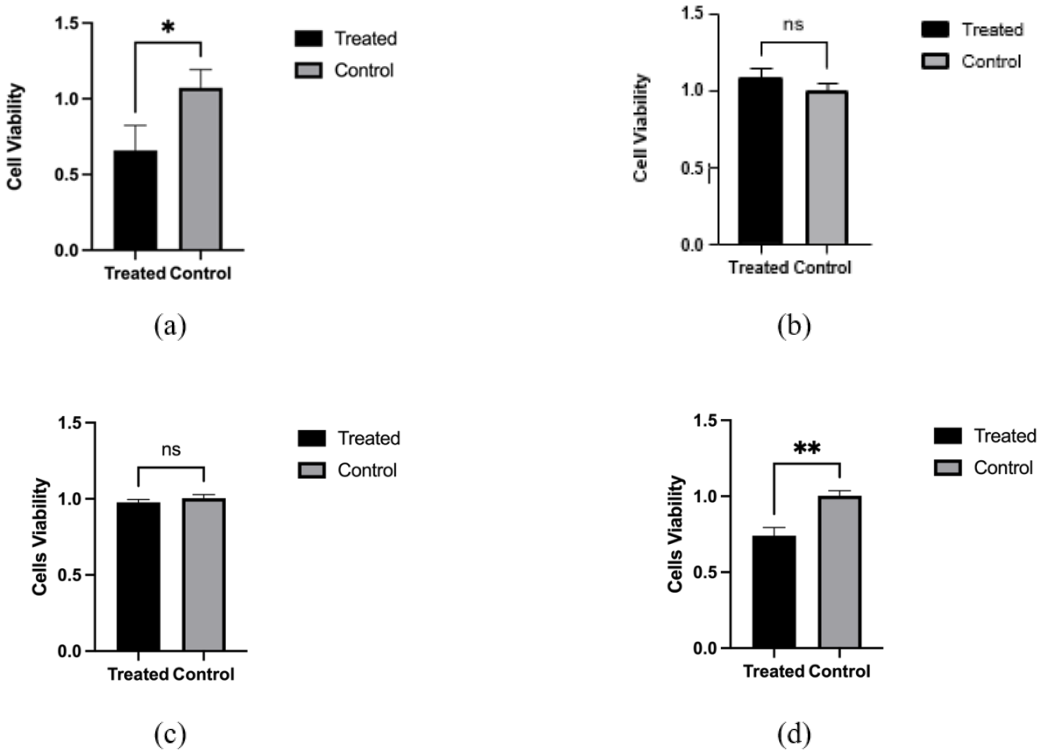


Figure 10 Bioptron PC3 exposure: (a) 10 minutes exposure; (b) 15 minutes exposure; (c) 20 minutes exposure; (d) 20 minutes exposure with 10 minutes of intermission

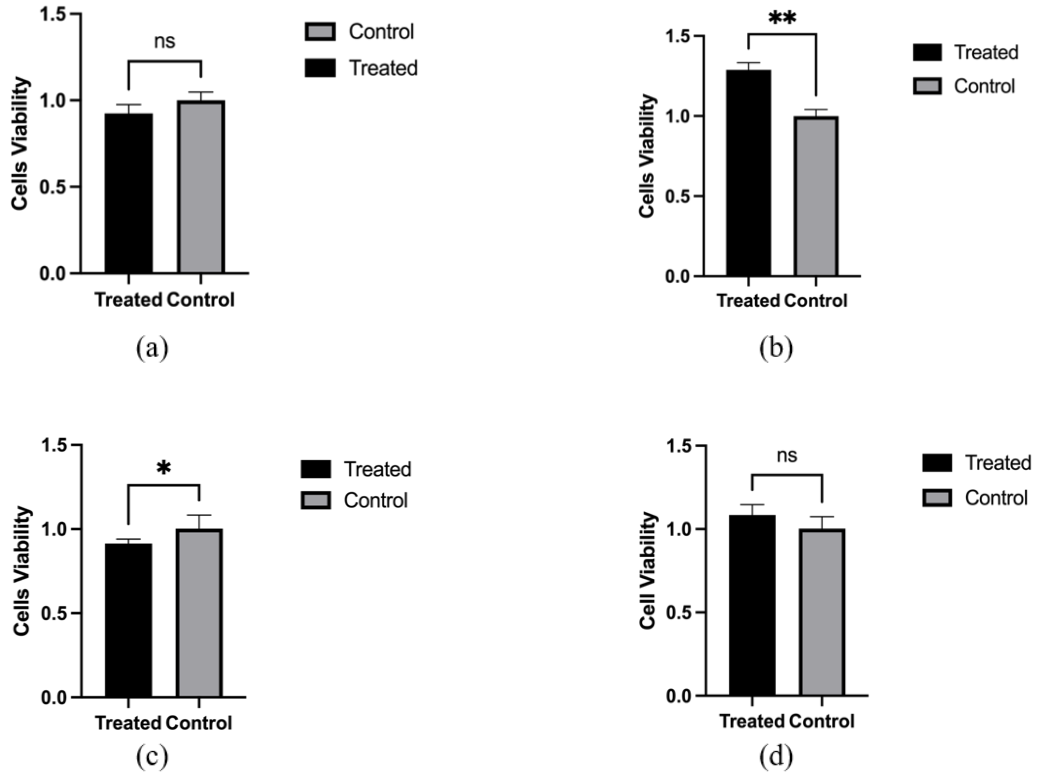


Figure 11 Vielight PC3 exposure: (a) 10 minutes exposure; (b) 15 minutes exposure; (c) 20 minutes exposure; (d) 20 minutes exposure with 10 minutes of intermission

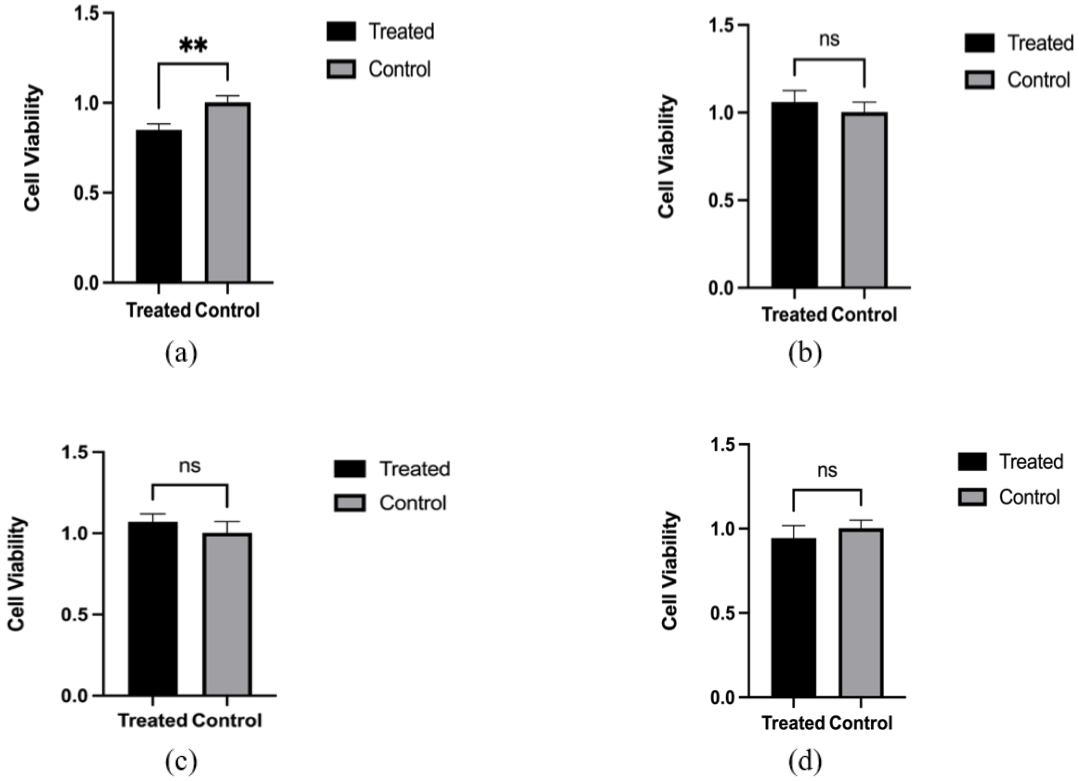


Figure 12 Bioptron PC3 medium exposure: (a) 10 minutes exposure; (b) 15 minutes exposure; (c) 20 minutes exposure; (d) 20 minutes exposure with 10 minutes of intermission

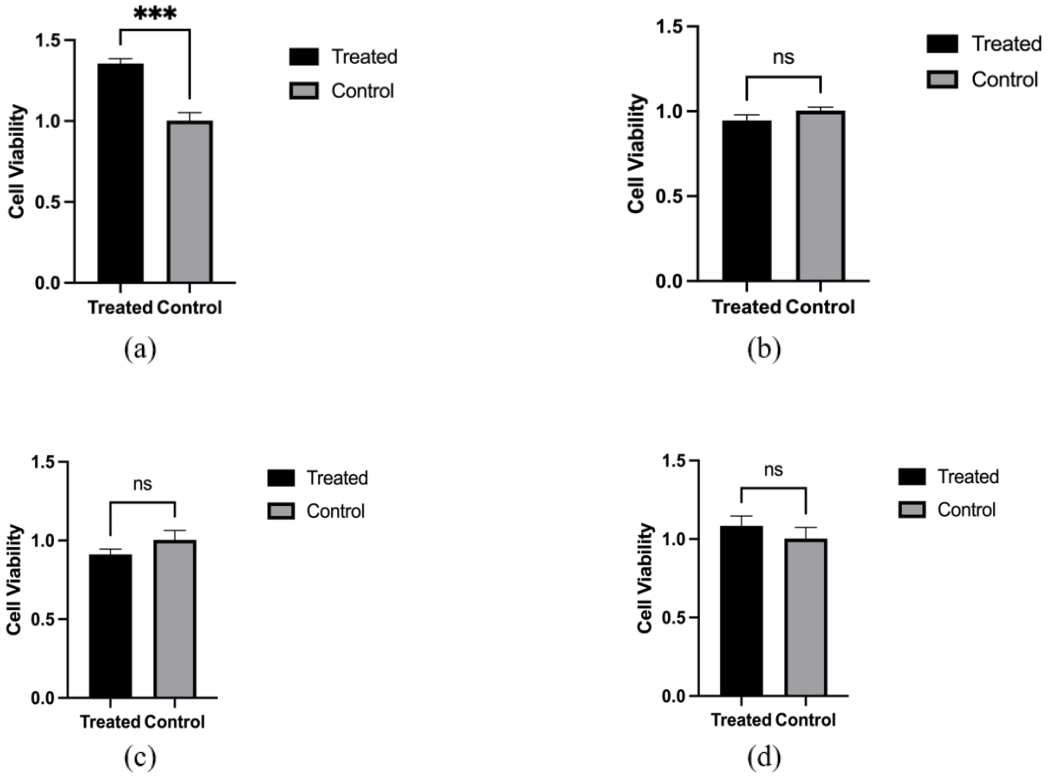


Figure 13 Vielight PC3 medium exposure: (a) 10 minutes exposure; (b) 15 minutes exposure; (c) 20 minutes exposure; (d) 20 minutes exposure with 10 minutes of intermission

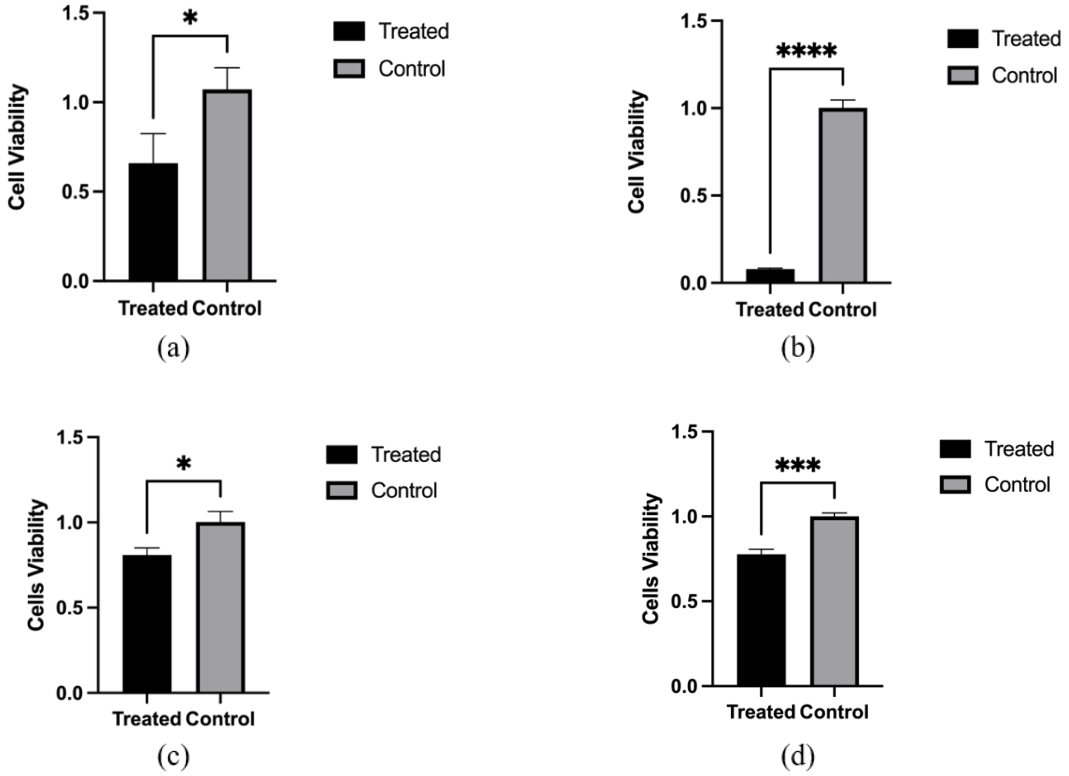


Figure 14 PC3 day 1 and day 7 exposure: (a) Bioptron - 10 minutes exposure, day 1; (b) Bioptron - 10 minutes exposure, day 7; (c) Vielight - 10 minutes exposure, day 1, 125 mm from the spot; (d) Vielight - 10 minutes exposure, day 7, 125 mm from the spot.

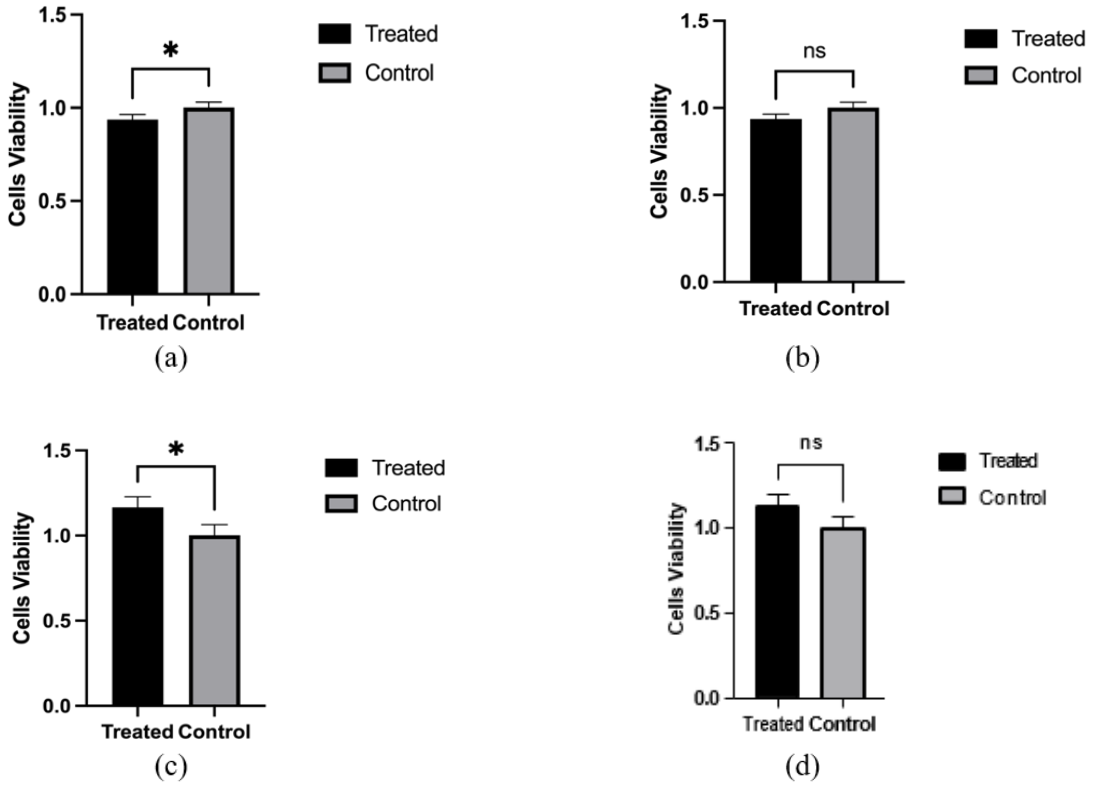


Figure 15 Bioptron HeLa exposure: (a) 10 minutes exposure; (b) 15 minutes exposure; (c) 20 minutes exposure; (d) 20 minutes exposure with 10 minutes of intermission

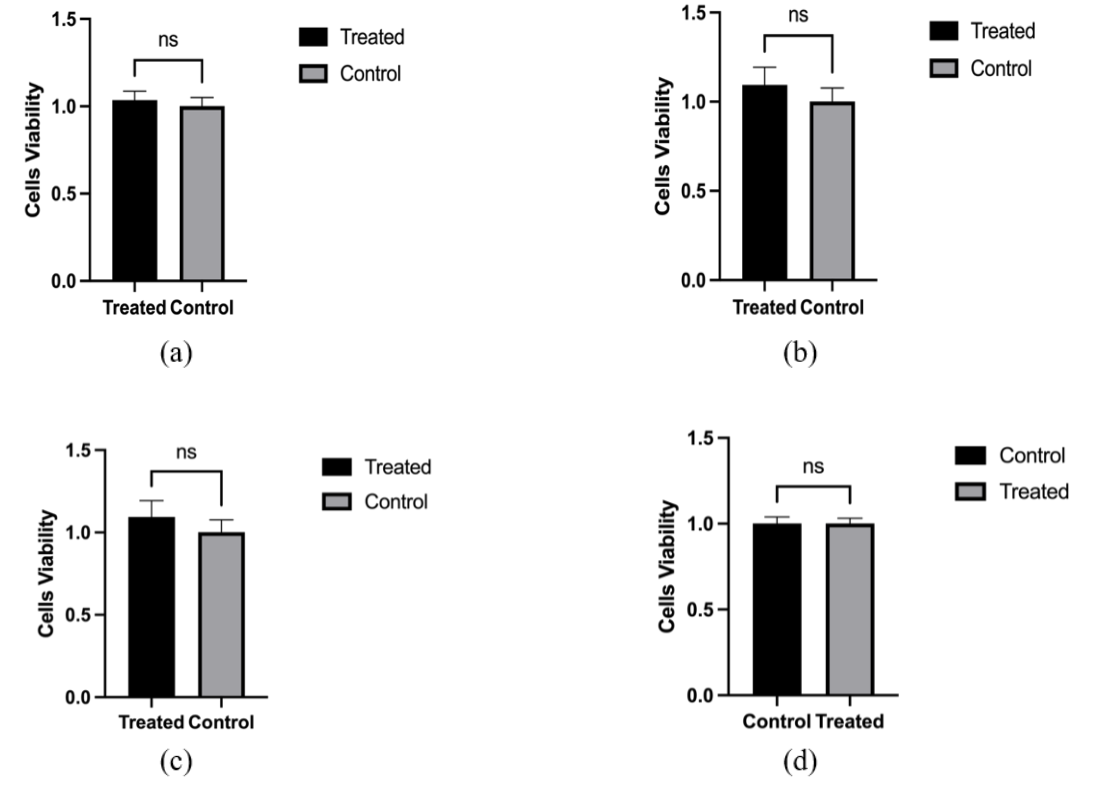


Figure 16 Vielight HeLa exposure: (a) 15 minutes exposure; (b) 33 minutes exposure; (c) 60 minutes exposure; (d) 30 minutes exposure with 15 minutes of intermission

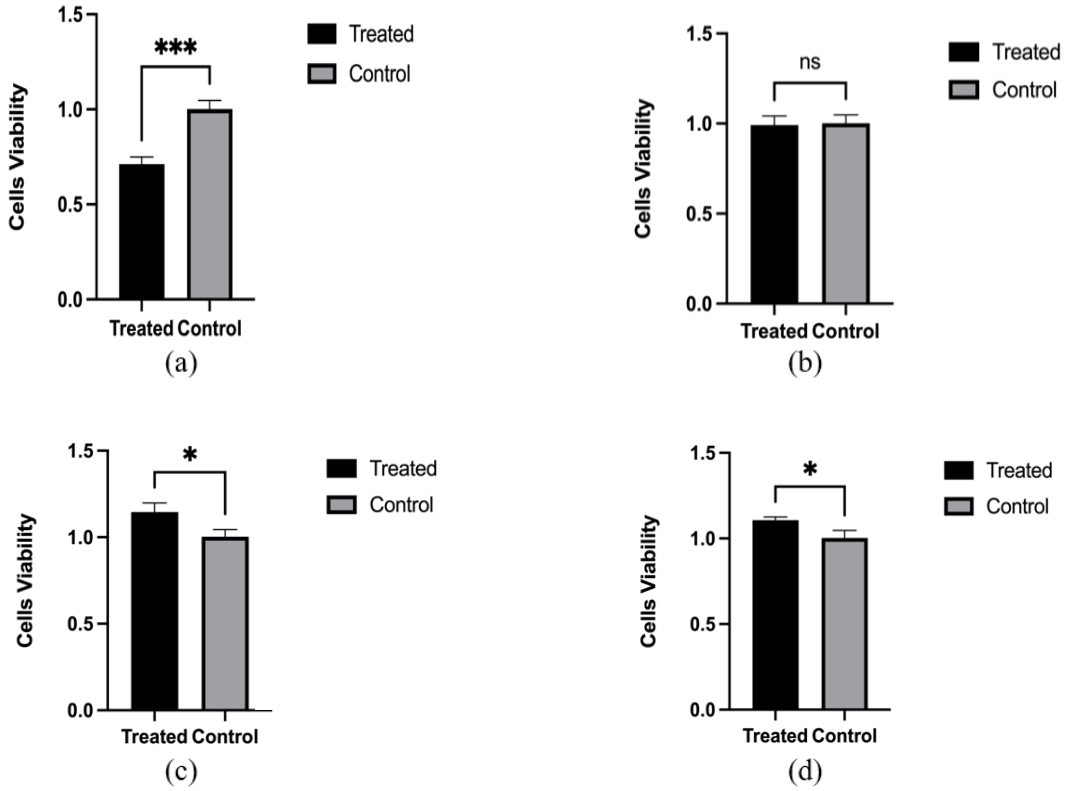


Figure 17 Bioptron MCF7 exposure: (a) 10 minutes exposure; (b) 15 minutes exposure; (c) 20 minutes exposure; (d) 20 minutes exposure with 10 minutes of intermission

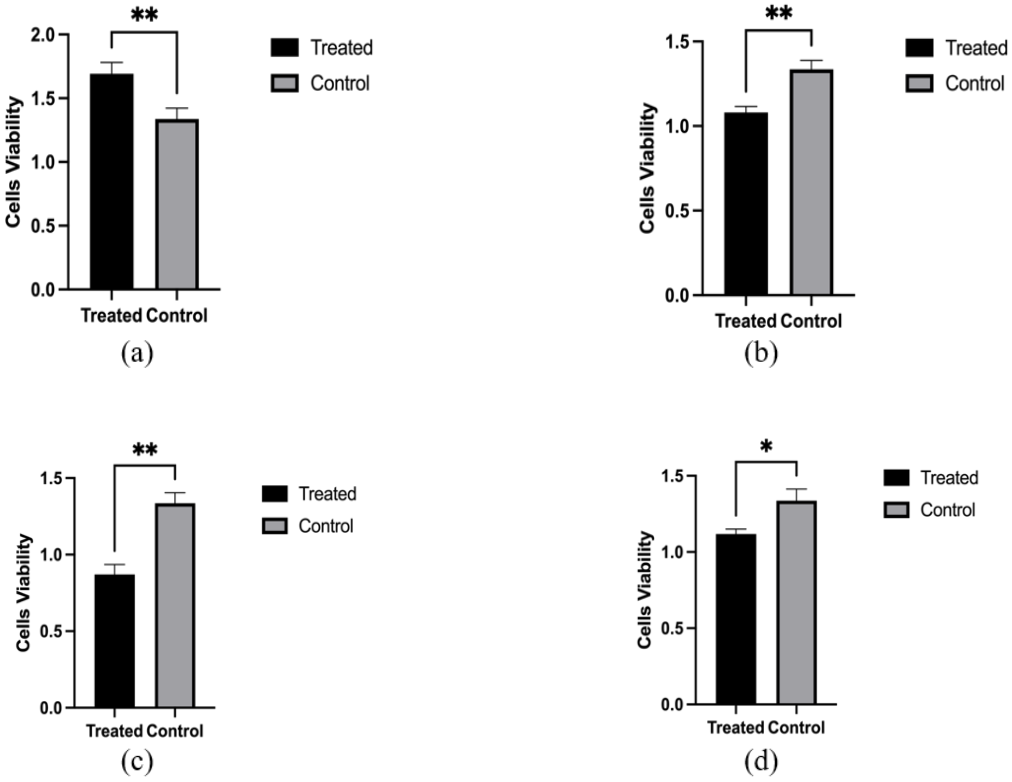


Figure 18 Vielight MCF7 exposure: (a) 15 minutes exposure; (b) 33 minutes exposure; (c) 60 minutes exposure; (d) 30 minutes exposure with 15 minutes of intermission

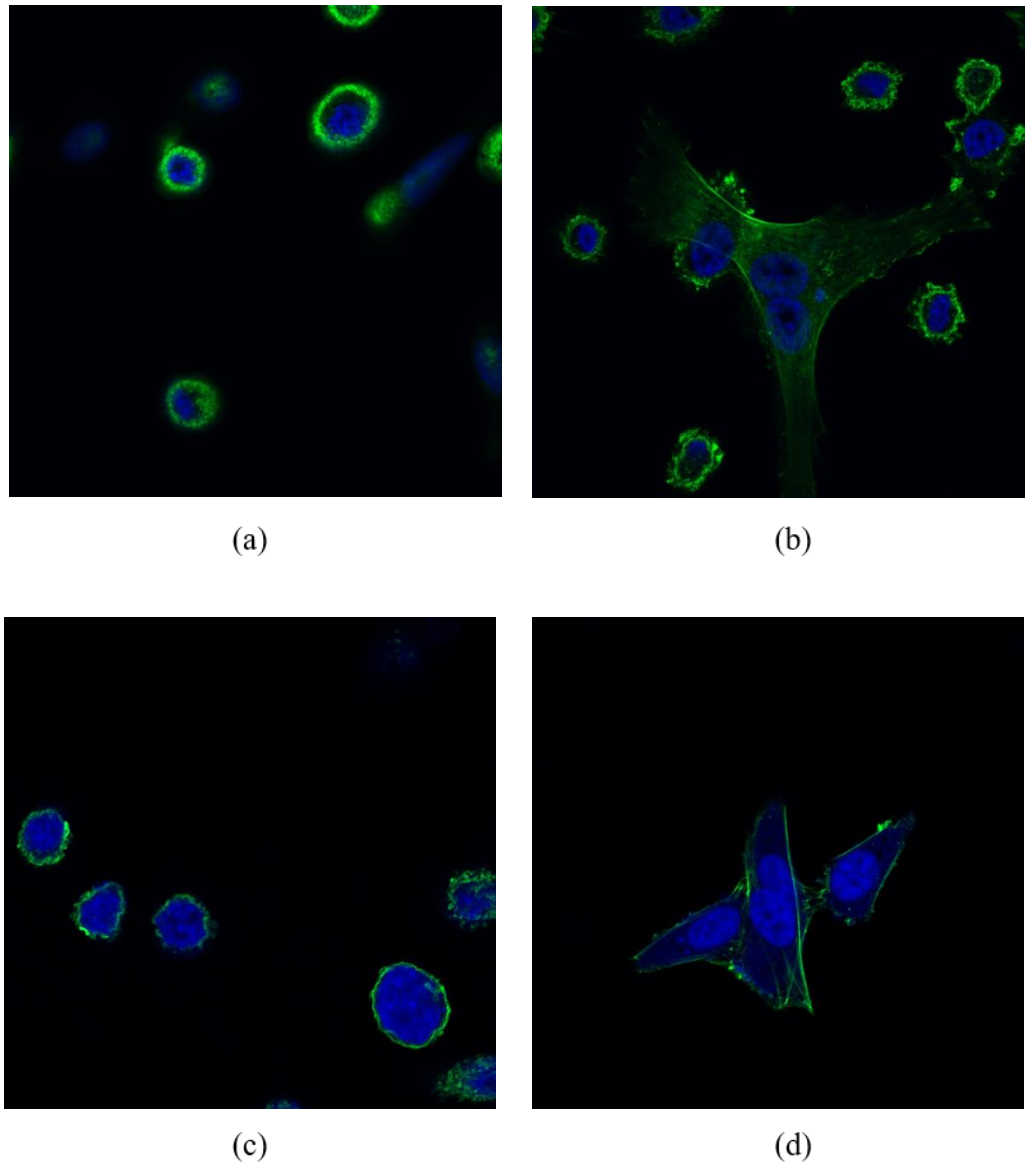


Figure 19 PC3 Actin staining. (a) Bioptron, 10-minutes exposed, treated; (b) Bioptron, 10-minutes exposed, control; (c) Vielight, 15-minutes exposed at a distance of 125 mm, treated; (d) Vielight, 15-minutes exposed at a distance of 125 mm, control.

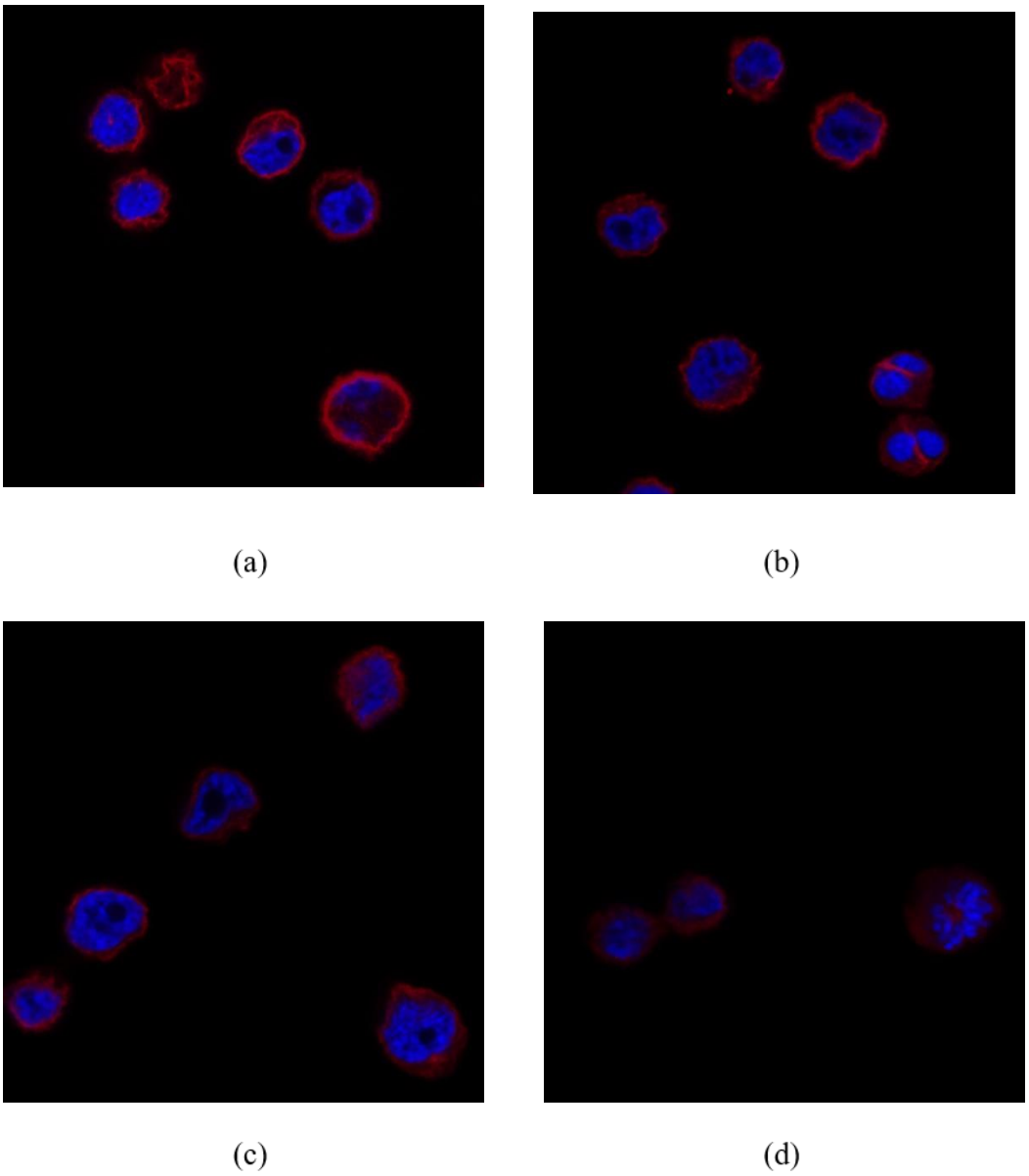


Figure 20 PC3 Tubulin staining. (a) Bioptron, 10-minutes exposed, treated; (b) Bioptron, 10-minutes exposed, control; (c) Vielight, 15-minutes exposed at a distance of 125 mm, treated; (d) Vielight, 15-minutes exposed at a distance of 125 mm, control.

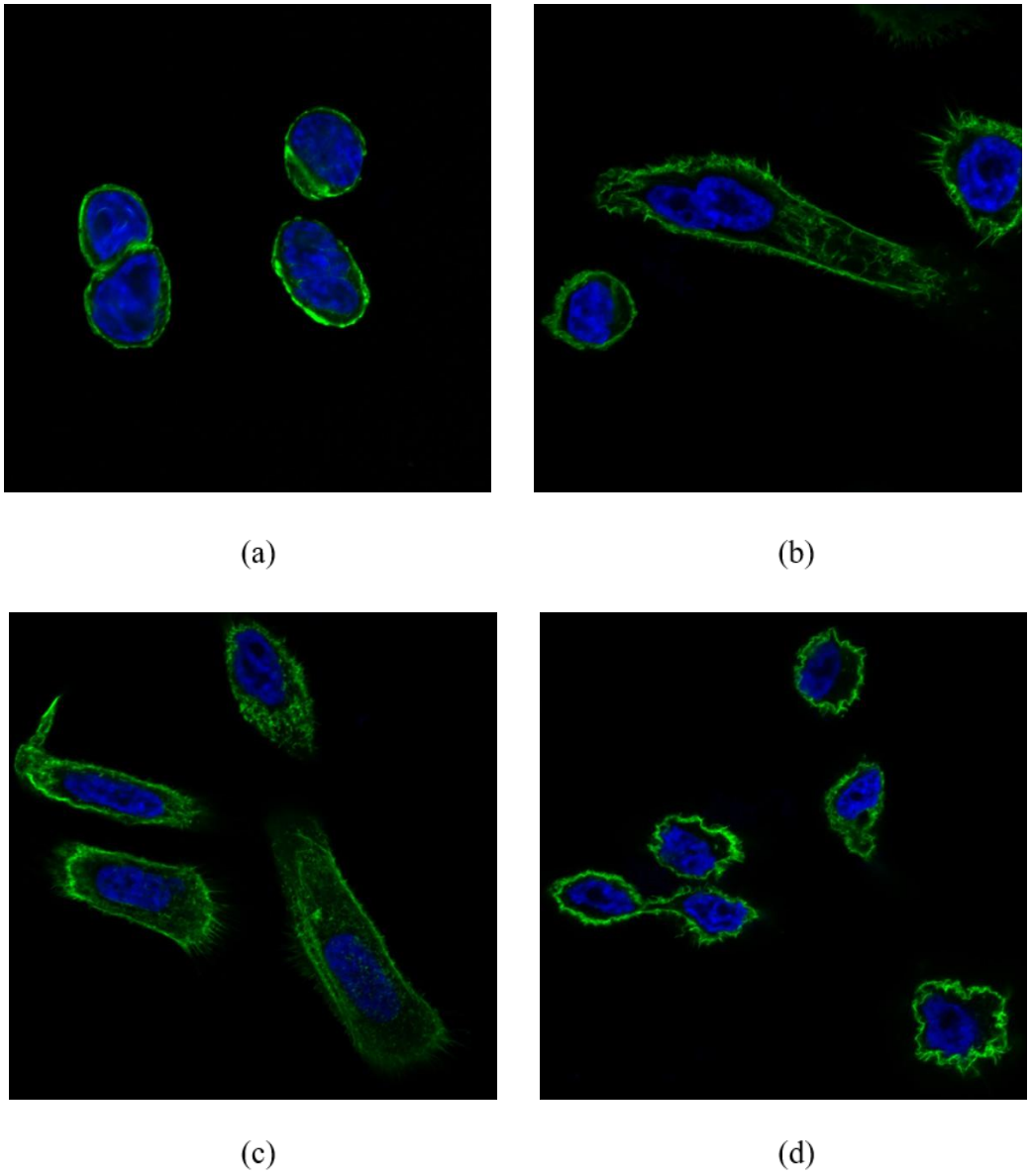


Figure 21 PC3 Actin staining. (a) Bioptron, 20-minutes exposed, treated; (b) Bioptron, 20-minutes exposed, control; (c) Vielight, 20-minutes exposed at a distance of 125 mm, treated; (d) Vielight, 20-minutes exposed at a distance of 125 mm, control.

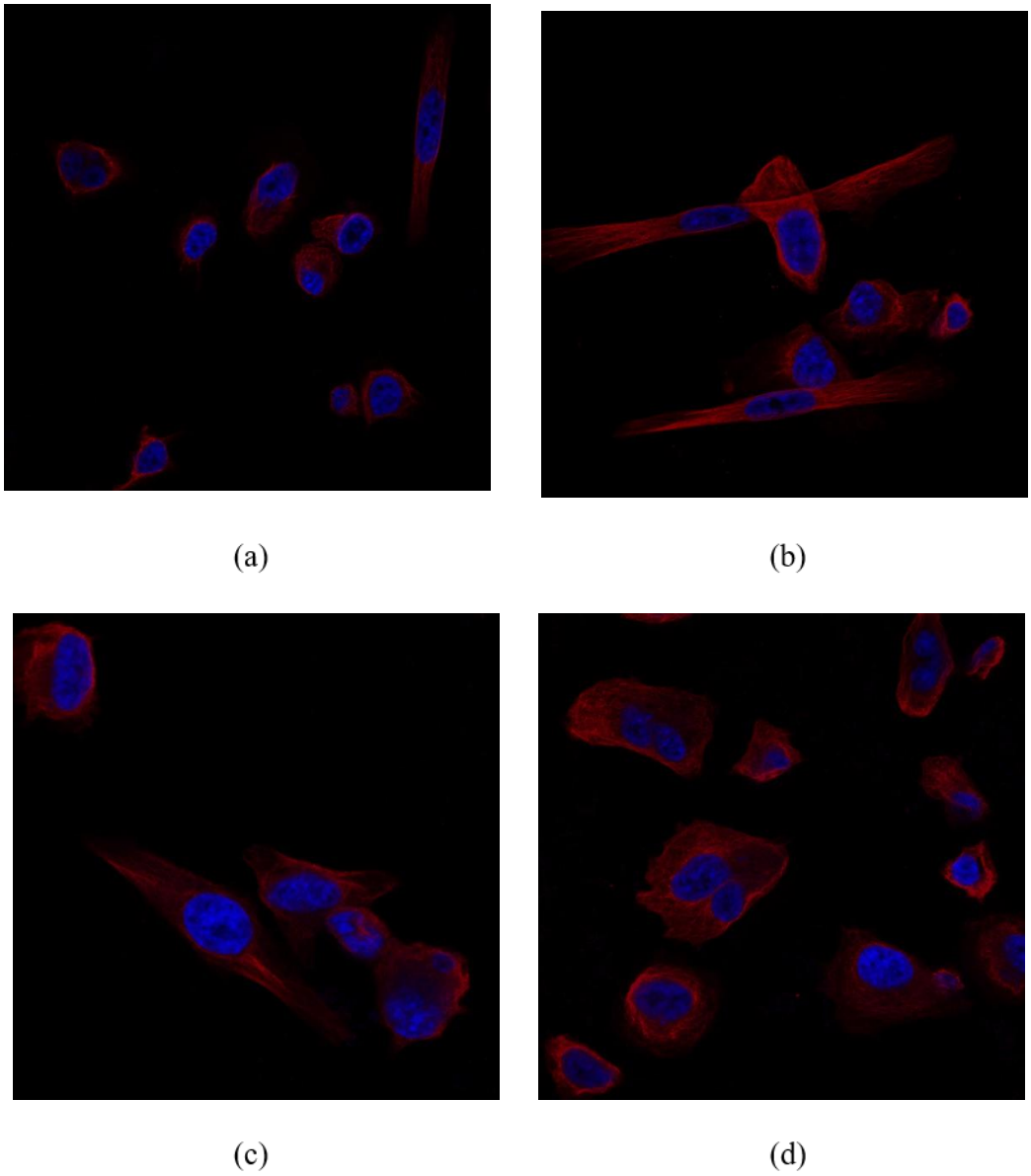


Figure 22 Tubulin staining. (a) Bioptron, 20-minutes exposed, treated; (b) Bioptron, 20-minutes exposed, control; (c) Vielight, 20-minutes exposed at a distance of 125 mm, treated; (d) Vielight, 20-minutes exposed at a distance of 125 mm, control.

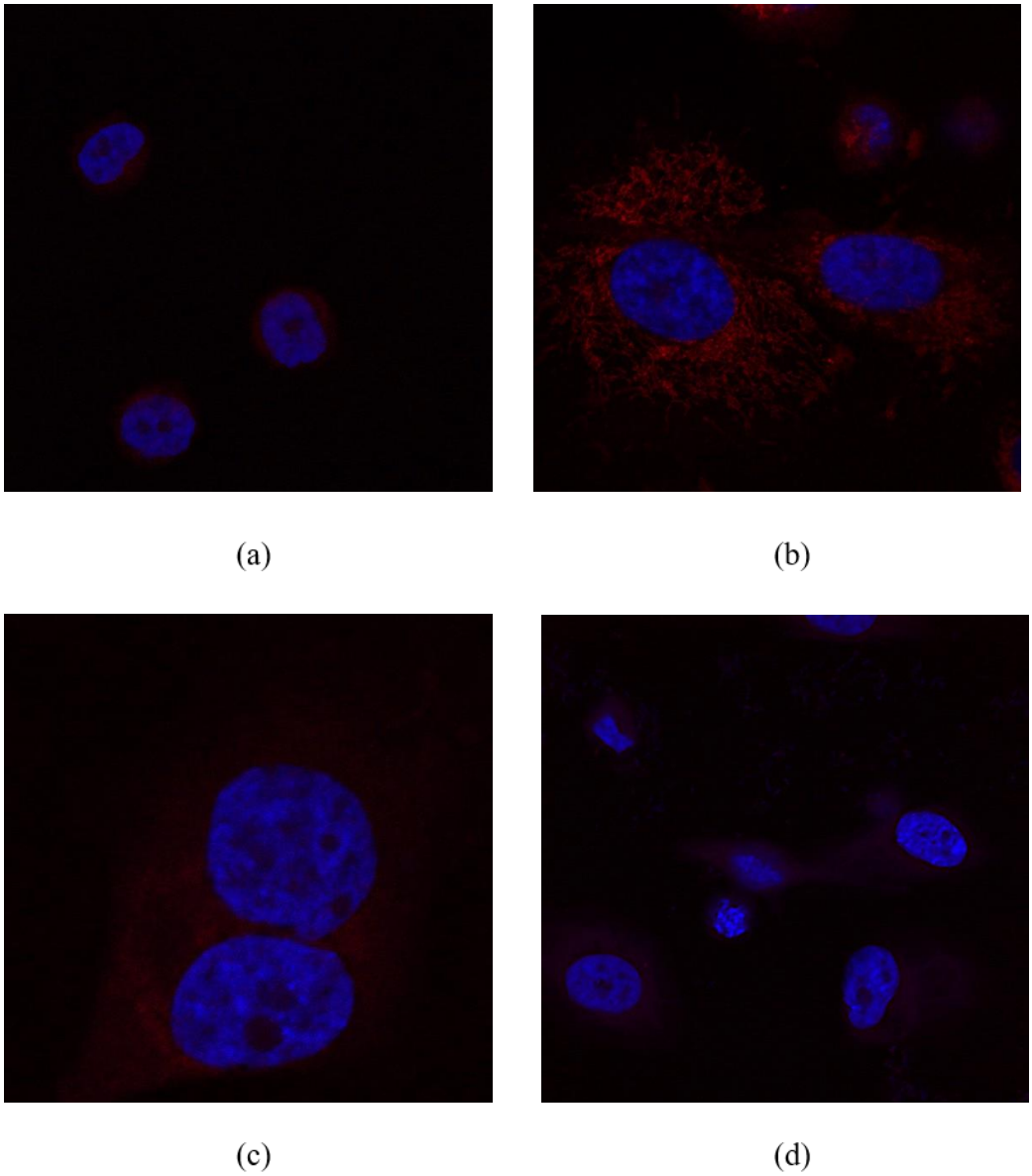


Figure 23 PC3 Mitochondria staining. (a) Bioptron, 10-minutes exposed, treated; (b) Bioptron, 10-minutes exposed, control; (c) Vielight, 15-minutes exposed at a distance of 125 mm, treated; (d) Vielight, 15-minutes exposed at a distance of 125 mm, control.

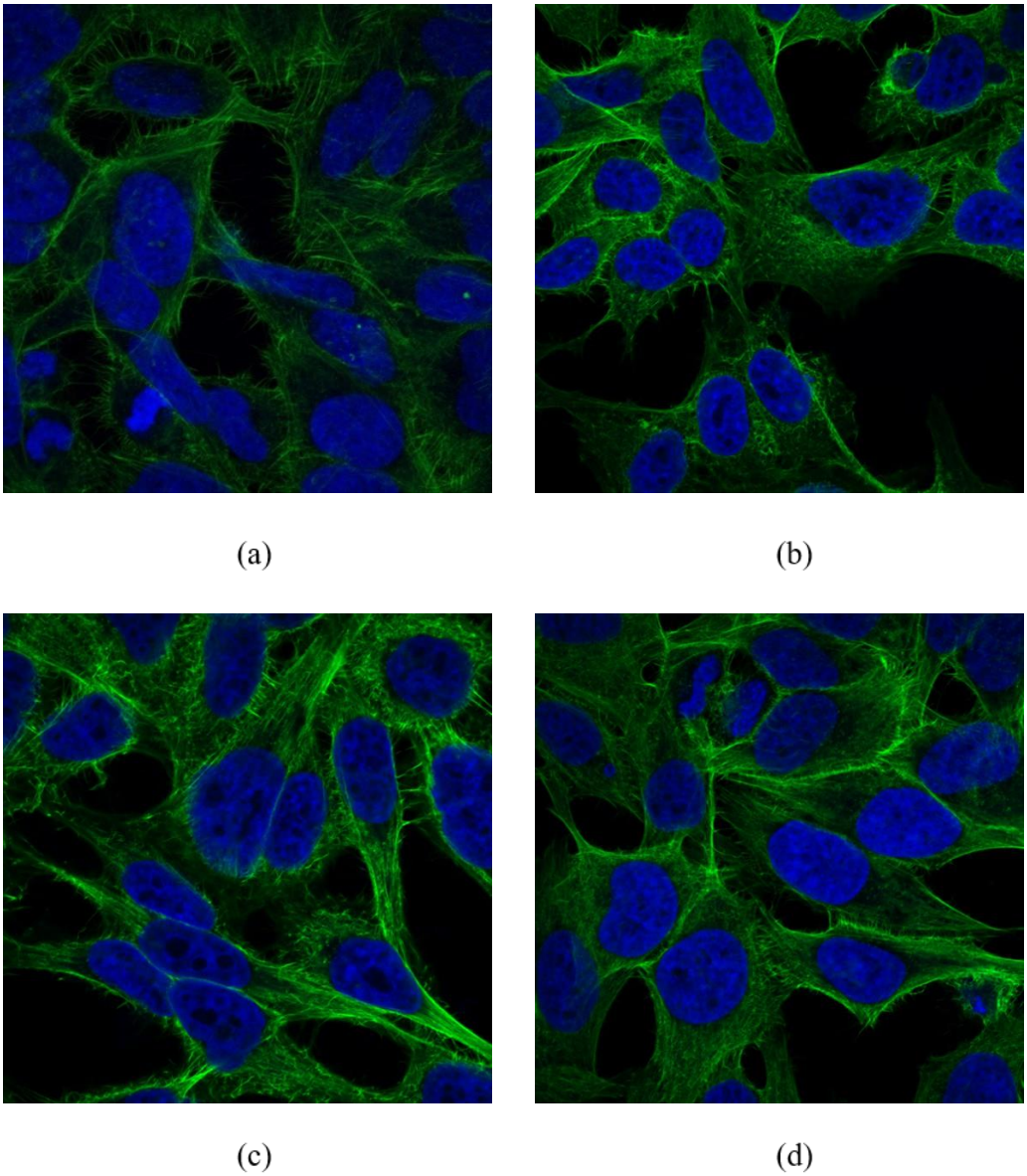


Figure 24 HeLa Actin staining. (a) Bioptron, 10-minutes exposed, treated; (b) Bioptron, 10-minutes exposed, control; (c) Vielight, 15-minutes exposed at a distance of 125 mm, treated; (d) Vielight, 15-minutes exposed at a distance of 125 mm, control.

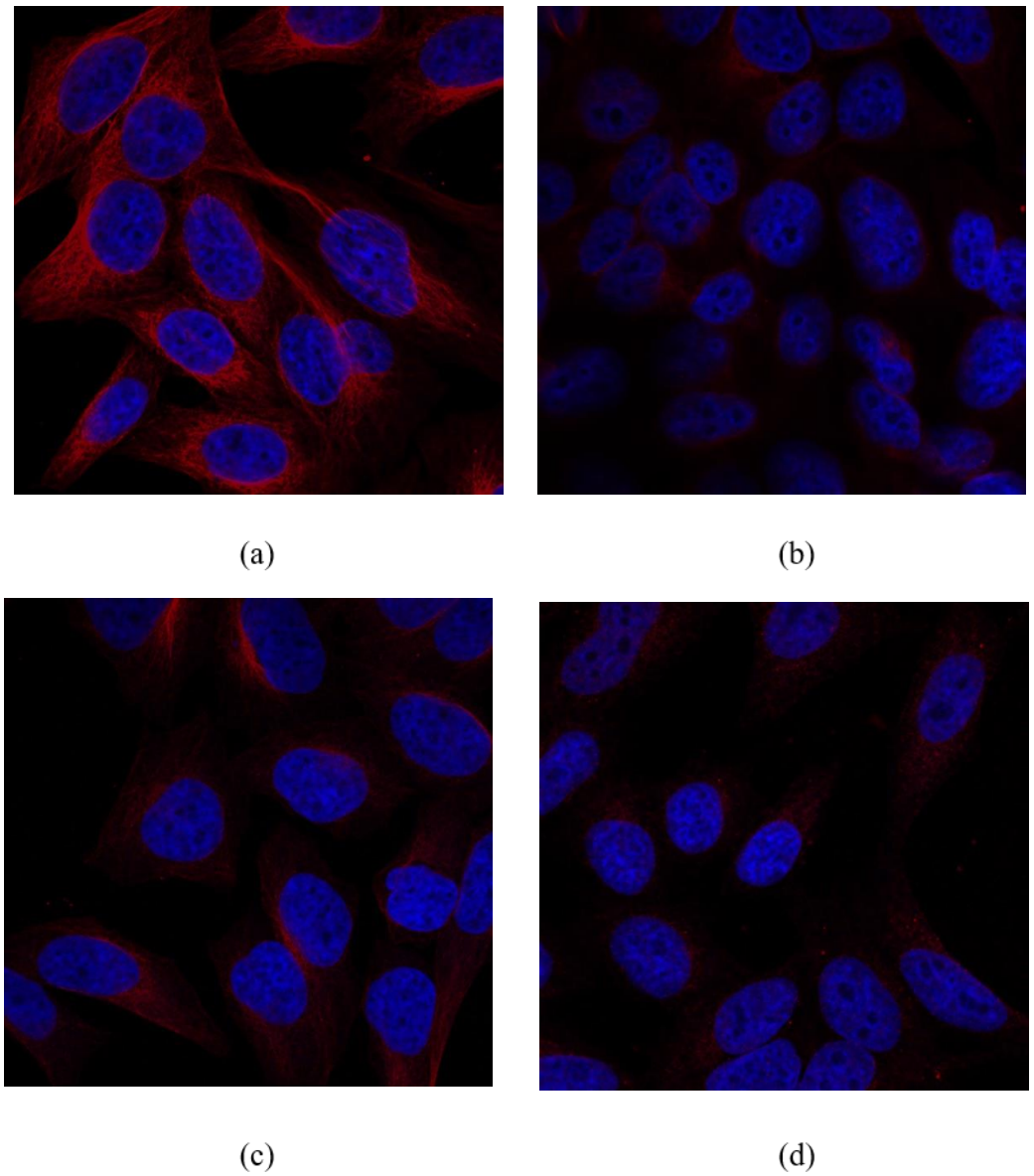


Figure 25 HeLa Tubulin staining. (a) Bioptron, 10-minutes exposed, treated; (b) Bioptron, 10-minutes exposed, control; (c) Vielight, 15-minutes exposed at a distance of 125 mm, treated; (d) Vielight, 15-minutes exposed at a distance of 125 mm, control.

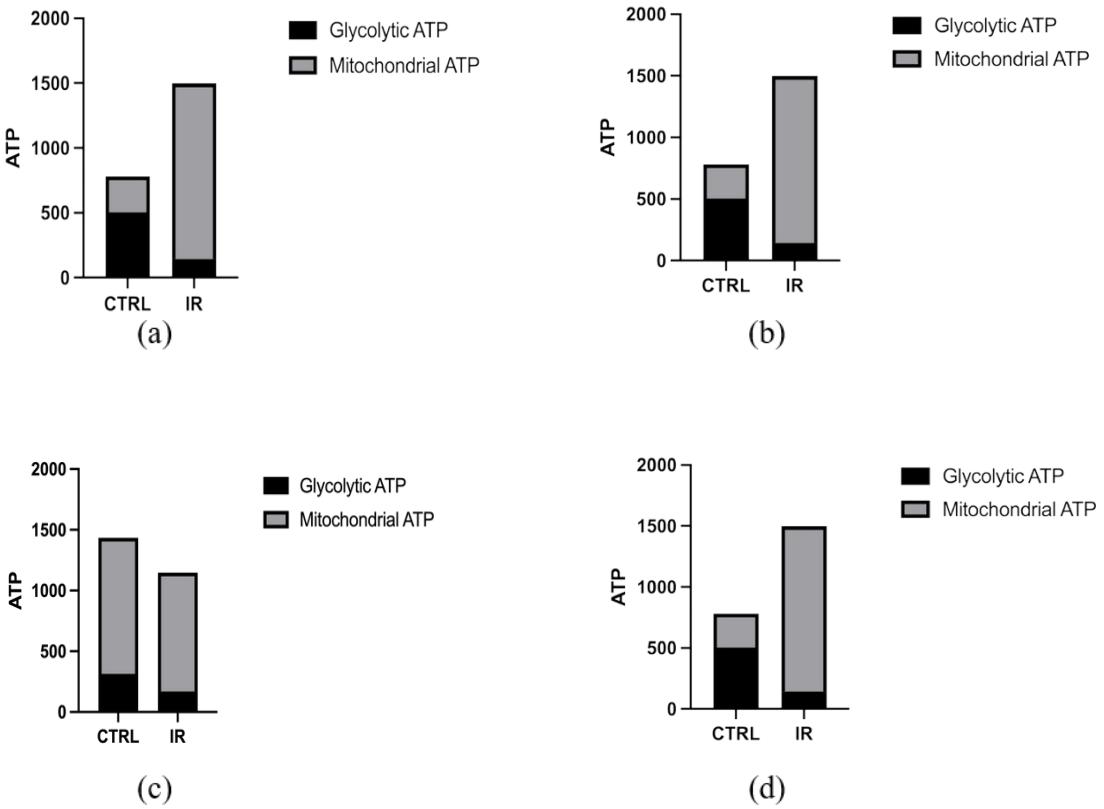


Figure 26 PC3 ATP assay: (a) Vielight, 15-minutes exposed at a distance of 125 mm; (b) Bioptron, 10-minutes exposed, experiment 1; (c) Bioptron, 10-minutes exposed, experiment 2; (d) Bioptron, 10-minutes exposed, experiment 3

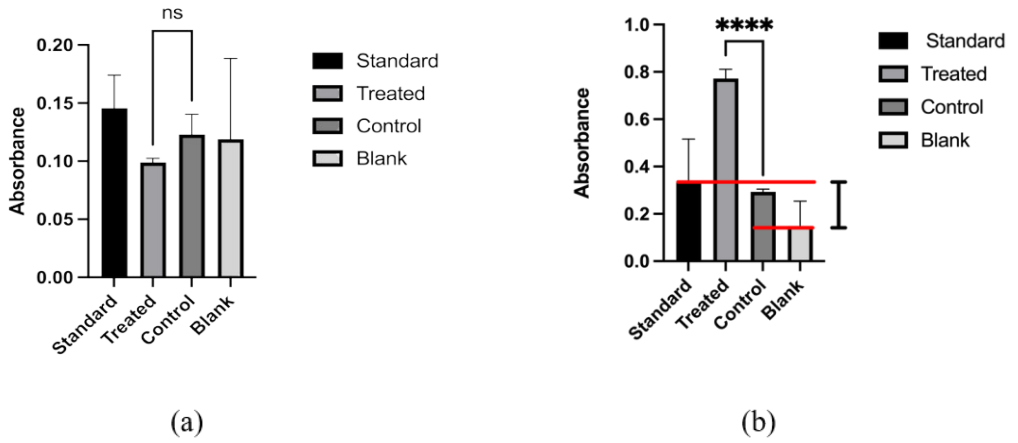


Figure 27 PC3 Lactate assay: (a) Vielight, 15-minutes exposed at a distance of 125 mm; (b) Bioptron, 10-minutes exposed.

# 5.2 Alzheimer's disease

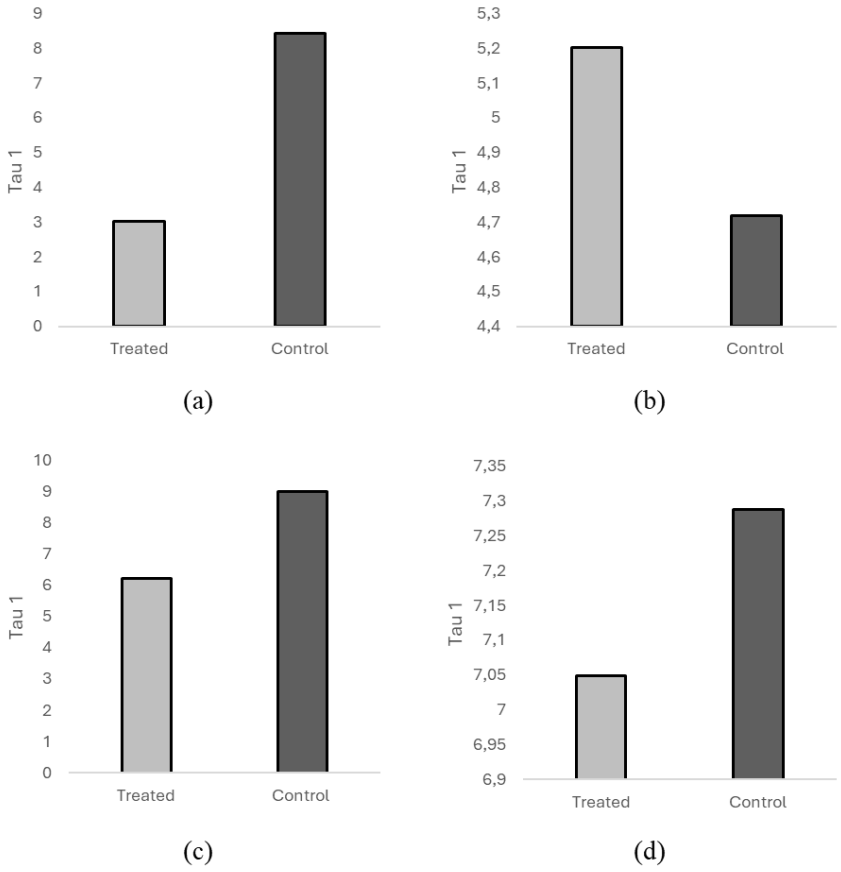


Figure 28 Levels of Tau 1 measured in Rat 1, Bioptron exposure (a) Warm sample, 10 minutes exposure; (b) Warm sample, 20 minutes exposure; (c) Cold sample, 10 minutes exposure; (d) Cold sample, 20 minutes exposure

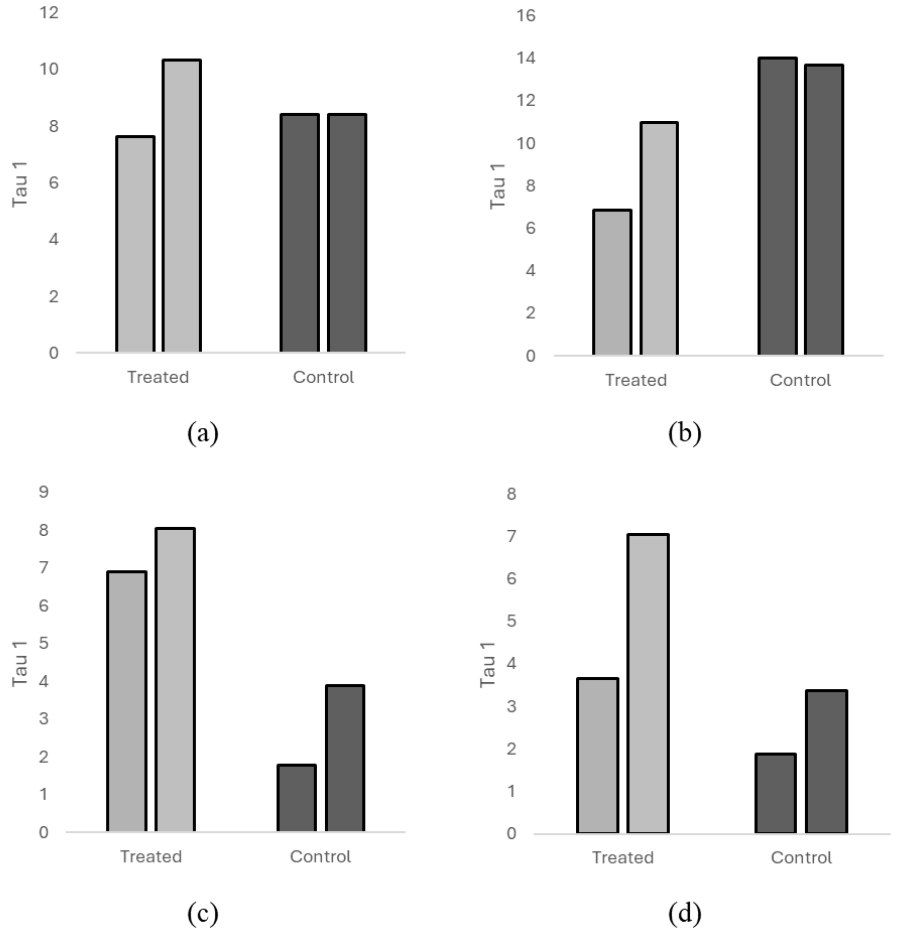


Figure 29 Levels of Tau 1 measured in Rat 2, Bioptron exposure (a) Warm sample, 10 minutes exposure; (b) Warm sample, 20 minutes exposure; (c) Cold sample, 10 minutes exposure; (d) Cold sample, 20 minutes exposure

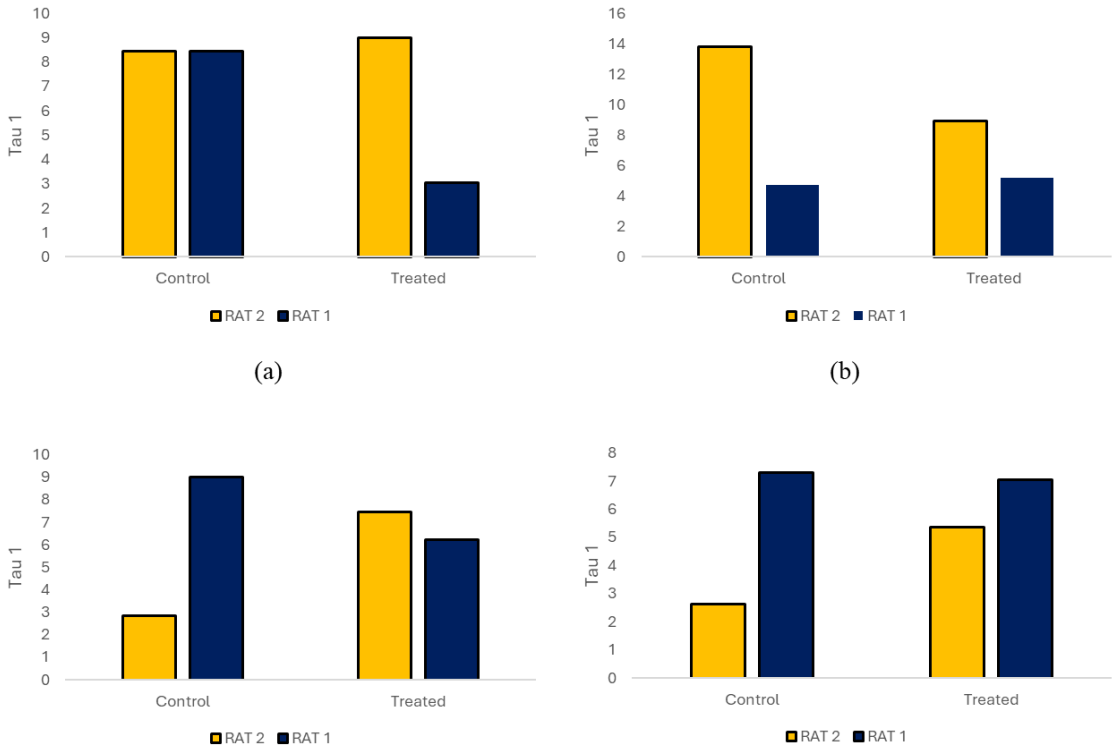


Figure 30 Levels of Tau 1 compared between rat 1 and 2, Bioptron exposure (a) Warm sample, 10 minutes exposure; (b) Warm sample, 20 minutes exposure; (c) Cold sample, 10 minutes exposure; (d) Cold sample, 20 minutes exposure

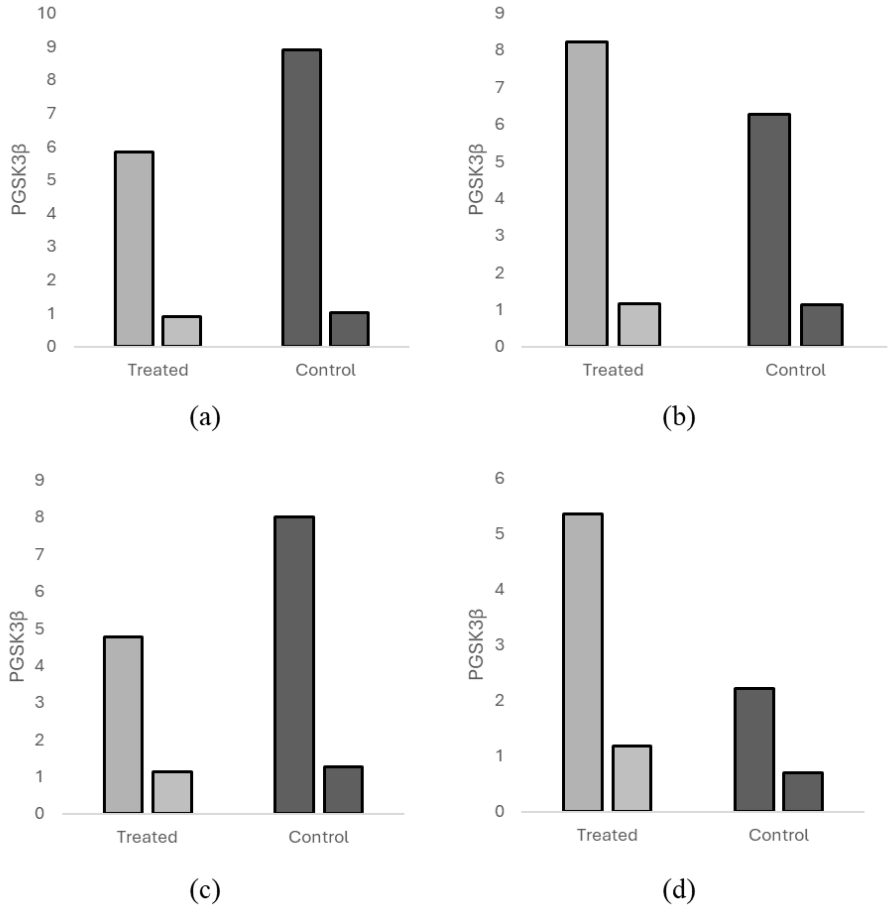


Figure 31 Levels of PGSK3β measured in Rat 1, Bioptron exposure (a) Warm sample, 10 minutes exposure; (b) Warm sample, 20 minutes exposure; (c) Cold sample, 10 minutes exposure; (d) Cold sample, 20 minutes exposure

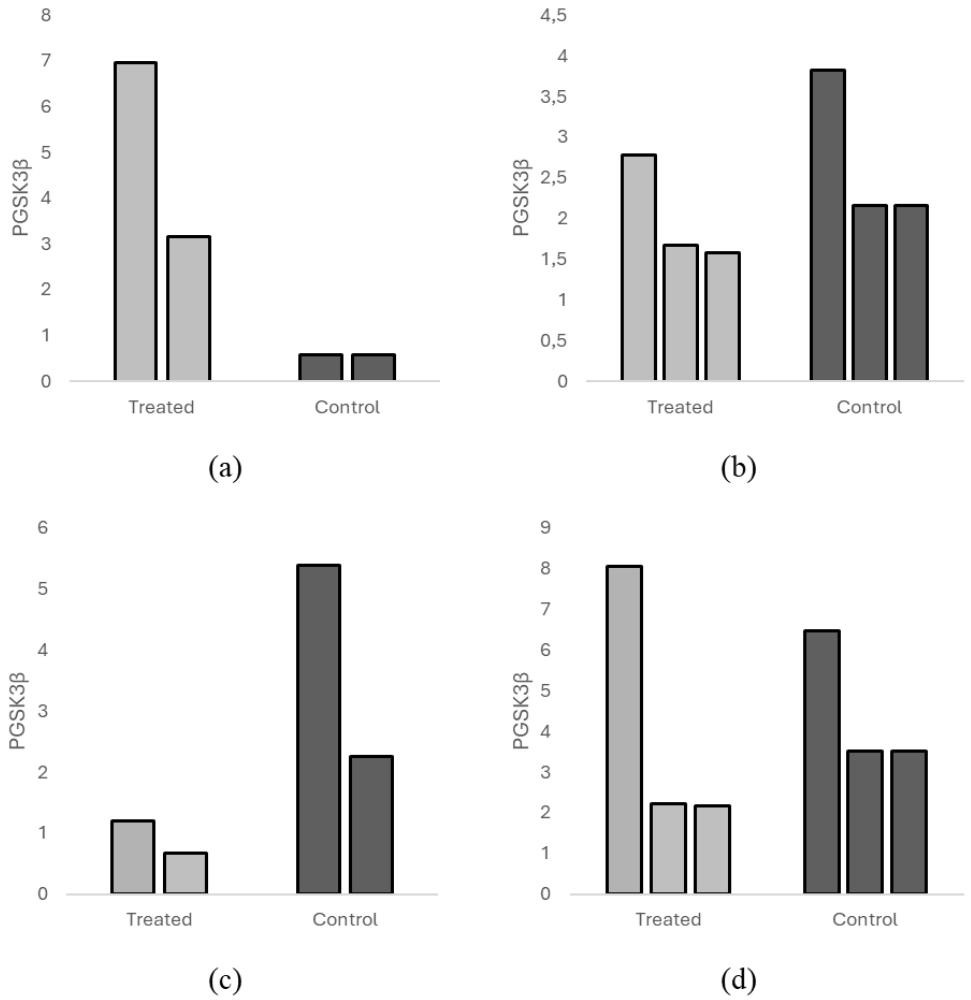


Figure 32 Levels of PGSK3β measured in Rat 2, Bioptron exposure (a) Warm sample, 10 minutes exposure; (b) Warm sample, 20 minutes exposure; (c) Cold sample, 10 minutes exposure; (d) Cold sample, 20 minutes exposure

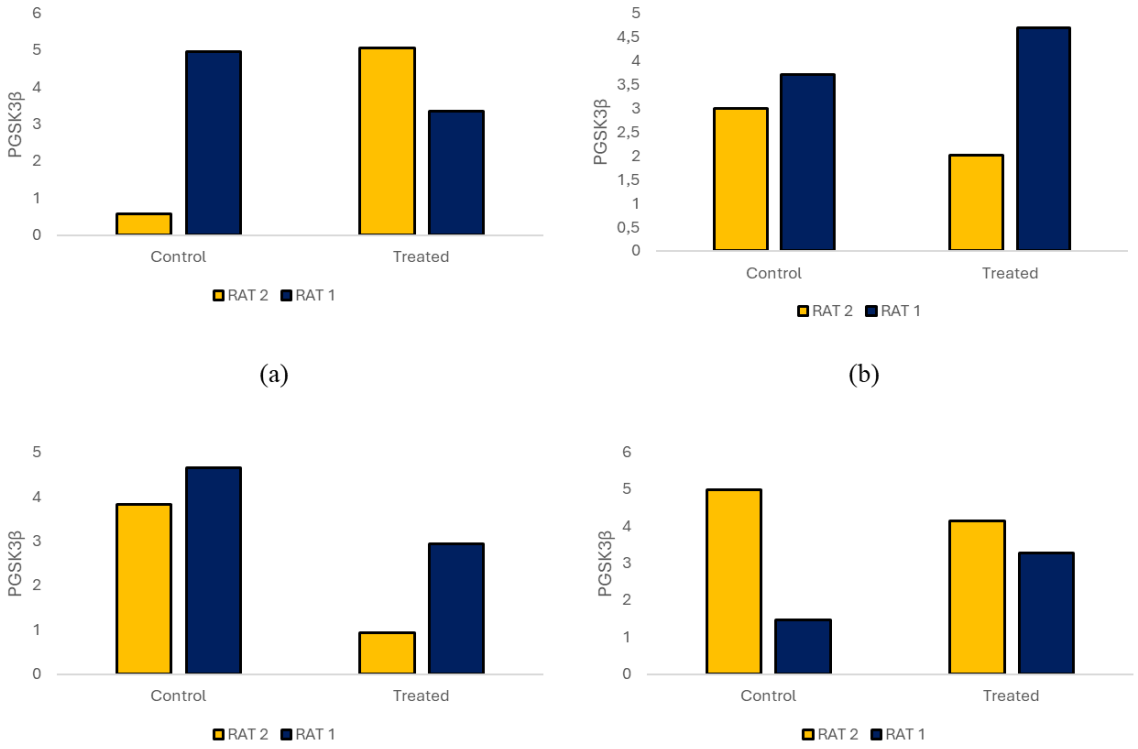


Figure 33 Levels of PGSK3β compared between rat 1 and 2, Bioptron exposure (a) Warm sample, 10 minutes exposure; (b) Warm sample, 20 minutes exposure; (c) Cold sample, 10 minutes exposure; (d) Cold sample, 20 minutes exposure

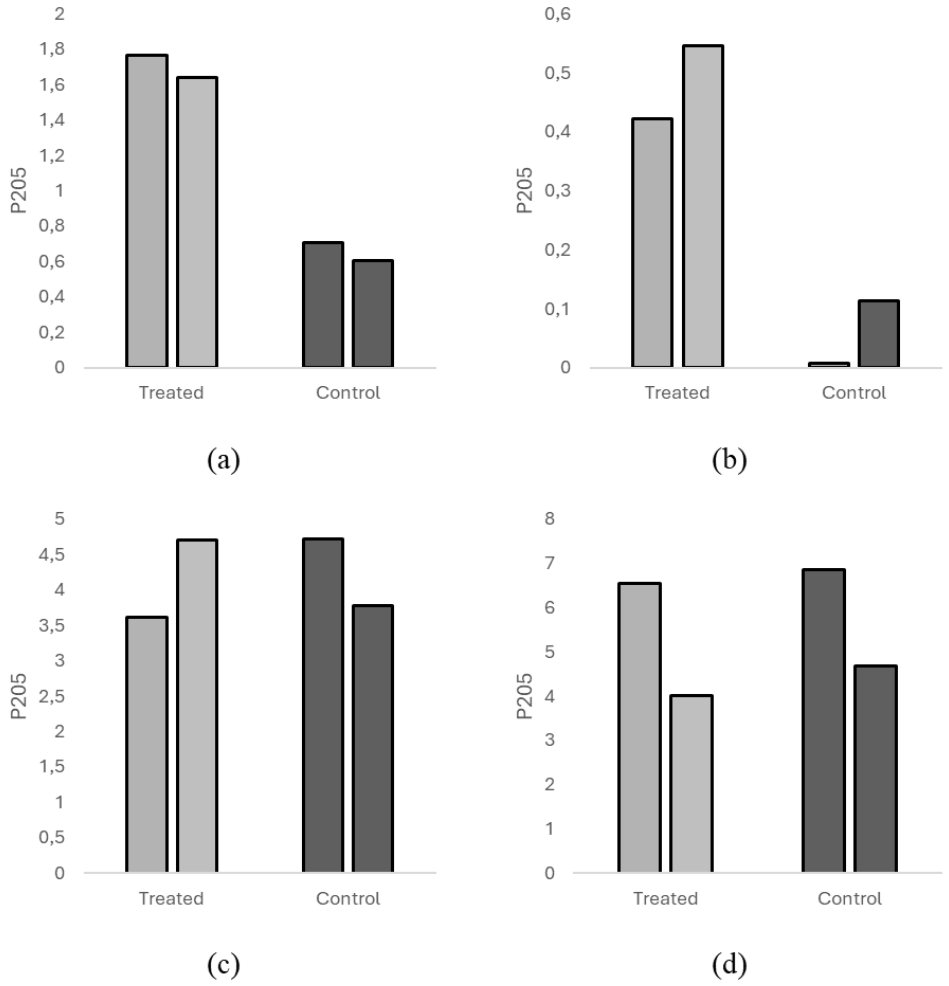


Figure 34 Levels of P205 measured in Rat 1, Bioptron exposure (a) Warm sample, 10 minutes exposure; (b) Warm sample, 20 minutes exposure; (c) Cold sample, 10 minutes exposure; (d) Cold sample, 20 minutes exposure

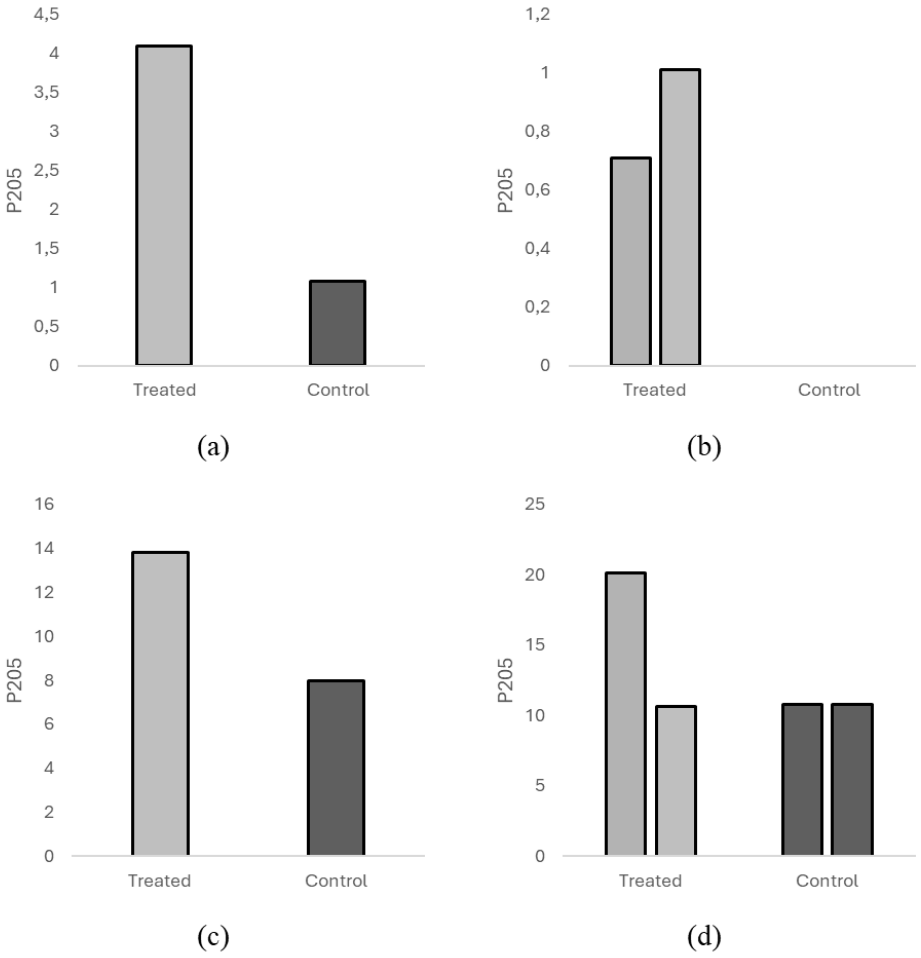


Figure 35 Levels of P205 measured in Rat 2, Bioptron exposure (a) Warm sample, 10 minutes exposure; (b) Warm sample, 20 minutes exposure; (c) Cold sample, 10 minutes exposure; (d) Cold sample, 20 minutes exposure

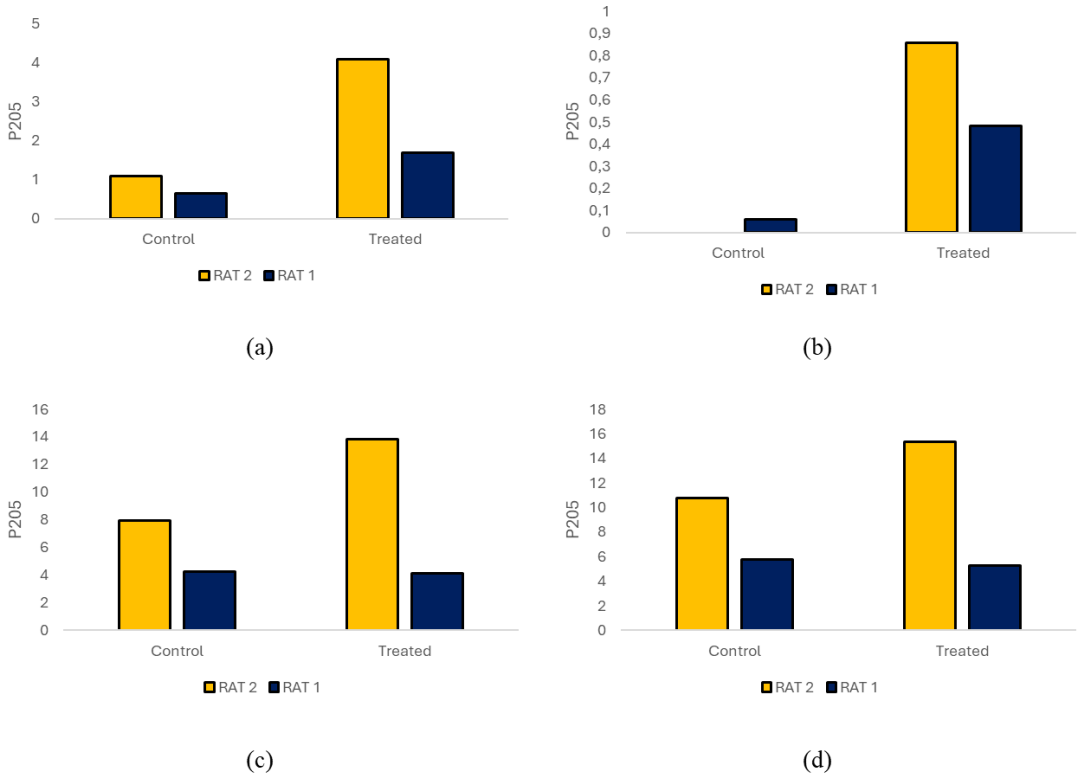


Figure 36 Levels of P205 compared between rat 1 and 2, Bioptron exposure (a) Warm sample, 10 minutes exposure; (b) Warm sample, 20 minutes exposure; (c) Cold sample, 10 minutes exposure; (d) Cold sample, 20 minutes exposure

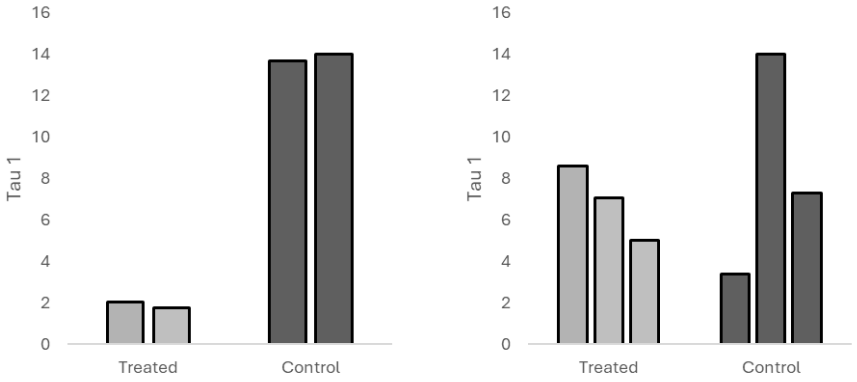


Figure 37 Levels of Tau 1 measured in Rat 2, VieLight exposure (a) Warm sample, 20 minutes exposure; (c) Cold sample, 20 minutes exposure

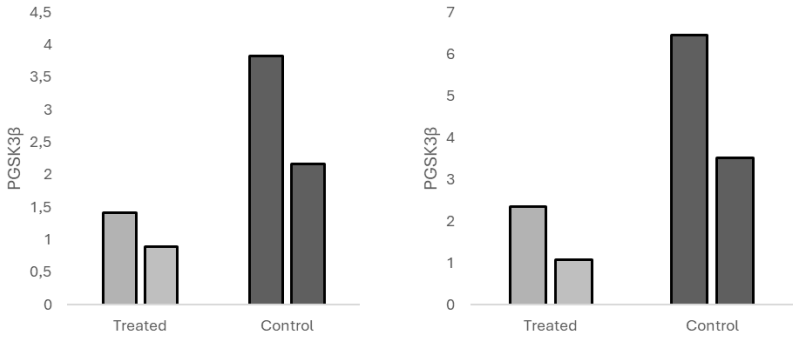


Figure 38 Levels of PGSK3β measured in Rat 2, VieLight exposure (a) Warm sample, 20 minutes exposure; (c) Cold sample, 20 minutes exposure

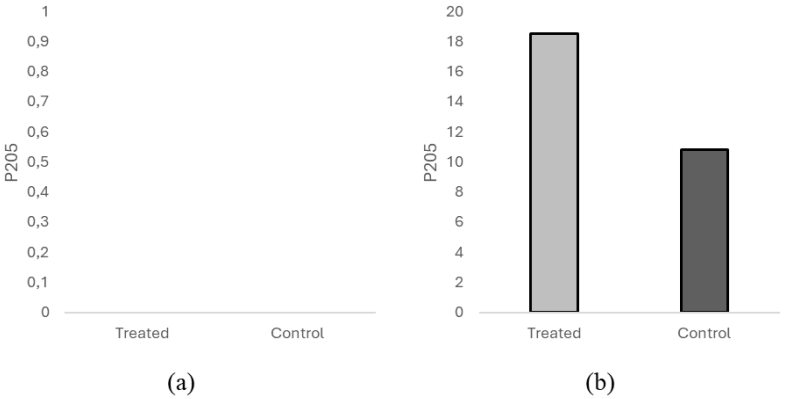


Figure 39 Levels of P205 measured in Rat 2, VieLight exposure (a) Warm sample, 20 minutes exposure; (c) Cold sample, 20 minutes exposure

# 6 DISCUSSIONS

## 6.1 Cancer disease

The potential therapeutic benefits of photobiomodulation (PBM) in cancer treatment are an ongoing debate, with inconsistent findings across various in vitro and in vivo studies (Hamblin, 2018b; Tam et al., 2020). The efficacy of PBM appears to be intricately linked to several key factors, including the wavelength of light used, dosage, target cell line, and specific exposure conditions (Bensadoun et al., 2020b; Robijns et al., 2021b, 2022b; Zein et al., 2018b). This variability underscores the complexity of PBM's mechanisms of action and their interaction with the diverse nature of cancer cells: while some studies report promising anti-tumor effects, others have observed negligible impacts or even potential tumor-promoting effects under certain circumstances (Ando et al., 2011; Baxter et al., 2017b; Robijns et al., 2021a). This contradiction emphasizes the necessity for more systematic investigations to decode the complex interplay between PBM and the molecular landscapes of different cancer types (Jo et al., 2023; Kara et al., 2018).

Our study aimed to elucidate these variations by systematically assessing the viability responses of three cancer cell lines (PC3, HeLa, and MCF7) under varying irradiation conditions. We employed two distinct light sources: the NeuroPro Device Module A (Vielight, Toronto, Canada) emitting near-infrared light at 810 nm, and the Bioptron Pro 1 device (Zepter, Zurich, Switzerland) producing hyperpolarized light with a spectrum range of 350-3400 nm and a polarization degree exceeding 95% (590-1550 nm).
In this investigation, the experimental protocol maintained a uniform beam spot distance of 125 mm throughout all irradiation scenarios. Then, to examinate different conditions varying the time parameter, the experiments were categorized into four groups, detailed in the Materials and Methods section (10, 15, 20, and 20 minutes with a 10-minute break in between).
A power density of 60 mW/cm2 was chosen for NeuroPro-exposed samples, in line with previous studies, facilitating comparisons with the Bioptron device's fixed power output of 40 mW/cm2.

Based on the results obtained regarding the viability of exposed cells, it must be noted that the hyperpolarized light seems efficient for shorter exposure intervals with respect to Neuropro-irradiated cells which led to a significant reduction in cells only after 20 minutes of exposure. In the latter case, we observed that longer time exposure reduced cell viability. Interestingly, 15 minutes of exposure was associated with an increase in cell proliferation and metabolism but when the interval is lengthened to 20 minutes, we observed a significant decrease in cell viability. It is crucial to notice that such trend is still valid for the Bioptron, observing that the outcome of both first (10 minutes) and the fourth (20 minutes with a 10-minute break in between) group is significantly reduced in terms of viability.

Regarding the re-irradiation experiments, the idea was to get some hints about the duration of eventual effects on cells by the EMFs applied. As Figure 14.b and Figure 14.d suggest, both devices demonstrated significant results, leading to a decrease in viability. These findings indicate that multiple exposures to irradiation result in increased cell death. However, the effect is much stronger in the case of Bioptron. More elucidations are needed in this case, to further

understand how the EMFs effects the cells in time. Hence, a next step will be testing other cell lines as we did for the above experiments explained.

Moreover, the role of the medium has been investigated to see if it effects the results in terms of beneficial effects produced by such light therapies. As expected, it appears to exist a direct involvement of the medium when exposed to the NIR spectrum. It is already known, that bound molecules interacting with aqueous solution can absorb the radiation, possibly limiting the efficacy of the therapy (Serhan et al., 2019; Szymborska-Małek et al., 2018).

Proving that, the viability of exposed media following 10 minutes exposure is significantly higher in value than the direct irradiation on cells' one; considering then the 15- and 20-minutes medium exposure, the resulting trend indicates a time-dependent decrease in viability. Hence, the leading hypothesis suggested is the screening effect of the medium over an approximately 10-minutes interval when exposed to irradiation in the NIR (NeuroPro), which drove us to test a longer time expo-sure for avoiding such effect and favor a better performance in terms of therapy efficiency and efficacy.

However, it is important to notice that such screening phenomenon does not seem to be present in the case of the hyperpolarized light, which is the reason why the exposure intervals have not been changed over the experiments.

To further validate the window optimization for both Bioptron and Vielight devices, the energy fluence (dose) was set at 2.4 J/cm$^2$ for testing two distinct cell lines, HeLa and MCF7.
The results show a decrease in viability due to a longer time exposure, that was significantly confirmed in the case of the MCF7 cell line, but not in the HeLa cells for the NeuroPro irradiation. This is not surprising because HeLa cells have previously been shown not to respond to the NIR irradiation with such lower doses. Indeed, the scientific evidence show a slightly decrease in viability starting from an energy fluence of about 5 J/cm$^2$ (H. B. Kim et al., 2021). These observations underscore the importance of cell line-specific characteristics in cellular response to light irradiation. The viability trend observed in the case of Bioptron-irradiated samples was confirmed for HeLa cells. This trend was also observed for the first group (10 minutes) of MCF7 cells. However, for the 20-minute group with a 10-minute break, the trend was opposite, supporting the aforementioned hypothesis of dependence on the specific features of each cell line.
It is worth noting that for both HeLa and MCF7 cells, exposure for a duration of 15 minutes led to a decrease in viability, although not significantly, indicating a certain flexibility in choosing the exposure window up to a maximum of 20 minutes, beyond which a significant proliferation was observed.

Keeping track of the effect of a dose of 2.4 J/cm$^2$, we investigated the possible structural changes after the irradiation, using immunofluorescence staining, on PC3 and HeLa cell lines, considering the results obtained which were equal in trend for 10-minutes Bioptron-irradiated samples and 15-minutes NeuroPro-irradiated ones. Confirming again the idea of cell-line dependency, both actin and tubulin staining in PC3 and HeLa cells displayed different characteristics. In particular, the former highlighted a shrinkage of the cytoplasm toward the nucleus favoured by the actin filaments after the irradiation of Bioptron and Vielight as well; tubulin filaments instead do not show a relevant difference between treated and control samples considering both light therapies employed for the irradiation, even if a lightly dimmer signal is present in the control group of the Neuro-Pro-irradiated cells. For this reason, it is not possible to determine eventual change in the disassembly or assembly dynamic because of the light therapy.

In contrast, HeLa cells exhibited no significant alterations in cytoplasmic morphology. However, our findings suggest a propensity for microtubule assembly and reorganization within these cells under the experimental conditions employed.
The observed changes in tubulin staining patterns may reflect light-induced alterations in microtubule polymerization or depolymerization, which could impact cellular functions and viability, again with a feature dependent on the cell-line type.

Following the same line, ATP has been measured for both Bioptron and NeuroPro irradiation samples respectively after 10- and 15-minutes exposure.
For the case of NIR irradiation, there is a decrease in glycolytic ATP and lactate levels, suggesting that light exposure may modulate cellular metabolism, potentially reversing the Warburg effect and promoting a more oxidative phenotype. Indeed, such phenomenon is based on an "aerobic glycolysis", which consists in a favored glycolysis over the oxidative phosphorylation even when oxygen is available (Liberti & Locasale, 2016b; Otto, 2016b; Vander Heiden et al., 2009b; Ward & Thompson, 2012b). Mitochondria appear to be activated leading to a production of ATP which is about 5-fold bigger than the glycolytic one.
Surprisingly, the repetition of this experiments for the hyperpolarized light treatment led to three different results: an initial switch to glycolytic activity with an evident damage to mitochondria; the second one, resulted in an increased mitochondrial activity as well as the production of the glycolytic ATP; finally there is a decrease in glycolytic ATP followed by a 10-fold increase in the mitochondrial one, as it happens for samples irradiated by NeuroPro.
This suggest that it exists a correlation between the aggressiveness of the cancer cell type and its progressive growth in culture over time, explaining the contrasting results obtained in Bioptron irradiated samples together with a possible influence of the hyperpolarized light itself. This is consistent with a synergistic upregulation of both glycolytic and mitochondrial pathways, potentially reflecting a metabolic adaptation strategy to meet the increased energy demands associated with cellular repair and recovery processes.

To better understand such outcomes, further investigations are needed involving mitochondria as a target and genetic studies to ameliorate the characterization of PBM and hyperpolarized light applied to cancer cells and to develop a standardized protocol.

## 6.2 Alzheimer's disease

Photobiomodulation (PBM) has emerged as a promising therapeutic approach for Alzheimer's disease (AD), offering potential benefits in addressing the complex pathophysiology of this neurodegenerative disorder (Huang et al., 2024). The mechanisms of PBM in AD treatment are multifaceted, targeting various aspects of the disease's pathology, the studies have demonstrated that PBM can improve mitochondrial function, increase ATP production, and reduce oxidative stress, all of which are crucial for maintaining neuronal health and function (Ramanishankar et al., 2024; Huang et al., 2024). These effects collectively contribute to potential neuroprotection and cognitive improvement in AD patients.

Despite the promising findings, recent research has highlighted the need for further investigation into the efficacy of PBM for AD treatment. A randomized, blinded study using a mouse model of AD showed no preventive effect of PBM on behavioral tests or histological analyses (Sipion, 2023). This contradictory result underscores the complexity of AD pathology and the need for more comprehensive studies to establish standardized protocols and confirm the long-term efficacy of PBM in AD management.

Turning to our experimental findings, we focused on the effects of PBM on key proteins involved in AD pathology: Tau1, GSK3β, and p-tau205. Tau is a microtubule-associated protein that becomes hyperphosphorylated in AD, leading to the formation of neurofibrillary tangles (Lantero-Rodriguez et al., 2024).
Tau 1 is the non-phosphorylated form of tau protein, which plays a crucial role in maintaining microtubule stability in neurons (Saltmarche, 2017). In AD, the balance between phosphorylated and non-phosphorylated tau is disrupted, with a shift towards increased phosphorylation leading to the formation of neurofibrillary tangles (Lim, 2024). GSK3β is a kinase that plays a crucial role in tau phosphorylation and has been implicated in AD pathogenesis (Huang et al., 2024). P-tau205 is a specific phosphorylation site on tau that has recently gained attention as a potential biomarker for AD (Lantero-Rodriguez et al., 2024).
In our experiments, we examined the effects of two different irradiation devices (Vielight NeuroPro Alpha2 and Bioptron MedAll devices) at various time points, comparing warm and cold samples.

The observed changes in Tau 1 levels following PBM treatment suggest that this intervention may influence the phosphorylation state of tau proteins. Specifically, an increase in tau 1 levels could indicate a shift towards a more balanced tau phosphorylation state, potentially mitigating the formation of neurofibrillary tangles (Saltmarche, 2017). Indeed, in rat 2, two measurements confirmed this trend in both in 10- and 20- minutes exposure to HPL.

Regarding GSK3β, our results showed a decrease in GSK3β activation following PBM treatment more evident in the warm slices of rat 2 exposed for 10 minutes to Bioptron device. In the cold samples, the effects are variable depending on the time of exposure and the rat used. For this reason, is complicated to confirm or denied previous results, that generally shows an increase of phosphorylated kinase GSK3β (Squarcio et al., 2023).

For p-tau (specifically p-T205), we found increased levels in treated warm samples exposed to HPL for 20 minutes. In cold samples we found some contrasting results between the two rats.

Indeed, we cannot draw some conclusions about the slice that underwent a hypothermia.

The differences we observed between warm and cold samples are particularly intriguing, the temperature dependence in PBM on AD-related proteins, is still under development, but previous research suggests that tissue temperature may be an important factor in modulating the biological effects of PBM, possibly by affecting enzyme kinetics or cellular stress responses.

Overall, while our results provide intriguing insights into the potential of PBM for modulating AD-related proteins, they also underscore the complexity of this approach and the need for rigorous, systematic research to fully understand and optimize PBM for potential AD applications.

# 7 CONCLUSIONS AND FUTURE WORK

This thesis aimed to explore the potential therapeutic applications of photobiomodulation (PBM) and hyperpolarized light (HPL) in two distinct areas: cancer treatment and Alzheimer's disease (AD). By investigating the effects of these light-based therapies on various cellular processes and protein dynamics, we sought to contribute to the growing body of knowledge in these fields and potentially uncover new avenues for treatment.

In the cancer-focused portion of our study, we examined the effects of PBM and HPL on three cancer cell lines: PC3, HeLa, and MCF7. Our experiments revealed complex and often cell line-specific responses to light therapy. Key findings included differential responses to exposure duration, with short exposures to HPL generally leading to decreased cell viability across all cell lines, while longer exposures produced variable effects. Each cell line exhibited unique patterns of response to both PBM and HPL, highlighting the importance of tailoring light therapy protocols to specific cancer types.
Both PBM and HPL induced significant changes in cellular metabolism, often shifting the balance between glycolytic and mitochondrial ATP production. This suggests a potential for light therapy to modulate the Warburg effect, a hallmark of cancer metabolism. Immunofluorescence studies revealed alterations in cytoskeletal organization and mitochondrial morphology following light exposure, particularly in PC3 cells. Our experiments also suggested that the culture medium plays a role in mediating the effects of light therapy, potentially by absorbing or modifying the incoming radiation.

In the Alzheimer's disease portion of our study, we focused on the effects of PBM and HPL on key proteins involved in AD pathology, namely Tau1, pGSK3β, and p-tau205. We observed distinct responses to light therapy in warm (37°C) versus cold (25°C) brain slice samples, suggesting that temperature may be a crucial factor in modulating the effects of PBM and HPL in neural tissue. Both PBM and HPL appeared to influence the levels of non-phosphorylated Tau (Tau1) and phosphorylated Tau (p-tau205), although the effects were often variable and dependent on specific experimental conditions. Our results indicated that light therapy could modulate the activation of pGSK3β, a key kinase involved in Tau phosphorylation, although the effects were not always consistent across different experimental conditions.

Our research demonstrates the complex and promising potential of photobiomodulation and hyperpolarized light in addressing two of the most challenging medical conditions of our time: cancer and Alzheimer's disease. While our findings reveal intriguing possibilities for modulating cellular behavior and protein dynamics through light-based interventions, they also underscore the need for continued, rigorous research in this field. The cell-specific and condition-dependent nature of the observed effects highlights the importance of developing tailored, precise protocols for light therapy applications.

As we move forward, it is crucial to build upon these findings with more comprehensive studies that address the limitations of our current work. By expanding our understanding of the mechanisms underlying PBM and HPL effects, optimizing treatment parameters, and transitioning to in vivo and clinical studies, we can work towards harnessing the full potential of these innovative therapies.

# 8 BIBLIOGRAPHY


1. Amaroli, A., Arany, P., Pasquale, C., Benedicenti, S., Bosco, A., & Ravera, S. (2021). Improving Consistency of Photobiomodulation Therapy: A Novel Flat-Top Beam Hand-Piece versus Standard Gaussian Probes on Mitochondrial Activity. International Journal of Molecular Sciences, 22(15). https://doi.org/10.3390/ijms22157788

2. Anders, J. J., Arany, P. R., Baxter, G. D., & Lanzafame, R. J. (2019). Light- Emitting Diode Therapy and Low-Level Light Therapy Are Photobiomodulation Therapy. Photobiomodulation, Photomedicine, and Laser Surgery, 37(2), 63–65. https://doi.org/10.1089/photob.2018.4600

3. Ando, T., Xuan, W., Xu, T., Dai, T., Sharma, S. K., Kharkwal, G. B., Huang, Y., Wu, Q., Whalen, M. J., Sato, S., Obara, M., & Hamblin, M. R. (2011). Comparison of therapeutic effects between pulsed and continuous wave 810-nm wavelength laser irradiation for traumatic brain injury in mice. PLoS ONE, 6(10). https://doi.org/10.1371/journal.pone.0026212

4. Atay, T., Aksoy, B. A., Aydogan, N. H., Baydar, M. L., Yildiz, M., & Ozdemir, R. (2009). Effect of Electromagnetic Field Induced by Radio Frequency Waves at 900 to 1800 MHz on Bone Mineral Density of Iliac Bone Wings. Journal of Craniofacial Surgery, 20(5), 1556–1560. https://doi.org/10.1097/SCS.0b013e3181b78559

5. Atkins, P., & De Paula, J. (2006). Physical chemistry (Oxford University Press, Ed.; Eighth). W. H. Freeman and Company.

6. Baxter, G. D., Liu, L., Petrich, S., Gisselman, A. S., Chapple, C., Anders, J. J., & Tumilty, S. (2017a). Low level laser therapy (Photobiomodulation therapy) for breast cancer-related lymphedema: a systematic review. In BMC cancer (Vol. 17, Issue 1, p. 833). https://doi.org/10.1186/s12885- 017-3852-x

7. Baxter, G. D., Liu, L., Petrich, S., Gisselman, A. S., Chapple, C., Anders, J. J., & Tumilty, S. (2017b). Low level laser therapy (Photobiomodulation therapy) for breast cancer-related lymphedema: a systematic review. In BMC cancer (Vol. 17, Issue 1, p. 833). https://doi.org/10.1186/s12885- 017-3852-x

8. Belenkov, I. N., & Ryff, I. M. (1981). Comparison of echocardiographic and cardiac morphometric data in healthy persons and patients with heart failure of various origins. Kardiologiia, 21(3), 84–87.

9. Bensadoun, R. J., Epstein, J. B., Nair, R. G., Barasch, A., Raber-Durlacher, J. E., Migliorati, C., Genot-Klastersky, M. T., Treister, N., Arany, P., Lodewijckx, J., & Robijns, J. (2020a). Safety and efficacy of photobiomodulation therapy in oncology: A systematic review. In Cancer Medicine (Vol. 9, Issue 22, pp. 8279–8300). Blackwell Publishing Ltd. https://doi.org/10.1002/cam4.3582

10. Bensadoun, R. J., Epstein, J. B., Nair, R. G., Barasch, A., Raber-Durlacher, J. E.,

Migliorati, C., Genot-Klastersky, M. T., Treister, N., Arany, P., Lodewijckx, J., & Robijns, J. (2020b). Safety and efficacy of photobiomodulation therapy in oncology: A systematic review. In Cancer Medicine (Vol. 9, Issue 22, pp. 8279–8300). Blackwell Publishing Ltd. https://doi.org/10.1002/cam4.3582

11. BIOPTRON Hyperlight. (n.d.).

12. BLOOD CELLS PROTEINS. AIChE Annual Meeting, Conference Proceedings, 2019-November. https://doi.org/10.1039/x0xx00000x

13. Bohren, C. F., & Huffman, D. R. (1940). Absorption and Scattering of Light by Small Particles.

14. Born, M., & Wolf, E. (2019). Principles of Optics. Cambridge University Press.

15. Calabrese, E. J. (2001a). Nitric Oxide: Biphasic Dose Responses. Critical Reviews in Toxicology, 31(4–5), 489–501. https://doi.org/10.1080/20014091111776

16. Calabrese, E. J. (2001b). The Future of Hormesis: Where Do We Go from Here? Critical Reviews in Toxicology, 31(4–5), 637–648. https://doi.org/10.1080/20014091111901

17. Calabrese, E. J. (2002). Hormesis: changing view of the dose-response, a personal account of the history and current status. Mutation Research/Reviews in Mutation Research, 511(3), 181–189. https://doi.org/10.1016/S1383-5742(02)00013-3

18. Calabrese, E. J. (2004). Hormesis: a revolution in toxicology, risk assessment and medicine. EMBO Reports, 5(S1). https://doi.org/10.1038/sj.embor.7400222

19. Calabrese, E. J. (2013). Biphasic dose responses in biology, toxicology and medicine: Accounting for their generalizability and quantitative features. Environmental Pollution, 182, 452–460. https://doi.org/10.1016/j.envpol.2013.07.046

20. Calabrò, M., Rinaldi, C., Santoro, G., & Crisafulli, C. (2020). The biological pathways of Alzheimer disease: a review. AIMS Neuroscience, 8(1), 86-132. https://doi.org/10.3934/Neuroscience.2021005

21. Caliogna, L., Medetti, M., Bina, V., Brancato, A. M., Castelli, A., Jannelli, E., Ivone, A., Gastaldi, G., Annunziata, S., Mosconi, M., & Pasta, G. (2021). Pulsed Electromagnetic Fields in Bone Healing: Molecular Pathways and Clinical Applications. International Journal of Molecular Sciences, 22(14), 7403. https://doi.org/10.3390/ijms22147403

22. Ceccarelli, G., Bloise, N., Mantelli, M., Gastaldi, G., Fassina, L., Cusella De Angelis, M. G., Ferrari, D., Imbriani, M., & Visai, L. (2013). A Comparative Analysis of the In Vitro Effects of Pulsed Electromagnetic Field Treatment on Osteogenic Differentiation of Two Different Mesenchymal Cell Lineages. BioResearch Open Access, 2(4), 283–294. https://doi.org/10.1089/biores.2013.0016

23. Chao, L. L. (2019). Effects of home photobiomodulation treatments on cognitive and behavioral function, cerebral perfusion, and resting-state functional connectivity in patients with dementia: A pilot trial. Photobiomodulation, Photomedicine, and Laser Surgery, 37(3), 133-141. https://doi.org/10.1089/photob.2018.4555

24. Costantini, E., Marconi, G. D., Fonticoli, L., Aielli, L., Trubiani, O., Rajan, T. S., Pizzicannella, J., Reale, M., & Diomede, F. (2022). Improved osteogenic differentiation by extremely low electromagnetic field exposure: possible application for bone engineering. Histochemistry and Cell Biology, 158(4), 369–381. https://doi.org/10.1007/s00418-022-02126-9

25. Davisson, C., & Germer, L. H. (1927). Diffraction of Electrons by a Crystal of Nickel. Physical Review, 30(6), 705–740. https://doi.org/10.1103/PhysRev.30.705

26. De Broglie, L. (n.d.). Recherches sur la théorie des Quanta. https://theses.hal.science/tel-00006807

27. De Freitas, L. F., & Hamblin, M. R. (2016). Proposed Mechanisms of Photobiomodulation or Low-Level Light Therapy. IEEE Journal of Selected Topics in Quantum Electronics, 22(3), 348–364. https://doi.org/10.1109/JSTQE.2016.2561201

28. De Taboada, L., Yu, J., El-Amouri, S., Gattoni-Celli, S., Richieri, S., McCarthy, T., et al. (2011). Transcranial laser therapy attenuates amyloid-β peptide neuropathology in amyloid-β protein precursor transgenic mice. Journal of Alzheimer's Disease, 23, 521–535. https://doi.org/10.3233/JAD-2010-100894

29. Delacourte, A., & Defossez, A. (1986). Alzheimer's disease: Tau proteins, the promoting factors of microtubule assembly, are major components of paired helical filaments. Journal of the Neurological Sciences, 76(2-3), 173-186. https://doi.org/10.1016/0022-510x(86)90167-x

30. Dermatitis, Acne-Seasonal Affective Disorder-Sleeping Problems-Skin Aging.

31. DialoguesClinNeurosci-16-93. (n.d.).

32. Einstein, A. (1905a). Über einen die Erzeugung und Verwandlung des Lichtes betreffenden heuristischen Gesichtspunkt. Annalen Der Physik, 322(6), 132–148. https://doi.org/10.1002/andp.19053220607

33. Einstein, A. (1905b). Zur Elektrodynamik bewegter Körper. Annalen Der Physik, 322(10), 891–921. https://doi.org/10.1002/andp.19053221004

34. ENDOGENOUS ELECTROMAGNETIC FIELD OF THE HUMAN BODY. 10. www.arpnjournals.com

35. Fantin, V. R., St-Pierre, J., & Leder, P. (2006). Attenuation of LDH-A expression uncovers a link between glycolysis, mitochondrial physiology, and tumor maintenance. Cancer Cell, 9(6), 425–434. https://doi.org/10.1016/j.ccr.2006.04.023

36. Füllekrug, M., & Fraser-Smith, A. C. (2011). The Earth's electromagnetic environment. Geophysical Research Letters, 38(21), n/a-n/a. https://doi.org/10.1029/2011GL049572

37. Funk, R. H. W. (2015a). Endogenous electric fields as guiding cue for cell migration. In Frontiers in Physiology (Vol. 6, Issue MAY). Frontiers Media S.A. https://doi.org/10.3389/fphys.2015.00143

38. Funk, R. H. W. (2015b). Endogenous electric fields as guiding cue for cell migration. In Frontiers in Physiology (Vol. 6, Issue MAY). Frontiers Media S.A. https://doi.org/10.3389/fphys.2015.00143

39. Gaggi, N. L., Parincu, Z., Siu, K., Collins, K. A., & Iosifescu, D. V. (2024). Modulating the Mitochondria for Mood Disorders: Emerging Evidence for Transcranial Photobiomodulation in Major Depressive Disorder. Current Treatment Options in Psychiatry. https://doi.org/10.1007/s40501-024- 00321-0

40. Gerson, J. E., Mudher, A., & Kayed, R. (2016). Potential mechanisms and implications for the formation of tau oligomeric strains. Critical Reviews in Biochemistry and Molecular Biology, 51, 482-496. https://doi.org/10.1080/10409238.2016.1226251

41. Glass, G. E. (2023). Photobiomodulation: A Systematic Review of the Oncologic Safety of Low-Level Light Therapy for Aesthetic Skin Rejuvenation. In Aesthetic Surgery Journal (Vol. 43, Issue 5, pp. NP357– NP371). Oxford University Press. https://doi.org/10.1093/asj/sjad018

42. Goldstein, D. H. (2017). Polarized Light. CRC Press. https://doi.org/10.1201/b10436

43. Gonul, Y., Kunt, H., Senturk, İ., Korkmaz, M., Ahsen, A., Hazman, Ö., Bal, A., Genc, A., & Songur, A. (2016). Effects of electromagnetic radiation exposure on bone mineral density, thyroid, and oxidative stress index in electrical workers. OncoTargets and Therapy, 745. https://doi.org/10.2147/OTT.S94374

44. Gutfreund, H. (1995). Kinetics for the Life Sciences: Receptors, Transmitters and Catalysts. Cambridge University Press, Cambridge, UK. ISBN: 0-521-48027-2

45. Hamblin, M. R. (2016). Photobiomodulation or low-level laser therapy. In Journal of Biophotonics (Vol. 9, Issues 11–12, pp. 1122–1124). Wiley- VCH Verlag. https://doi.org/10.1002/jbio.201670113

46. Hamblin, M. R. (2018a). Mechanisms and Mitochondrial Redox Signaling in Photobiomodulation. Photochemistry and Photobiology, 94(2), 199–212. https://doi.org/10.1111/php.12864

47. Hamblin, M. R. (2018b). Mechanisms and Mitochondrial Redox Signaling in Photobiomodulation. Photochemistry and Photobiology, 94(2), 199–212. https://doi.org/10.1111/php.12864

48. Hamblin, M. R., Nelson, S. T., & Strahan, J. R. (2018). Photobiomodulation and Cancer: What Is the Truth? In Photomedicine and laser surgery (Vol. 36, Issue 5, pp. 241–245). https://doi.org/10.1089/pho.2017.4401

49. Hammerschlag, R., Levin, M., McCraty, R., Bat, N., Ives, J. A., Lutgendorf, S. K., & Oschman, J. L. (2015). Biofield physiology: A Framework for an emerging discipline. Global Advances in Health and Medicine, 4(1_suppl), gahmj.2015.015. https://doi.org/10.7453/gahmj.2015.015.suppl

50. Hardie, D. G. (2022). 100 years of the Warburg effect: a historical perspective.

Endocrine-Related Cancer, 29(12), T1–T13. https://doi.org/10.1530/ERC- 22-0173

51. Hecht, E. (2016). Optics (Pearson Education Limited, Ed.).

52. Heiskanen, V., & Hamblin, M. R. (2018). Photobiomodulation: Lasers: vs. light emitting diodes? In Photochemical and Photobiological Sciences (Vol. 17, Issue 8, pp. 1003–1017). Royal Society of Chemistry. https://doi.org/10.1039/c8pp00176f

53. Himmler, A., Drechsel, D., Kirschner, M. W., & Martin, D. W. Jr. (1989). Tau consists of a set of proteins with repeated C-terminal microtubule-binding domains and variable N-terminal domains. Molecular and Cellular Biology, 9(4), 1381-1388. https://doi.org/10.1128/mcb.9.4.1381-1388.1989

54. Huang, Z., Hamblin, M. R., & Zhang, Q. (2024). Photobiomodulation in experimental models of Alzheimer's disease: state-of-the-art and translational perspectives. Journal of Translational Medicine, 16(1), 114. https://doi.org/10.1186/s13195-024-01484-x

55. Ji, Q., Yan, S., Ding, J., Zeng, X., Liu, Z., Zhou, T., Wu, Z., Wei, W., Li, H., Liu, S., & Ai, S. (2024). Photobiomodulation improves depression symptoms: a systematic review and meta-analysis of randomized controlled trials. Frontiers in Psychiatry, 14. https://doi.org/10.3389/fpsyt.2023.1267415

56. Jo, I. Y., Byeon, H. K., Ban, M. J., Park, J. H., Lee, S. C., Won, Y. K., Eun, Y. S., Kim, J. Y., Yang, N. G., Lee, S. H., Lee, P., Heo, N. H., Jo, S., Seo, H., Kim, S., Song, H. Y., & Kim, J. E. (2023). Effect of a Novel Handheld Photobiomodulation Therapy Device in the Management of Chemoradiation Therapy-Induced Oral Mucositis in Head and Neck Cancer Patients: A Case Series Study. Photonics, 10(3). https://doi.org/10.3390/photonics10030241

57. Kara, C., Selamet, H., Gökmenoğlu, C., & Kara, N. (2018). Low level laser therapy induces increased viability and proliferation in isolated cancer cells. Cell Proliferation, 51(2). https://doi.org/10.1111/cpr.12417

58. Karran, E., Mercken, M., & De Strooper, B. (2011). The amyloid cascade hypothesis for Alzheimer's disease: an appraisal for the development of therapeutics. Nature Reviews Drug Discovery. https://doi.org/10.1038/nrd3505

59. Karu, T. I. (2014a). Cellular and molecular mechanisms of photobiomodulation (low-power laser therapy). IEEE Journal on Selected Topics in Quantum Electronics, 20(2). https://doi.org/10.1109/JSTQE.2013.2273411

60. Karu, T. I. (2014b). Cellular and molecular mechanisms of photobiomodulation (low-power laser therapy). IEEE Journal on Selected Topics in Quantum Electronics, 20(2). https://doi.org/10.1109/JSTQE.2013.2273411

61. Karu, T. I., Pyatibrat, L. V., & Afanasyeva, N. I. (2005). Cellular effects of low power laser therapy can be mediated by nitric oxide. Lasers in Surgery and Medicine, 36(4), 307–314. https://doi.org/10.1002/lsm.20148

62. Kim, H. B., Jeong, S., & Baik, K. Y. (2021). Preconditioning with near-infrared irradiation to enhance the irreversible electroporation efficiency in hela cells. Applied

Sciences (Switzerland), 11(18). https://doi.org/10.3390/app11188504

63. Kim, H. P. (2014). Lightening up Light Therapy: Activation of Retrograde Signaling Pathway by Photobiomodulation. Biomolecules & Therapeutics, 22(6), 491–496. https://doi.org/10.4062/biomolther.2014.083

64. Koruga, D. (2018). Hyperpolarized Light. Fundamentals of Nanobiomedical Photonics. Zepter Book World.

65. Kovacs, G. G. (2017). Tauopathies. Handbook of Clinical Neurology, 145, 355-368. https://doi.org/10.1016/B978-0-12-802395-2.00025-0

66. Lantero-Rodriguez, J., Montoliu-Gaya, L., Benedet, A. L., Vrillon, A., Dumurgier, J., Cognat, E., Brum, W. S., Rahmouni, N., Stevenson, J., Servaes, S., Therriault, J., Becker, B., Brinkmalm, G., Snellman, A., Huber, H., Kvartsberg, H., Ashton, N. J., Zetterberg, H., Paquet, C., Rosa-Neto, P., & Blennow, K. (2024). CSF p-tau205: a biomarker of tau pathology in Alzheimer's disease. Acta Neuropathologica, 147(1), 12. https://doi.org/10.1007/s00401-023-02659-w

67. Lei, T., Li, F., Liang, Z., Tang, C., Xie, K., Wang, P., Dong, X., Shan, S., Liu, J., Xu, Q., Luo, E., & Shen, G. (2017). Effects of four kinds of electromagnetic fields (EMF) with different frequency spectrum bands on ovariectomized osteoporosis in mice. Scientific Reports, 7(1), 553. https://doi.org/10.1038/s41598-017-00668-w

68. Levin, M. (2014). Molecular bioelectricity: how endogenous voltage potentials control cell behavior and instruct pattern regulation in vivo. Molecular Biology of the Cell, 25(24), 3835–3850. https://doi.org/10.1091/mbc.e13- 12-0708

69. Liberti, M. V., & Locasale, J. W. (2016a). The Warburg Effect: How Does it Benefit Cancer Cells? Trends in Biochemical Sciences, 41(3), 211–218. https://doi.org/10.1016/j.tibs.2015.12.001

70. Liberti, M. V., & Locasale, J. W. (2016b). The Warburg Effect: How Does it Benefit Cancer Cells? Trends in Biochemical Sciences, 41(3), 211–218. https://doi.org/10.1016/j.tibs.2015.12.001

71. Lim, L. (2024). Modifying Alzheimer's disease pathophysiology with photobiomodulation: model, evidence, and future with EEG-guided intervention. Frontiers in Neurology. https://doi.org/10.3389/fneur.2024.1407785

72. Luppi, M., Hitrec, T., Di Cristoforo, A., Squarcio, F., Stanzani, A., Occhinegro, A., Chiavetta, P., Tupone, D., Zamboni, G., Amici, R., & Cerri, M. (2019). Phosphorylation and Dephosphorylation of Tau Protein During Synthetic Torpor. Frontiers in Neuroanatomy. https://doi.org/10.3389/fnana.2019.00057

73. Ma, Q., Chen, C., Deng, P., Zhu, G., Lin, M., Zhang, L., Xu, S., He, M., Lu, Y., Duan, W., Pi, H., Cao, Z., Pei, L., Li, M., Liu, C., Zhang, Y., Zhong, M., Zhou, Z., & Yu, Z. (2016). Extremely Low-Frequency Electromagnetic Fields Promote In Vitro Neuronal Differentiation and Neurite Outgrowth of Embryonic Neural Stem Cells via Up-Regulating TRPC1. PLOS ONE, 11(3), e0150923. https://doi.org/10.1371/journal.pone.0150923

74. Markov, M. S. (Ed.). (2015a). Electromagnetic Fields in Biology and Medicine. CRC Press. https://doi.org/10.1201/b18148

75. Markov, M. S. (Ed.). (2015b). Electromagnetic Fields in Biology and Medicine. CRC Press. https://doi.org/10.1201/b18148

76. Marshall, C. J. (1997). Cold-adapted enzymes. Trends in Biotechnology, 15, 359-364. https://doi.org/10.1016/S0167-7799(97)01086-X

77. Martin, L., Latypova, X., Wilson, C. M., Magnaudeix, A., Perrin, M. L., Yardin, C., & Terro, F. (2013). Tau protein kinases: Involvement in Alzheimer's disease. Ageing Research Reviews. https://doi.org/10.1016/j.arr.2012.06.003

78. Masters, J. R. (2002). HeLa cells 50 years on: the good, the bad and the ugly. Nature Reviews Cancer, 2(4), 315–319. https://doi.org/10.1038/nrc775

79. May 1801: Thomas Young and the Nature of Light. (n.d.).

80. Medeiros, R., Baglietto-Vargas, D., & LaFerla, F. M. (2011). The Role of Tau in Alzheimer's Disease and Related Disorders. Journal of Alzheimer's Disease. https://doi.org/10.1111/j.1755-5949.2010.00177.x

81. Montazeri, K., Farhadi, M., Fekrazad, R., Chaibakhsh, S., & Mahmoudian, S. (2022). Photobiomodulation therapy in mood disorders: a systematic review. Lasers in Medical Science, 37(9), 3343–3351. https://doi.org/10.1007/s10103-022-03641-w

82. Moriyama, Y., Nguyen, J., Akens, M., Moriyama, E. H., & Lilge, L. (2009). In vivo effects of low level laser therapy on inducible nitric oxide synthase. Lasers in Surgery and Medicine, 41(3), 227–231. https://doi.org/10.1002/lsm.20745

83. Mukrasch, M. D., Bibow, S., Korukottu, J., Zweckstetter, M., e altri (2009). Structural Polymorphism of 441-Residue Tau at Single Residue Resolution. PLOS Biology, 7(2), e34. https://doi.org/10.1371/journal.pbio.1000034

84. Otto, A. M. (2016a). Warburg effect(s)-a biographical sketch of Otto Warburg and his impacts on tumor metabolism. Cancer & Metabolism, 4, 5. https://doi.org/10.1186/s40170-016-0145-9

85. Otto, A. M. (2016b). Warburg effect(s)-a biographical sketch of Otto Warburg and his impacts on tumor metabolism. Cancer & Metabolism, 4, 5. https://doi.org/10.1186/s40170-016-0145-9

86. Pascale, R. M., Calvisi, D. F., Simile, M. M., Feo, C. F., & Feo, F. (2020). The Warburg Effect 97 Years after Its Discovery. Cancers, 12(10), 2819. https://doi.org/10.3390/cancers12102819

87. Planel, E., Bretteville, A., Liu, L., Virag, L., Du, A. L., Yu, W. H., Dickson, D. W., Whittington, R. A., & Duff, K. E. (2009). Acceleration and persistence of neurofibrillary pathology in a mouse model of tauopathy following anesthesia. The FASEB Journal, 23, 2595-2604. https://doi.org/10.1096/fj.08-122424

88. Planel, E., Miyasaka, T., Launey, T., Chui, D. H., Tanemura, K., Sato, S., Murayama, O., Ishiguro, K., Tatebayashi, Y., & Takashima, A. (2004). Alterations in glucose metabolism induce hypothermia leading to Tau hyperphosphorylation through differential inhibition of kinase and phosphatase activities: implications for Alzheimer's disease. The Journal of Neuroscience, 24, 2401-2411. https://doi.org/10.1523/JNEUROSCI.5561-03.2004

89. Popović, Z., & Popović, B. D. (1999). Introductory Electromagnetics (Vol. 20). Prentice-Hall.

90. Purushothuman, S., Johnstone, D. M., Nandasena, C., van Eersel, J., Ittner, L. M., Mitrofanis, J., & Stone, J. (2015). Near infrared light mitigates cerebellar pathology in transgenic mouse models of dementia. Neuroscience Letters, 591, 155-159. https://doi.org/10.1016/j.neulet.2015.02.037

91. R Hamblin, M. (2017a). Mechanisms and applications of the anti-inflammatory effects of photobiomodulation. AIMS Biophysics, 4(3), 337–361. https://doi.org/10.3934/biophy.2017.3.337

92. R Hamblin, M. (2017b). Mechanisms and applications of the anti-inflammatory effects of photobiomodulation. AIMS Biophysics, 4(3), 337–361. https://doi.org/10.3934/biophy.2017.3.337

93. Raeissadat, S. A., Rayegani, S. M., Rezaei, S., Sedighipour, L., Hasan Bahrami, M., Eliaspour, D., & Karimzadeh, A. (2014). The Effect of Polarized Polychromatic Noncoherent Light (Bioptron) Therapy on Patients with Carpal Tunnel Syndrome. In Original Article Journal of Lasers in Medical Sciences (Vol. 5).

94. Raines, J. K. (1981a). ELECTROMAGNETIC FIELD INTERACTIONS WITH THE HUMAN BODY: OBSERVED EFFECTS AND THEORIES.

95. Raines, J. K. (1981b). ELECTROMAGNETIC FIELD INTERACTIONS WITH THE HUMAN BODY: OBSERVED EFFECTS AND THEORIES.

96. Ramanishankar, A., Singh, A. S., Begum, R. F., Jayasankar, N., Nayeem, A., Prajapati, B. G., & Nirenjen, S. (2024). Unleashing light's healing power: an overview of photobiomodulation for Alzheimer's treatment. Future Science OA, 10(1), FSO922. https://doi.org/10.2144/fsoa-2023-0155

97. Ravera, S., Colombo, E., Pasquale, C., Benedicenti, S., Solimei, L., Signore, A., & Amaroli, A. (2021). Mitochondrial Bioenergetic, Photobiomodulation and Trigeminal Branches Nerve Damage, What's the Connection? A Review. International Journal of Molecular Sciences, 22(9), 4347. https://doi.org/10.3390/ijms22094347

98. Ravera, S., Ferrando, S., Agas, D., De Angelis, N., Raffetto, M., Sabbieti, M. G., Signore, A., Benedicenti, S., & Amaroli, A. (2019). 1064 nm Nd:YAG laser light affects transmembrane mitochondria respiratory chain complexes. Journal of Biophotonics, 12(9). https://doi.org/10.1002/jbio.201900101

99. Rein, G. (2004). Bioinformation Within the Biofield: Beyond Bioelectromagnetics. In

THE JOURNAL OF ALTERNATIVE AND COMPLEMENTARY MEDICINE (Vol. 10, Issue 1).

100. Robijns, J., Lodewijckx, J., Claes, S., Van Bever, L., Pannekoeke, L., Censabella, S., Bussé, L., Colson, D., Kaminski, I., Broux, V., Puts, S., Vanmechelen, S., Timmermans, A., Noé, L., Bulens, P., Govers, M., Maes, A., & Mebis, J. (2021a). Photobiomodulation therapy for the prevention of acute radiation dermatitis in head and neck cancer patients (DERMISHEAD trial). Radiotherapy and Oncology, 158, 268–275. https://doi.org/10.1016/j.radonc.2021.03.002

101. Robijns, J., Lodewijckx, J., Claes, S., Van Bever, L., Pannekoeke, L., Censabella, S., Bussé, L., Colson, D., Kaminski, I., Broux, V., Puts, S.,Vanmechelen, S., Timmermans, A., Noé, L., Bulens, P., Govers, M., Maes, A., & Mebis, J. (2021b). Photobiomodulation therapy for the prevention of acute radiation dermatitis in head and neck cancer patients (DERMISHEAD trial). Radiotherapy and Oncology, 158, 268–275. https://doi.org/10.1016/j.radonc.2021.03.002

102. Robijns, J., Nair, R. G., Lodewijckx, J., Arany, P., Barasch, A., Bjordal, J. M., Bossi, P., Chilles, A., Corby, P. M., Epstein, J. B., Elad, S., Fekrazad, R.,Fregnani, E. R., Genot, M. T., Ibarra, A. M. C., Hamblin, M. R., Heiskanen, V., Hu, K., Klastersky, J., … Bensadoun, R. J. (2022a). Photobiomodulation therapy in management of cancer therapy-induced side effects: WALT position paper 2022. In Frontiers in Oncology (Vol. 12). Frontiers Media S.A. https://doi.org/10.3389/fonc.2022.927685

103. Romano, G. (2011). On the Laws of Electromagnetic Induction. https://www.researchgate.net/publication/51892073

104. Saltmarche, A. E., Naeser, M. A., Ho, K. F., Hamblin, M. R., & Lim, L. (2017). Significant improvement in cognition in mild to moderately severe dementia cases treated with transcranial plus intranasal photobiomodulation: Case series report. Photomedicine and Laser Surgery, 35(8), 432–441. https://doi.org/10.1089/pho.2016.4227

105. Serhan, M., Sprowls, M., Jackemeyer, D., Long, M., Perez, I. D., Maret, W., Tao, N., & Forzani, E. (2019). NEAR INFRARED LIGHT INDUCES POSTTRANSLATIONAL MODIFICATIONS OF HUMAN RED

106. Sipion, M., Ferreira, F. M., Scholler, J., Brana, C., Gora, M., Kouvas, G., Barthet, G., & Sobolewski, A. (2023). A randomized, blinded study of photobiomodulation in a mouse model of Alzheimer's disease showed no preventive effect. Scientific Reports, 13(1), 19828. https://doi.org/10.1038/s41598-023-47039-2

107. Squarcio, F., Hitrec, T., Piscitiello, E., Cerri, M., Giovannini, C., Martelli, D., Occhinegro, A., Taddei, L., Tupone, D., Amici, R., & Luppi, M. (2023). Synthetic torpor triggers a regulated mechanism in the rat brain, favoring the reversibility of Tau protein hyperphosphorylation. Frontiers in Physiology. https://doi.org/10.3389/fphys.2023.1129278

108. Staelens, M., Di Gregorio, E., Kalra, A. P., Le, H. T., Hosseinkhah, N., Karimpoor, M., Lim, L., & Tuszyński, J. A. (2022). Near-Infrared Photobiomodulation of Living Cells, Tubulin, and Microtubules In Vitro. Frontiers in Medical Technology, 4. https://doi.org/10.3389/fmedt.2022.871196

109. Su, B., Wang, X., Drew, K. L., Perry, G., Smith, M. A., & Zhu, X. (2008). Physiological regulation of Tau phosphorylation during hibernation. Journal of Neurochemistry, 105, 2098-2108. https://doi.org/10.1111/j.1471-4159.2008.05294.x

110. Szymborska-Małek, K., Komorowska, M., & Gąsior-Głogowska, M. (2018). Effects of Near Infrared Radiation on DNA. DLS and ATR-FTIR Study Spectrochimica Acta - Part A: Molecular and Biomolecular Spectroscopy, 188, 258–267. https://doi.org/10.1016/j.saa.2017.07.004

111. Tai, S., Sun, Y., Squires, J. M., Zhang, H., Oh, W. K., Liang, C., & Huang, J. (2011). PC3 is a cell line characteristic of prostatic small cell carcinoma. The Prostate, 71(15), 1668–1679. https://doi.org/10.1002/pros.21383 Tam, S. Y., Tam, V. C. W., Ramkumar, S., Khaw, M. L., Law, H. K. W., & Lee, S. W. Y. (2020). Review on the Cellular Mechanisms of Low- Level Laser Therapy Use in Oncology. In Frontiers in Oncology (Vol. 10). Frontiers Media S.A. https://doi.org/10.3389/fonc.2020.01255

112. Thar, R., & Kühl, M. (2004a). Propagation of electromagnetic radiation in mitochondria? Journal of Theoretical Biology, 230(2), 261–270. https://doi.org/10.1016/j.jtbi.2004.05.021

113. The Bakerian Lecture. Experiments and calculations relative to physical optics. (1804). Philosophical Transactions of the Royal Society of London, 94, 1–16. https://doi.org/10.1098/rstl.1804.0001

114. Tian, H., Zhu, H., Gao, C., Shi, M., Yang, D., Jin, M., Wang, F., & Sui, X. (2023a). System-level biological effects of extremely low-frequency electromagnetic fields: an in vivo experimental review. Frontiers in Neuroscience, 17. https://doi.org/10.3389/fnins.2023.1247021

115. Vainio, R., Desorgher, L., Heynderickx, D., Storini, M., Flückiger, E., Horne, R. B., Kovaltsov, G. A., Kudela, K., Laurenza, M., McKenna-Lawlor, S., Rothkaehl, H., & Usoskin, I. G. (2009). Dynamics of the Earth's particle radiation environment. Space Science Reviews, 147(3–4), 187–231. https://doi.org/10.1007/s11214-009-9496-7

116. Vander Heiden, M. G., Cantley, L. C., & Thompson, C. B. (2009a). Understanding the Warburg effect: the metabolic requirements of cell proliferation. Science (New York, N.Y.), 324(5930), 1029–1033. https://doi.org/10.1126/science.1160809

117. Vander Heiden, M. G., Cantley, L. C., & Thompson, C. B. (2009b). Understanding the Warburg effect: the metabolic requirements of cell proliferation. Science (New York, N.Y.), 324(5930), 1029–1033. https://doi.org/10.1126/science.1160809

118. Vecchia P., Matthes R., Zielgelberger G., Lin J., Saunders R., & Swerdlow A. (Eds.). (2009). Exposure to high frequency electromagnetic fields, biological effects and health consequences (100 kHz–300 GHz) (ICNIRP 16/2009).

119. Wang, Y., & Mandelkow, E. (2016). Tau in physiology and pathology. Nature Reviews Neuroscience, 17, 5-21. https://doi.org/10.1038/nrn.2015.1

120. Ward, P. S., & Thompson, C. B. (2012a). Metabolic Reprogramming: A Cancer Hallmark Even Warburg Did Not Anticipate. Cancer Cell, 21(3), 297–308. https://doi.org/10.1016/j.ccr.2012.02.014

121. Ward, P. S., & Thompson, C. B. (2012b). Metabolic Reprogramming: A Cancer Hallmark Even Warburg Did Not Anticipate. Cancer Cell, 21(3), 297–308. https://doi.org/10.1016/j.ccr.2012.02.014

122. Weingarten, M. D., Lockwood, A. H., Hwo, S. Y., & Kirschner, M. W. (1975). A protein factor essential for microtubule assembly. Proceedings of the National Academy of Sciences of the United States of America, 72, 1858-1862. https://doi.org/10.1073/pnas.72.5.1858

123. Welsh, J. (2013). Animal Models for Studying Prevention and Treatment of Breast Cancer. In Animal Models for the Study of Human Disease (pp. 997–1018). Elsevier. https://doi.org/10.1016/B978-0-12-415894-8.00040-3

124. Wiginton, J., Brazdzionis, J., Patchana, T., Savla, P., Hung, J., Zhang, Y., & Miulli, D. E. (2022). Measuring Electromagnetic Field Activity Generated by Neurons In Vivo by Humans With Thoughts of Repetitive Motor Activities and Emotional Thoughts. Cureus, 14(3), e23332. https://doi.org/10.7759/cureus.23332

125. Willemse, M., Tuszynski, J., & Fertig, B. (n.d.). Hyperlight Therapy A breakthrough for Healing and Enhancing Your Well-Being Clinically proven efficacy for treating: Chronic Wounds-Rheumatoid Symptoms-Back Pain-Shoulder and Neck Pain-Sport Injuries-Skin Diseases: Psoriasis,

126. Yadikar, H., Torres, I., Aiello, G., Kurup, M., Yang, Z., Lin, F., Kobeissy, F., Yost, R., & Wang, K. K. (2020). Screening of tau protein kinase inhibitors in a tauopathy-relevant cell-based model of tau hyperphosphorylation and oligomerization. PLOS ONE, 15(7). https://doi.org/10.1371/journal.pone.0224952

127. Yang, L., Wu, C., Parker, E., Li, Y., Dong, Y., Tucker, L., et al. (2022). Non-invasive photobiomodulation treatment in an Alzheimer Disease-like transgenic rat model. Theranostics, 12, 2205–2231. https://doi.org/10.7150/thno.70756

128. Zein, R., Selting, W., & Hamblin, M. R. (2018a). Review of light parameters and photobiomodulation efficacy: dive into complexity. Journal of Biomedical Optics, 23(12), 1. https://doi.org/10.1117/1.JBO.23.12.120901

129. Zein, R., Selting, W., & Hamblin, M. R. (2018b). Review of light parameters and photobiomodulation efficacy: dive into complexity. Journal of Biomedical Optics, 23(12), 1. https://doi.org/10.1117/1.JBO.23.12.120901

130. Zhang, B., Xie, Y., Ni, Z., & Chen, L. (2020). Effects and Mechanisms of Exogenous Electromagnetic Field on Bone Cells: A Review. Bioelectromagnetics, 41(4), 263–278. https://doi.org/10.1002/bem.22258

131. Zhang, R., Zhou, T., Samanta, S., Luo, Z., Li, S., Xu, H., et al. (2022). Synergistic photobiomodulation with 808-nm and 1064-nm lasers to reduce the β-amyloid

neurotoxicity in the in vitro Alzheimer's disease models. Frontiers in Neuroimaging, 1, 903531. https://doi.org/10.3389/fnimg.2022.903531

132. Zomorrodi, R., Loheswaran, G., Pushparaj, A., & Lim, L. (2019). Pulsed Near Infrared Transcranial and Intranasal Photobiomodulation Significantly Modulates Neural Oscillations: a pilot exploratory study. Scientific Reports, 9(1), 6309. https://doi.org/10.1038/s41598-019-42693-x

133. Zura, S., Jalil, A., Abdullah, H., & Taib, M. N. (2015a). DETECTION OF ENDOGENOUS ELECTROMAGNETIC FIELD OF THE HUMAN BODY. 10. www.arpnjournals.com

134. Zura, S., Jalil, A., Abdullah, H., & Taib, M. N. (2015b). DETECTION OF ENDOGENOUS ELECTROMAGNETIC FIELD OF THE HUMAN BODY. 10. www.arpnjournals.com